UNIVERSITÉ DE SHERBROOKE
Faculté de génie
Département de génie mécanique

RÉCUPÉRATION DES DÉCHETS THERMIQUES DANS LES USINES D'ALUMINIUM À TRAVERS LES MACHINES STIRLING

WASTE HEAT RECOVERY IN ALUMINUM PLANTS BY MEANS OF STIRLING ENGINES

Thèse de doctorat
Specialité: génie mécanique

Franco CASCELLA

Sherbrooke (Québec) Canada

Octobre 2018

JURY MEMBERS

Mikhail SORIN

Supervisor

Alberto TEYSSEDOU

Co-supervisor

Clara SANTATO

Examiner

Luc FRÉCHETTE

Examiner

Gervais SOUCY

Examiner

"Fu una sera di gennaio, che mio padre mi portò
Su una barca senza vela che sapeva dove andare,
A gettare la mia rete dietro al faro, poi mi disse, figlio mio
Questa rete è la tua vita, manda a fondo tutti i sogni,
Come un giorno ho fatto io."

Lucio Dalla, Edoardo De Angelis, *Sulla rotta di Cristoforo Colombo*

Alla forza di mio padre
e al sorriso di mia madre

RÉSUMÉ

Parmi tous les secteurs industriels, celui de la production d'aluminium est l'un des plus importants consommateurs d'énergie : les processus les plus modernes nécessitent une quantité d'énergie électrique comprise entre 11 et 15 MW h par tonne d'aluminium produite. La plus grande partie de cette énergie est nécessaire pour réaliser le processus d'électrolyse qui produit de l'aluminium (c'est-à-dire, le procédé Hall-Héroult). La moitié de cette énergie est perdue sous forme de déchets thermiques.
Tous les producteurs d'aluminium financent des projets de recherche privés pour trouver des solutions qui améliorent l'efficacité énergétique de leurs usines. Ceci est réalisé par l'analyse des sources de pertes thermiques et par la suite par la valorisation de ces pertes. Par exemple, la chaleur gaspillée dans l'usine d'aluminium peut être utilisée aux fins de chauffage urbain ou pour produire de la puissance électrique. Dans les deux cas, un effet utile (c'est-à-dire, l'énergie thermique ou électrique) est produit à travers une source de chaleur qui serait autrement perdue.
Le déchet thermique qui a été largement analysé dans la littérature scientifique est la libération des gaz d'échappement à haute température depuis l'usine d'aluminium vers l'environnement. Plusieurs solutions pour récupérer cette forme d'énergie thermique ont été proposées. Mais ces solutions n'ont pas été appliquées en raison de leurs coûts d'investissement élevés. Ceci est la raison pour laquelle d'autres formes de récupération et de conversion des rejets thermiques doivent être étudiées. Il est bien connu qu'une grande différence de température se produit entre les parois de la cuve électrolytique (dans lesquelles l'aluminium est produit) et l'air ambiant ; plus précisément, la surface de paroi a une température comprise entre 200°C et 400°C, tandis que l'air est à la température ambiante. Par conséquent, des phénomènes de transfert de chaleur tels que la convection naturelle et le rayonnement thermique apparaissent. Aujourd'hui, les technologies en mesure de récupérer et de convertir cette forme de chaleur (comme par exemple, les échangeurs de chaleur installés sur la paroi latérale) ne sont pas suffisamment au point, donc davantage de recherche dans ce domaine est nécessaire.
L'objectif de cette thèse est d'étudier la récupération des déchets thermiques et leur conversion en puissance utile. Après une brève introduction, une revue de la littérature existante est réalisée afin de mettre en évidence les sources de gaspillage thermique dans le procédé de Hall-Héroult et les technologies disponibles pour les récupérer et les valoriser en respectant les critères de sécurité de l'usine. Il est donc proposé de récupérer les déchets thermiques de la paroi de la cuve par rayonnement (et, dans une moindre mesure, par conduction) et de les convertir en puissance utile à travers des machines Stirling. La récupération des déchets et leur conversion ont été traitées par l'auteur dans deux articles scientifiques présentés dans cette thèse. Les derniers chapitres de la thèse sont dédiés à la discussion de ce projet de recherche et aux travaux futurs.

Mots-clés : Récupération des déchets thermiques, équations de conservation, CFD, analogie électrique, circuit équivalente, moteur Stirling

ABSTRACT

Among all industrial sectors, the aluminum-production industry is one of the most energy intensive: most up-to-date processes require a quantity of electrical energy ranging between 11 and 15 MW h per ton of produced aluminum. Most of this energy is needed to sustain the electrolysis process that produces aluminum, namely, the Hall-Héroult process; however, a detailed analysis of a conventional aluminum production line demonstrates that almost half of the aforementioned energy is lost under the form of heat.
The aluminum companies fund private research projects to find solutions that increase the energy efficiency of their smelters. This is accomplished by analyzing the thermal losses and the possibility of converting them into useful power. For instance, heat wasted in the aluminum plant can be the source for space or district heating. Another solution consists in introducing a heat engine that uses the thermal waste to generate electrical power. In both cases, a useful output (i.e. thermal or electrical power) is produced by means of energy that would be otherwise wasted.
There is a thermal waste that has been widely analyzed in the scientific literature, namely the release of exhaust gases at high temperature from the aluminum plant to the environment. Several solutions to recover this form of energy loss have been proposed (for instance, the introduction of an organic Rankine engine); however, these technologies have not been implemented because of their high capital costs. This is the reason why other forms of thermal waste must be investigated. It is well known that there is a considerable temperature difference between the walls of the electrolytic cell (in which aluminum is produced) and the surrounding air; more precisely, the wall surface has a temperature between 200°C and 400°C, while the air and the surrounding walls are at ambient temperature. Therefore, heat transfer phenomena arise, such as natural convection and thermal radiation. Nowadays, technologies able to recover these forms of heat (as sidewall heat exchangers) are not sufficiently advanced; hence, further research in this field is needed.
The main objective of this thesis is to study the recovery and the conversion of the electrolysis cell thermal wastes occurring at the pot sidewall. After a brief introduction, the literature review is presented. The review highlights the sources of thermal waste in the Hall-Héroult process; then the (few) technologies able to harvest them without affecting the safety of the smelter are listed. Therefore, it is proposed to recover the cell-sidewall heat wastes by thermal radiation (and, to a lesser extent, by conduction) and to convert them into useful power by means of the Stirling engine technology. The recovery of the thermal losses and their conversion are the main topics of two scientific papers presented in this thesis. Finally, in the last chapters of this document, this research project and future works are discussed.

Keywords: Thermal wastes recovery, conservation equations, CFD, electrical analogy, equivalent circuit, Stirling engine

ACKNOWLEDGEMENTS

The first page of this dissertation states that I am its author. I strongly believe that this statement is unfair. True, I spent most of the last two years writing this document; however, its fulfillment would have never been possible without the help of the people who accompanied me on this journey. These people deserve to be considered as coauthors of this dissertation; since (unfortunately) this is not possible, I will try to show my gratitude to them here.

I would like to start with my supervisor, Professor Mikhail Sorin, and my co-supervisor, Professor Alberto Teyssedou. Working with these professors was a growth experience in which I learned what actually means to undertake and accomplish a research project. Over the past four years, Professor Sorin has provided any kind of support a PhD student may need. From the beginning of my studies, he gave me all the means required to succeed my research; in particular, when my first scholarship ended in 2017, he promptly provided me with an essential financial aid. But most importantly, he has always believed in my ideas (even the most unattainable) and in my capacities to work with other researchers. Professor Alberto Teyssedou's help was also fundamental. He has done more than his institutional role demanded, by revising all my drafts and giving precious advices about my research topics. He also considered me for what became one of the most satisfying experience of my doctorate, that is, being responsible for the practical tutorials of the "Physics Thermodynamic" course. Above all, I am thankful for all those discussions we had, related not only to my research, but also to astrophysics, politics, books, and, sometimes, love.

I would like to mention the researchers with whom I worked: Professor Fabien Formosa of the Université Savoie Mont Blanc, who had the time to provide his essential point of view about the Stirling engine technology; Simon Gaboury, of the Rio Tinto Arvida R&D Center, for providing the precious data about the Alma electrolysis cells; Steven L. Rickman, of the NASA Engineering and Safety Center, and the NASA TFAWS committee, for letting me give a talk about OpenFOAM at TFAWS 2017; and Giuliana Litrico, former PhD student at Sherbrooke University, for having the time to answer my questions about OpenFOAM and for being my Italian friend in Sherbrooke.

Non posso fare a meno di ringraziare la mia famiglia, mio padre Cosimo, mia madre Lidia e mia sorella Cinzia. Questo lavoro è dedicato principalmente a loro, non solo per aver acettato la mia assenza, ma soptattutto per avermi insegnato che l'unico modo per guardare al futuro è con ottimismo e che la speranza non è mai vana. Sono enormemente grato anche ai miei zii, Zio Silvio, Zia Anna, Zio Giordano e Zio Enzo, per il supporto che mi mostrano ogni giorno.

Je désire aussi remercier ma belle famille, Francois et Roselyne, qui m'ont aidé à corriger tous les documents que j'ai rédigé en français, incluant cette thèse. Merci Francois pour toutes les bonnes bouteilles de vin que tu as apportées depuis la France et merci Roselyne de me dire que j'ai toujours raison. Et surtout merci à vous de m'avoir accueilli dans votre famille comme un *figlio mio*.

Je souhaite aussi remercier mes collègues de bureau, Étienne, Darren, Akila, Ahmed Falat,

Ahmed Naceur, Atyab et Aaron ; les échanges d'idées avec chacun d'entre vous m'ont permis d'améliorer mes connaissances et mes compétences de chercheur. Un merci particulier va aussi à tous mes amis du Club d'Aviron de Montréal.
"Il lavoro è quella cosa noiosa che si fa fra una pausa caffè e l'altra", diceva un comico italiano in uno dei suoi spettacoli. Allora, come non poter ricordare chi ha supportato questa tesi in questi anni? Grazie a Gianniantonio, Daria e Stefano, Eduardo e Filippo, per aver accettato i miei continui e insistenti inviti a prendersi un caffè da me. Un ringraziamento speciale va anche a quegli amici che ogni giorno non smettono mai di starmi vicino: Nunzio, con cui condivido le mie radici, e Lidia e Paolo, per le serate "Nuovo Cinema Cascella", Chloé e Nello, per il tempo passato a prendersi in giro e mai sul serio, Valeria, la cui pazzia è una continua fonte d'ispirazione, Roberto, compagno di pizza fritta (e di altre leccornie) e Alessandra (o, in amicizia, Cassi), per avermi insegnato che certi legami di amicizia sono veramente indissolubili.
Pour finir, mon plus grand remerciement va à ma compagne de vie, sans laquelle la rédaction de cette thèse aurait été impossible. Durant ces quatre ans, il n'y a pas eu un jour où elle n'a été présente pour me soutenir, même dans les moments les plus difficiles ; chaque fois qu'il y avait un présage de tristesse, elle l'a promptement chassé ; mais surtout, elle a su m'accepter dans mes limites. La confiance énorme qu'elle m'a témoignée est devenue une composante fondamentale et irremplaçable de ma vie ; grâce à cette confiance, synonyme d'un amour immense, j'ai compris que le paradis se trouve ici, sur cette terre, avec elle. Merci de donner un sens à tout ce que je fais dans ma vie. Je t'aime, Carine.

TABLE OF CONTENTS

1 INTRODUCTION **1**
- 1.1 Energy harvesting in aluminum smelters . . . 1
- 1.2 Overall objectives of the research . . . 3
- 1.3 Proposed methodology . . . 5
- 1.4 Plan of the thesis . . . 7

2 LITERATURE REVIEW AND OBJECTIVES OF THE THESIS **9**
- 2.1 Aluminum production: a general overview . . . 9
  - 2.1.1 Hall-Héroult process . . . 9
  - 2.1.2 Mass balance of the electrolysis cell . . . 11
  - 2.1.3 Electrolysis cell energy balance . . . 14
- 2.2 Recovery of the thermal wastes in the aluminum production industry . . . 17
  - 2.2.1 Recovery of exhaust heat loss . . . 20
  - 2.2.2 Thermal recovery of heat flux through the walls of electrolytic cells 22
- 2.3 Conversion of thermal wastes into useful work . . . 30
  - 2.3.1 Conversion of exhaust low-grade heat wastes by means of ORC engines 32
  - 2.3.2 Conversion of low-grade sidewall heat flux . . . 34
- 2.4 Specific objectives of the research . . . 40
  - 2.4.1 Waste-heat recovery by thermal radiation and conversion using Stirling engines . . . 40
  - 2.4.2 Principal contributions of the present work . . . 43
  - 2.4.3 Release of residual cooling heat . . . 45

3 PROOF OF CONCEPT TO RECOVER THERMAL WASTES FROM ALUMINUM ELECTROLYSIS CELLS USING STIRLING ENGINES **47**
- 3.1 Abstract . . . 49
- 3.2 Introduction . . . 49
- 3.3 Cooling the pots in aluminum smelters . . . 51
- 3.4 The numerical model . . . 52
  - 3.4.1 The integration domain . . . 52
  - 3.4.2 Conservation equations . . . 54
  - 3.4.3 Boundary conditions . . . 56
  - 3.4.4 Validation of the numerical model . . . 58
- 3.5 Modeling waste heat recovery from aluminum electrolysis cells . . . 63
  - 3.5.1 Assessment of convergence . . . 63
  - 3.5.2 Numerical results . . . 64
- 3.6 Conversion of sidewall thermal losses into useful power . . . 68
- 3.7 Conclusion . . . 70

4 MODELING THE OPERATION OF STIRLING ENGINES BY MEANS OF AN EQUIVALENT ELECTRICAL CIRCUIT **73**

4.1 Abstract . . . 75
4.2 Introduction . . . 75
4.3 Description of the model . . . 77
4.3.1 Expansion and compression chambers . . . 79
4.3.2 Heater and cooler . . . 80
4.3.3 Regenerator . . . 83
4.3.4 Displacer and power piston . . . 86
4.4 Results and discussion . . . 88
4.4.1 Validation of the model . . . 90
4.4.2 Analyses of the proposed model . . . 91
4.4.3 Discussion . . . 91
4.5 Conclusion . . . 92

5 DISCUSSION 95
5.1 The operation of a Stirling engine converting the radiative thermal wastes from the pot sidewalls . . . 95
5.1.1 Validity of the proposed coupling approach . . . 100
5.2 Economic analysis . . . 102
5.3 Future perspectives . . . 106
5.4 Research assessment . . . 111

6 CONCLUSION FRANÇAISE 113
6.1 Résumé de la recherche . . . 113
6.2 Contributions scientifiques . . . 115
6.3 Travaux futurs . . . 117

7 ENGLISH CONCLUSION 119
7.1 Summary of the research . . . 119
7.2 Scientific contributions . . . 121
7.3 Future works . . . 122

A THE HALL-HÉROULT PROCESS: THEORETICAL ENERGY AND ACTUAL REACTIONS 125
A.1 Theoretical energy for the Hall-Héroult process . . . 125
A.2 Actual reactions in the Hall-Héroult process . . . 126

B RADIATION HEAT EXCHANGERS: A GENERAL OVERVIEW 129

C THE $k\varepsilon$ AND THE $k\omega$ TURBULENCE MODELS 133

D GENERAL TRANSPORT EQUATION IN THE FINITE VOLUME METHOD 135

E THE SEMI IMPLICIT METHOD FOR PRESSURE LINKED EQUATIONS (SIMPLE) OF PATANKAR [19] 137

F RE-1000 TECHNICAL DATA [49] **139**

LIST OF REFERENCES **141**

LIST OF FIGURES

1.1 Aluminium plant in Alma, QC [10]. 3

2.1 Sketch of the electrolysis cell used to produce aluminum at industrial scale. 10
2.2 Relevant materials flowing through the cell control volume. 11
2.3 Relevant energy flows through the cell control volume. 14
2.4 Photos of typical cell operations: (a) introduction of bath corrections; (b) anode change. 16
2.5 (a) Inner geometry of a modern electrolysis cell [27] and (b) thermal simulation of a 500 kA cell [35]. 17
2.6 Electrolysis cell energy balances from three studies found in the scientific literature. 18
2.7 District heating scheme for the town of Akranes, proposed by Fleer et al. [4]. 21
2.8 Pot cooling strategies: (a) flow of external air cooling the pot evaluated by means of CFD [34]; (b) scheme of localized jet cooling [33]. 23
2.9 Sketch of a sidewall heat exchanger. 24
2.10 (a) Radiation from an infinitesimal surface $d\sigma$ in the direction of the conical element $d\Omega$; (b) infrared light radiation from the walls of a pot (b). 25
2.11 Schematic description of the control volume used in Equation 9. 28
2.12 Heat flux at the collector as a function of its temperature and distance estimated by Equation 9. 30
2.13 ORC engine configurations: (a) the exhausts heat is transferred to the organic working fluid of the ORC; (b) a water loopp is used to transfer heat of the exhausts to the organic working fluid. 32
2.14 Design and exploded view of the proposed thermoelectric generator. 35
2.15 Thermodynamic diagrams describing a Stirling cycle: ideal Stirling cycle in the pV (a) and Ts (b) diagram and real versus ideal Stirling cycle (c). . . . 37
2.16 Design and exploded Stirling machine under analysis [13]. 39
2.17 Comparison of the performance of Stirling engines with thermoelectric generators: (a) comparison of measured thermodynamic efficiencies of various Stirling engines proposed in the literature [13, 69, 72-74] with thermoelectric-module as a function of the hot-source temperature for the same cool temperature (T_k = 20°C); (b) comparison of the useful work converted by Stirling engines proposed in the literature with the work obtained by thermoelectric modules as a function of the hot-source temperature for the same cool temperature (T_k = 20°C). 43

3.1 Top view of the control volume. 53
3.2 Computational domain used to perform the simulations: (a) bottom surface of the fluid region; (b) mesh refinement around the air inlet nozzles. 54

3.3 Comparison of cylindrical fin temperature distributions calculated using Equation 9 and the numerical simulations performed using both $k\varepsilon$ and $k\omega$ turbulence models. . . . 60
3.4 Comparison of CFD simulations with results obtained using Schlichting formulas [84]: (a) flow velocity distribution; (b) flow temperature profile. . 62
3.5 Convergence behavior as a function of the number of iterations. (a) variations of the residuals; (b) radiative thermal power at the Stirling engine heat collector. . . . 65
3.6 Effect of the sidewall thermal power flux on the collector average temperature and the thermal power flux recovered by radiation. . . . 66
3.7 Effect of inlet air cooling conditions on the thermal collector: (a) average temperature and radiation flux upon the collector as a function of the air-nozzle inlet velocity; (b) collector average surface temperature. . . . 67

4.1 Simplified sketch of a Stirling engine. . . . 78
4.2 Sketch of the engine under analysis [49]. . . . 79
4.3 Equivalent circuit for the compression/expansion chamber. . . . 80
4.4 Equivalent circuit for both heater and cooler. . . . 83
4.5 Equivalent circuit for the regenerator. . . . 85
4.6 Forces acting on the displacer. . . . 86
4.7 Equivalent electrical circuit of the displacer. . . . 87
4.8 Power piston force balance. . . . 87
4.9 Equivalent electrical circuit of the power piston. . . . 88
4.10 Equivalent electrical network for the RE-1000 Stirling engine. . . . 89
4.11 Electrical analogy model predictions (design working conditions): (a) power piston motion; (b) compression pressure; (c) pressure-volume diagram of the compression space. . . . 90
4.12 Predictions of the model in off-design operating conditions: (a) frequency; (b) compression pressure amplitude; (c) piston stroke. . . . 91
4.13 Power evaluation from the electrical analogy model as a function of the mean pressure (a), the heater temperature (b) and the cooler temperature (c). . 92

5.1 Operation of the Stirling engine as a function of various values of the scale factor ε: (a) piston stroke $|x_p|$ and (b) frequency f as a function of the heater temperature T_h; (c) piston stroke $|x_p|$ and (d) frequency f as a function of the engine mean pressure $\overline{p}$. . . . 97
5.2 Operation of the Stirling engine as a function of various values of the scale factor ε: power output as a function of (a) the heater temperature T_h and (b) the engine mean pressure $\overline{p}$. . . . 100
5.3 Economic analysis: bar plots showing the Stirling engine investment cash flows under different scenarios. . . . 104
5.4 Sankey diagram for the proposed recovery-and-conversion system. . . . 111

B.1 Stationary collector configurations: flat–plate (a), compound parabolic (b) and evacuated tube collectors (c) [117, 118]. . . . 129

B.2 Sun-tracking collector configurations: (a) parabolic trough collector, (b) Fresnel reflector, (c) Parabolic dish reflectors and (d) heliostat field collectors [117, 118]. 130
B.3 Brayton power engine for space application. 131

D.1 Control volume V_p for the definition of the FVM. 135

LIST OF TABLES

2.1 Statistical analysis of energy distributions (data from Figure 2.6). 20
2.2 Second-principle analysis of the thermal wastes. 31

3.1 Physical properties of materials and surfaces. 54
3.2 RMS errors for the $k\varepsilon$ and $k\omega$ turbulence models. 63
3.3 Effect of the distance between the pot sidewall and the surface of the thermal collector exposed to radiation heat transfer ($u_{jet} = 25\ \mathrm{m\,s^{-1}}$, $T_{jet} = 20°\mathrm{C}$). 66

4.1 Working conditions of the RE-1000 engine. 89

5.1 Characteristic variables of the Stirling unit under analysis. 98

A.1 Constants to evaluate enthalpy and entropy of species 125
A.2 Thermodynamic data 127

LIST OF SYMBOLS

Letters	
A	Surface area [m^2]
Be	Beale Number [-]
C	Equivalent capacitor [$m^4\,s\,kg^{-1}$]
c_f	Friction factor coefficient [-]
c_p	Specific heat [$J\,kg^{-1}K^{-1}$]
D, d	Diameter [m]
d_h	Hydraulic diameter [m]
F_d	Damping force [N]
F_{ij}	View factor [-]
f	Frequency [Hz]
g	Source term in the time domain [m^3s^{-1}]
$\vec{g}$	gravitational acceleration [$m\,s^{-2}$]
h	Convective heat transfer coefficient [$W\,m^{-2}K^{-1}$]
I	Turbulent intensity [-]
k	Turbulent kinetic energy [m^2s^{-2}]
k	Thermal conductivity [$W\,m^{-1}K^{-1}$]
$\mathscr{L}$	Laplace-transform operator
L	Equivalent inductor [$kg\,m^{-4}$]
l	Mixing length [m]
m	Mass [kg]
n	Exponential coefficient in $F_d = \alpha\dot{x}^n$ [-]
Nu	Nusselt number [-]
P, p	Pressure [Pa]
P	Perimeter [m]
Pr	Prandtl number [-]
Q	Radiative power [W]
$\dot{q}$	Heat flux [Wm^{-2}]
$\Re$	Real part [-]
R	Equivalent resistor [$kg\,s^{-1}m^{-4}$]
R	Gas constant [$J\,kg^{-1}K^{-1}$]
$\overline{R}$	Universal gas constant [$\overline{R} = 8.314\ J\,mol^{-1}K^{-1}$]
Re	Reynolds number [-]
s	Laplace variable
T, t	Temperature [°C]
t	Temporal coordinate [s]
V	Volume [m^3]
$\dot{V}$, $\dot{v}$	Volumetric flow rate [m^3s]
$\dot{W}$	Useful power [W]
U, u	Velocity [$m\,s^{-1}$]
x	Spatial coordinate [m]

$\lvert x_p \rvert$	Piston stroke [m]
y^+	Dimensionless distance from the wall [-]

Greek Letters	
α	Dimensional coefficient in $F_d = \alpha \dot{x}^n$ [N]
β	Volumetric thermal expansion coefficient [K^{-1}]
γ	Heat capacity ratio [-]
δ	Kronecker delta [-]
ε	Regenerator porosity [-]
ε	Coefficient of emission [-]
ε	Dissipation rate [$m^2 s^{-3}$]
ε	Scale factor [-]
η	Thermodynamic efficiency [-]
θ	Dimensionless temperature [-]
κ	Friction factor [s^{-1}]
λ	Eigenvalue [-]
μ	Shear viscosity [Pa s]
ν_t	Turbulent viscosity [$m^2 s^{-1}$]
ξ	Dimensionless space coordinate [-]
ρ	Density [$kg\,m^{-3}$]
σ	Stefan-Boltzmann constant [$\sigma = 5.67 \times 10^{-8} W\,m^{-2} K^{-4}$]
τ	Temporal coordinate [s]
Ψ, ψ	Generic variable
ω	Turbulence frequency [s^{-1}]

Subscripts	
c	Collector
c	Compression chamber
d	Displacer
e	Expansion chamber
H	Free Stream
h	Heater
HT	Heat exchanger
k	Cooler
m	Maximal
o	Outlet
p	Power piston
r	Regenerator
s	Metallic matrix
s	Surface
sw	Sidewall
w	Wall
max	Maximum value
rms	Root mean square

Other symbols	
$\dot{[\,]}$	First derivative with respect to time
$\ddot{[\,]}$	Second derivative with respect to time
$\overline{[\,]}$	Mean variable
$[\,]'$	Fluctuating variable
$\vec{[\,]}$	Vector

LIST OF ACRONYMS

Acronym	Definition
CFD	Computational Fluid Dynamic
DNS	Direct Numerical Simulations
EPRI	Electric Power Research Institute
FPSE	Free-Piston Stirling Engines
IRR	Internal Rate of Return
LES	Large Eddy Simulations
LTD	Low Temperature Difference
MHD	Magnetohydrodynamics
NPV	Net Present Value
OpenFOAM	Open source Field Operation And Manipulation
ORC	Organic Rankine Cycle
PDE	Partial Differential Equation
R&D	Research and Development
RANS	Reynolds Averaged Navier-Stokes
RE-1000	Research Engine (nominal power 1000 W)
ROI	Returns On Investment
SIMPLE	Semi-Implicit Method for Pressure Linked Equations

CHAPTER 1

INTRODUCTION

1.1 Energy harvesting in aluminum smelters

The continuously increasing energy demand in both developed and under-developing countries is a problem that our society has to face. The main issue lies beneath the fact that most of the world energy needs are met by non-renewable resources, above all, oil, coal and natural gas [1]; there is no question that the use of these resources has a profound impact on the environment, since they are responsible for air pollution and the greenhouse effect [2].

Among the three sectors of the economy, the secondary one (i.e. manufacturing) is particularly affected by these issues, since the energy demand of some industrial plants is particularly high; therefore, the only resources capable of satisfying their needs are non-renewable. As a consequence, governments regulate these industries by introducing laws limiting the externalities due to the consumption of these resources (above all, carbon dioxide and other pollutants); for instance, the temperature and the composition of exhaust gas of a combustion process are precisely defined by these regulations. If these laws are not respected, a payment of the Pigouvian tax is imposed [3]. In order to reduce these externalities, engineers and researchers are looking for solutions that may decrease the demand, or increase the energy efficiency, of industrial factories.

An industrial sector which is particularly energy intensive is the production of primary aluminum. In order to produce a ton of aluminum, a quantity of energy between 11 and 15 MW h is needed[1] [4–6]. Most of the energy demand is required to sustain the electrolysis process of aluminum smelting, namely, the Hall-Héroult process [7]. The problems that aluminum producers are facing are not related to the enormous energy consumption, but to the energy efficiency of the process itself, because roughly half of the input power is released to the environment under the form of thermal power [6]. That being said, aluminum producers are interested in recovering these thermal wastes and eventually converting them into useful power.

In the scientific literature, two main sources of thermal wastes have been identified: the thermal energy loss due to the release of process exhaust gases (which have a tempera-

[1] Due to these large amounts of energy, most aluminum factories usually have their own power station nearby.

ture of about 100°C) and the heat lost through the walls of the electrolytic cells (usually called pots) in which aluminum is produced [6]. Solutions to recover the former source of thermal waste have been studied in the open literature. One of the proposed ideas is to introduce a power generation system that uses the exhaust gases as the heat source. Such a system is based on the Organic Rankine Cycle (ORC) engine [4]; in fact, because of its low evaporation temperature, an organic working fluid assures the good operation of the ORC engine [8]. Another idea is to use the exhaust gases for district heating. In this case, the thermodynamic potential of the gases is sent to a nearby location in need of heat for either residential or commercial purposes [4]. These two options are certainly valid. From a the thermodynamic viewpoint, an increase of the energy efficiency of the industrial plant is achieved; from the environmental viewpoint, one of the two outputs, that is, either electric or thermal power is converted from an energy source that would be otherwise wasted (so, the carbon footprint is low). Nonetheless, these solutions require enormous investments [5]. Therefore, aluminum producers are rarely interested in these waste-heat recovery systems as their Returns On Investment (ROI) are not attractive [4]. As an example, the Rio Tinto® case should be mentioned. In the Americas, the most important producer and vendor of aluminum is Rio Tinto [9]: in order to increase the energy efficiency of their Canadian plants, Rio Tinto has funded (and keeps on funding) research-and-development (R&D) projects on waste heat recovery. In particular, a recent collaboration with HydroQuebéc® was launched. The main objective of this collaboration is to analyze a specific case study, that is, the Rio Tinto aluminum facility located in Alma, QC, namely the *Usine Alma* (Figure 1.1).

This Rio Tinto facility, built in 2001 with a capital cost of $ 2.9 billion, works 24 hours per day and consumes 660 MW to produce 440,000 tons of aluminum per year [10]. Since a huge amount of this power is lost under the form of heat, Rio Tinto and HydroQuebéc are working together to find a reliable solution to recover these losses. The results of this collaboration can be found in a confidential report released by the Shawinigan Energy Technology Laboratory [5]. In this report, the temperature of the exhaust gases has been analyzed as a function of the season; the possibility of using these gases as a heat source of an ORC engine has been investigated. Therefore, it is shown that at least 550 kW could be converted by means of this technology; however, an economic study has been implemented and it has shown that the introduction of this solution is not economically profitable [5].

The considerations listed above justify the need of studying the second source of thermal

® Rio Tinto is a registered trademark.
® HydroQuebéc is a registered trademark.

Figure 1.1 Aluminium plant in Alma, QC [10].

waste recovery, that is, the heat losses occurring from the electrolytic cell walls. As previously mentioned, the scientific literature does not provide enough information on this topic [11]; still, the cell wall temperature varies between 200 and 400°C [12] while the environment surrounding the cell is at ambient temperature. Thus, heat losses such as those due to natural convection and to radiation have a good potential for being converted into useful energy.

1.2 Overall objectives of the research

This research work aims at answering the following question:

Is it possible to increase the energy efficiency of aluminum smelters?

Or, in more detail,

Can the thermal wastes of the pot sidewalls be recovered? If the answer to this question is affirmative, which technologies are best suited to accomplish this task? Furthermore, is the conversion of the thermal wastes feasible? If so, which energy conversion system should be used?

In order to find the answers to these questions, we propose to undertake a research project which covers the following topics:

1. **To analyze the different sources of heat waste in a typical aluminum plant.** Two main sources of thermal waste have been highlighted, that is, the exhaust and the cell surface heat losses. However, in order to have a better understanding of the

causes of these losses, an analysis of the aluminum production process is required. In this way, it is possible to understand not only the nature of the aforementioned thermal losses, but also the feasibility of either reducing or recovering them.

2. **To estimate the recoverable heat losses.** Once the several waste heat sources in the aluminum production line are determined, another issue arises, that is, recovering them by means of heat exchangers. The problem is not limited to just predict the operation of a heat exchanger placed in a section of the production line where the thermal losses occur. In fact, a mandatory requirement for this component is that it must not affect the aluminum production at all. Thus, the operation of this heat exchanger should not impact the safety level of the aluminum plant. Recovering heat from the exhausts has been widely analyzed because it is accomplished without affecting neither the aluminum production nor the plant safety. An interesting subject that has not been studied yet [11] is the recovery of heat wasted on the electrolysis cell walls. This topic is addressed in this thesis by considering radiative heat exchangers recovering the pot wall wastes. These heat exchangers are worthy of studying because their operation has a small influence on the safety of the plant; therefore, determining the operation of these systems (i.e. how much heat can be recovered as a function of the cell operation) is a fundamental subject of the work presented in this thesis.

3. **To estimate and analyze the recoverable heat.** Once the thermal energy is recovered, it must be converted into other forms of useful energy. Several solutions are available. Most of the works in the open literature proposes to couple the exhausts of the aluminum plant to an ORC engine in order to generate electrical power. It has been shown that it is possible to produce useful power from the exhaust gases, despite their low thermodynamic potential (that is, the low temperature difference between the hot and the cold sources); however, the investment related to an ORC engine is too high and the pay-back time is too long [5, 6]. A similar problem is encountered when the recovered heat is used for district heating; in this case, the issue lies behind the introduction of a network carrying thermal energy, which is challenging on both technical and economic viewpoints. For these reasons, it is necessary to find alternative solutions. In this thesis, we propose to examine the Stirling engine technology, since it is a high-efficiency conversion system for low grade heat. An example of such an engine is the Stirling machine developed by Formosa et al. [13], which could be used for these purposes, since it converts heat from a thermodynamic reservoir at 150°C; its measured efficiency is half that of an ideal Carnot engine working under

the same temperature levels. The interest for these engines is also justified by the fact that they can convert a radiative heat source into into useful energy [14, 15]. According to the author's point of view, this is a safe and convenient way to convert the heat wasted along the aluminum production line; therefore, in the framework of this thesis, a theoretical model able to predict the operation of Stirling engines is outlined.

4. **To evaluate the validity of the proposed solution.** As previously mentioned, few research on the recovery of the thermal wastes of the electrolysis cell sidewalls has been undertaken. Nonetheless, there exists a well-tested technology able to convert these losses into useful work [16]. Indeed, the thermoelectric modules can accomplish this task by turning a temperature gradient into a difference of electrical potential [17]. Then, it is mandatory to show that the solution proposed in this thesis brings a considerable advantage with respect to the use of thermoelectric modules. The nature of this advantage, which may be either thermodynamic or economic, will be discussed throughout this document.

The methodology followed in this thesis to accomplish these objectives is outlined in the following section.

1.3 Proposed methodology

The base of every research project is a detailed review of the scientific literature. In this thesis, the literature review aims to fulfill the following objectives. The first one is to present the Hall-Héroult industrial process by describing the pot (that is, electrolysis reactor where aluminum is produced); then, a detailed mass and energy balance of the pot is carried out from the data found in the open literature. Such analysis allow us to acquire the necessary knowledge about the nature of the electrolysis cell thermal losses. That being said, it is possible to define other objectives of the literature review, which are to identify the technologies able not only to recover but also to convert these energy losses without affecting the safety of the aluminum smelter. Therefore, the interest in the recovery of the losses by radiation and their conversion by means of Stirling engines will be emphasized. The recovery and the conversion of the thermal wastes will be studied in this thesis by following two distinct theoretical approaches.

In order to estimate the thermal losses from the sidewall, a complex heat transfer problem needs to be solved; as it will be described later, the heat transfer modes occurring at the sidewall are: conduction, forced and natural convection, and radiation. All these modes must be considered to evaluate the pot thermal losses. This can be done by solving

a system of Partial Differential Equations (PDE) defining the conservation of physical quantities such as the continuity, momentum and energy. A widely used approach to solve the Navier-Stokes equations (that is, the conservation of both mass and momentum) coupled with the proper energy balance is the Computational Fluid Dynamic (CFD) theory [18–20]. In this way, it is possible to obtain a numerical approximation for the solution of the system of the aforementioned PDEs; thus, the estimation of the radiative heat flux from the sidewall is outlined. Usually, the numerical solution is carried out by using a proper software; in this work, the version 5.0 of OpenFOAM (for "Open source Field Operation And Manipulation") has been used to carry the simulations. OpenFOAM 5.0 is an open-source C++ library of models of the above mentioned (and many other continuous mechanic) equations [21]. These models follow a friendly syntax, making their understanding straightforward for the user. Furthermore, OpenFOAM 5.0 offers utilities for both pre- and post-processing, as well as for parallel and remote computing.

Several factors justify the use of Stirling engine as a safe and low-grade-heat conversion system. For instance, a configuration of a Stirling engine able to generate useful work from solar radiation has been extensively discussed in the literature [22]. Nonetheless, when estimating the rate of conversion of the thermal losses into useful work, manifold difficulties arise. For instance, it is not easy to predict the performance of the engine because it involves several interrelated physical phenomena. Also, a configuration of a Stirling engine converting low grade radiative wastes in industrial plants has never been considered before. The Stirling machine like the one we are proposing (that is, an engine that generates power from the recovered heat) does not exist yet, thus, it needs to be designed and manufactured. How is it possible to justify the fulfillment of such a complex project, if we have no clue about the operation of the proposed engine? We assumed that it is possible to overtake this difficulty by using the electrical analogy theory to model the operation of the engine. The electrical analogy theory is based on the analysis of the conservation equations applied to each component of the engine (power pistons, heat exchangers...); then, by establishing the analogy between the characteristic variables of the engine (i.e. the pressure and the velocity of the working fluid) and those of an electrical circuit (i.e, current intensity and electrical potential difference), an equivalent electrical circuit is written down. Afterwards, the variations of the current and electrical potential drop in the circuit are equivalent to those of the velocity and pressure differentials in the engine. The electrical circuit obtained from this theory is a powerful tool because it predicts the behaviour of any type of Stirling engine of any dimension (because it is based on the conservation equations applied to components present in the Stirling engine).

Moreover, the prediction of the complex operation of these engines becomes easier since it is reduced to the analysis of an electrical circuit [23].

1.4 Plan of the thesis

In this document, the research undertaken within the framework of this doctorate will be outlined. Chapter 2 is consecrated to the review of the literature of this research project. Thus, as previously mentioned, an analysis of the electrolysis cell is performed in order to identify the technologies able to recover and convert the pot thermal wastes. The most important contributions of this research are presented in Chapters 3 and 4. These chapters list two peer-reviewed articles, that is, "Proof of concept to recover thermal wastes from aluminum electrolysis cells using Stirling engines" and "Modeling the dynamic and thermodynamic operation of Stirling engines by means of an equivalent electrical circuit", both published in Energy Conversion and Management. In these articles, the topics of the recovery and conversion are separately treated. The coupling of these two distinct research subjects and a preliminary economic analysis of the investment of the proposed solution are the main topics of Chapter 5. Finally, the concluding remarks of this thesis and the future perspectives of this research are listed in Chapters 6 and 7, redacted in both French and English, respectively.

CHAPTER 2

LITERATURE REVIEW AND OBJECTIVES OF THE THESIS

In this chapter, the literature review of the topics listed in the previous chapter will be presented. Section 2.1 is an overview of the aluminum production process; it will be explained how to produce aluminum by electrolysis. Thereafter, the recovery of the main sources of heat losses during the aluminum production process will be discussed in Section 2.2. Once these sources are examined, the technologies used to convert them into useful work will be outlined in Section 2.3. Based on these considerations, the proposed research project is briefly described in Section 2.4.

2.1 Aluminum production: a general overview

The production of primary aluminum is an extremely energy-intensive process. In order to produce a ton of aluminum, a quantity of energy ranging from 11 and 15 MW h is required; however, almost half of this energy is transferred to the environment under the form of heat [6]. In order to clarify this aspect, it is necessary to understand the industrial process used to produce primary aluminum.

2.1.1 Hall-Héroult process

The only industrial method known to date to produce primary aluminum (that is, aluminum not derived from recycling) is the Hall-Héroult process [24]. This process takes the name from their inventors, Charles Martin Hall [25, 26] and Paul Héroult [7], who independently discovered the procedure to make aluminum by means of electrolysis.
Electrolysis is an electrochemical process in which non-spontaneous chemical reactions occur. In the Hall-Héroult process, the reactants are alumina (Al_2O_3) and graphite, while the products are aluminum and carbon dioxide, according to the overall reaction:

$$Al_2O_3 + \frac{3}{2}C \longrightarrow 2\,Al + \frac{3}{2}CO_2 \qquad (R\,1)$$

A general sketch of the Hall-Héroult electrolytic cell (the reactor where electrolysis occurs) is shown in Figure 2.1. The role of the electrolyte is performed by melted cryolite

(Na_3AlF_6). Cryolite is a mineral that can be found in nature; however, most of the cryolite mines are exhausted. Hence, nowadays cryolite is synthetically produced in industrial plants according to the overall reaction [24]:

$$6\,HF + 2NaOH + NaAlO_2 \longrightarrow Na_3AlF_6 + 4\,H_2O \qquad (R\,2)$$

The cryolitic bath is continuously fed with alumina; in this way, the dissociation of this oxide into Al^{3+} and O^{2-} takes place. Once a difference of electrochemical potential is applied to the two electrodes, Reaction R 1 occurs. The oxygen ions migrate towards the surface of the anode[1] where graphite is oxidized according to the following reaction:

$$2\,O^{2-} + C \longrightarrow CO_2 + 4\,e^- \qquad (R\,3)$$

Instead, the aluminum ions migrate to the cathode (the positive electrode) which is made of carbon coke; here, the aluminum ions are reduced according to the following reaction:

$$Al^{3+} + 3\,e^- \longrightarrow Al \qquad (R\,4)$$

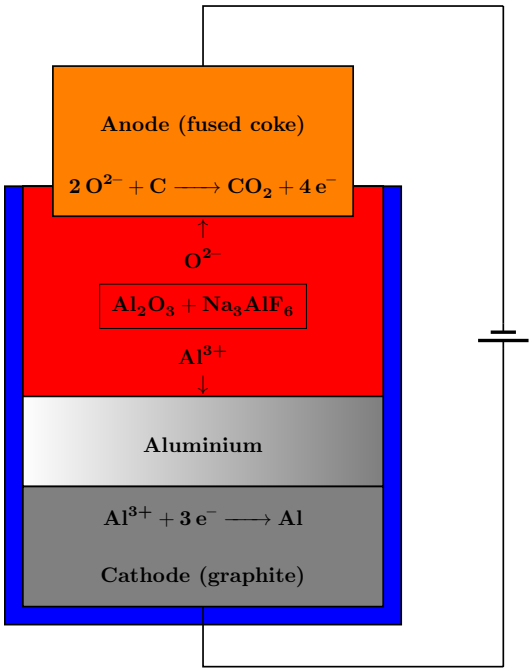

Figure 2.1 Sketch of the electrolysis cell used to produce aluminum at industrial scale.

[1]The anode of the electrolysis cell is made from a mixture of petroleum coke, coal tar pitch and previously used anode residuals (also known as butts) [24].

Once the melted aluminum is electrodeposited at the bottom of the electrolytic cell (or rather, at the cathode surface), it is possible to spill it out of the cell and to send it to the foundries, where it will be subjected to further thermomechanical operations.
From the process described above, the mass and the energy balance can be performed to a control volume of electrolysis cell (Figure 2.1). The material inputs are the reactants of Reaction R 1, while the outputs are the products of the aforementioned reaction. Therefore, in order to produce one ton of aluminum, the cell should be fed with 0.33 t of graphite and 1.89 t of alumina [24]; also, the production of 1.22 t of carbon dioxide is observed. According to this mass balance, the energy required for Reaction R 1 can be estimated (recall that this reaction is endothermic); this value is equal to the enthalpy of the reaction, that is, about 6 MWh/t_{Al} (see Appendix A) [27] .
The mass and the energy balances performed to the electrolytic cell of Figure 2.1 represent a strong simplification of the industrial Hall-Héroult process. More details about the actual production of aluminum should be listed. These details will be presented below in order to estimate the real mass and energy flows across the cell control volume. This is a fundamental aspect necessary to understand the thermal waste due to the aluminum production.

2.1.2 Mass balance of the electrolysis cell

Figure 2.2 shows the electrolysis-cell control volume, where the red-dashed line defines its boundaries, as proposed by Gusberti et al. [28]. According to Reaction R 1, the only materials crossing the aforementioned control volume boundaries are be alumina (i.e. the input), aluminum and dioxide carbon (i.e. the outputs). However, as shown in Figure 2.2, there are other chemical species flowing through the control volume. In the following paragraphs, these species (and their effects on the cell operation) will be listed.
As previously mentioned, in order to produce one ton of aluminum, the electrolytic bath

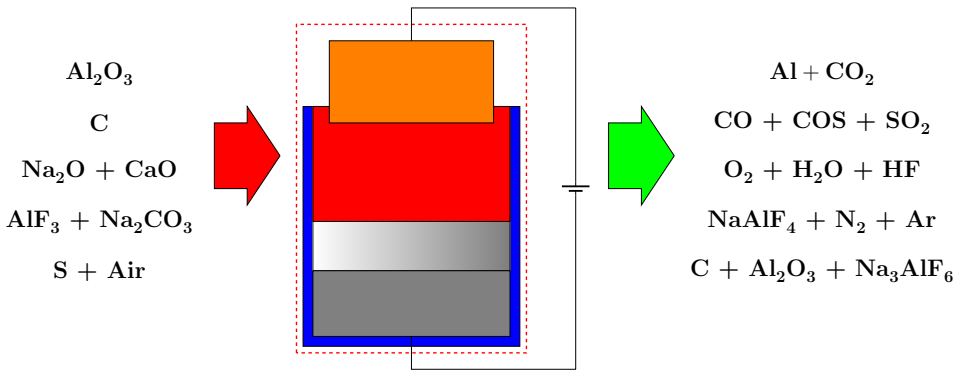

Figure 2.2 Relevant materials flowing through the cell control volume.

must be fed with 1.89 t of alumina; however, this is an estimation and the real value for alumina feeding is different. Several reasons can explain this aspect.

- The alumina entering in the cell brings some impurities. Since the alumina has a degree of purity of about 98%, the actual alumina feeding should increase; thus, accordingly, 1.93 t/t_{Al} are required [24, 28].
- Part of the produced aluminum can react with the carbon dioxide, according to the following reaction:

$$3\,CO_2 + 2\,Al \longrightarrow Al_2O_3 + 3\,CO \tag{R 5}$$

  The occurrence of this reaction decreases the need of alumina in the bath (as it will be seen in the following paragraphs, this is not the only reaction taking place in the bath and producing alumina).
- In modern cells, a layer of solid alumina (usually called crust) covers the electrolytic bath [16]. During some routine operations, such as aluminum tapping and anode replacement, this layer breaks and its fragments may fall into the bath[2]. This event changes the concentration of alumina in the bath, which should be between 2 and 4% in mass [24].

All these aspects must be taken into account to predict the required alumina feeding. This is not an easy task, since the occurrence of the events listed above is quite complex.
The actual rate of consumption of carbon is different than its stoichiometric value which is 0.33 t/t_{Al}. Effectively, a portion of the anode material is not used. On the one hand, it is lost to the environment under the form of dusts. On the other hand, it may react with the oxygen and the carbon dioxide:

$$C + O_2 \longrightarrow CO_2 \tag{R 6}$$

$$C + CO_2 \longrightarrow 2\,CO \tag{R 7}$$

$$2\,CO + O_2 \longrightarrow 2\,CO_2 \tag{R 8}$$

Also, traces of sulfur (1.5-3% in volume) are present in the carbon anode. The sulfur is undesired, since it reacts with the alumina and the graphite of the anode to give carbonyl

[2]For instance, Figure 2.4a presented in the following section shows an operator breaking this layer.

sulfide:

$$3\,C + Al_2O_3 + 3\,S \longrightarrow 2\,Al + 3\,OCS \tag{R 9}$$

$$2\,COS + 3\,O_2 \longrightarrow 2\,CO_2 + 2\,SO_2 \tag{R 10}$$

The graphite of the anode is continuously consumed to produce aluminium (Reaction R 1); therefore, the anode must be replaced once each month [4, 24]. During this routine operation, the cell is open, allowing the surrounding air to enter into the cell (the pressure inside the cell is lower than the atmospheric one). Therefore, another input should be considered, that is, the air; its chemical composition, except for the presence of moisture, is inert. In fact, the water molecules reacts with fluorides in the bath (see below), thus:

$$2\,AlF_3 + 3\,H_2O \longrightarrow Al_2O_3 + 6\,HF \tag{R 11}$$

$$Na_3AlF_6 + 2\,AlF_3 \longrightarrow 3\,NaAlF_4 \tag{R 12}$$

$$3\,NaAlF_4 + 3\,H_2O \longrightarrow Al_2O_3 + Na_3AlF_6 + 6\,HF \tag{R 13}$$

The effects of the impurities (that is, chemical compounds not participating to the production of aluminum) should be mentioned as well. These are introduced through operation correcting the bath chemistry under the form of Na_2O, CaO, AlF_3 and H_2O. In order to control any effects due to Na_2O and CaO, AlF_3 is added in the bath. The fluorides react with the impurities according to the following reactions:

$$3\,Na_2O + 4\,AlF_3 \longrightarrow 2\,Na_3AlF_6 + Al_2O_3 \tag{R 14}$$

and

$$3\,CaO + 2\,AlF_3 \longrightarrow 3\,CaF_2 + Al_2O_3 \tag{R 15}$$

In Reaction R 15, the formation of calcium fluoride is accepted (and in some cases, promoted), since it decreases the melting point of the cryolite from 1011°C to 960°C. However, the fluorides concentration should be lower than 10-13% in volume; thus, sodium carbonate is added to the bath [24, 28]:

$$4\,AlF_3 + 3\,Na_2CO_3 \longrightarrow 2Na_3AlF_6 + Al_2O_3 + 3\,CO_2 \tag{R 16}$$

It is paramount to monitor the occurrence of all these reactions (and the effects of these on the cell operation) whose rates range between few minutes to several days [29]. Despite

its importance, it should be recalled that performing such a monitoring is a complex task. The most important output is aluminum; its amount is predicted by the Faraday's law of electrolysis: the amount of produced aluminum is directly proportional to the cell electrical current [30]. Furthermore, gaseous species leave the cell under the form of CO_2 (not only due to Reaction R 1, but also to Reactions R 6, R 8, R 10 andR 16), CO (Reactions R 5 and R 7), OCS (Reaction R 9), SO_2 (Reaction R 10), HF (Reactions R 11 and R 13), $NaAlF_4$ (Reaction R 12), O_2, N_2, H_2O and Ar (dues to the inert air). Other material outputs are graphite (anode replacement), cryolite and alumina (bath cleaning).

2.1.3 Electrolysis cell energy balance

Following the procedure presented by Gusberti et al. [28], the first law of Thermodynamic is applied to the control volume defined in Figure 2.3. In other words, the difference between the power entering and leaving the control volume must equal the accumulated energy rate [31]. A relevant input is the electric power due to the electrical potential and current applied to the electrodes, while a loss of heat occurs throughout the boundaries (e.g. thermal resistances between the inner bath at 960°C and the outer air at room temperature). In order to perform the energy balance, it is required to know the enthalpies of each specie crossing the control volume, as well as the flow rates evaluated from the mass balance. Obviously, at steady-state conditions, the rate of accumulated energy is null, while it is different from zero at transient conditions, that is, during the operating practices (for instance, aluminum tapping or any other operation in which the cell is open). Therefore, it can be stated:

$$\left.\frac{\mathrm{d}E}{\mathrm{d}t}\right|_{CV} = V_{cell}I + \sum \dot{m}_{in}\left[\overline{h}_f^o + \overline{h}\left(T_p\right) - \overline{h}^o\right]_{in} - \sum \dot{m}_{out}\left[\overline{h}_f^o + \overline{h}\left(T_p\right) - \overline{h}^o\right]_{out} - \dot{Q}_{loss} \quad (1)$$

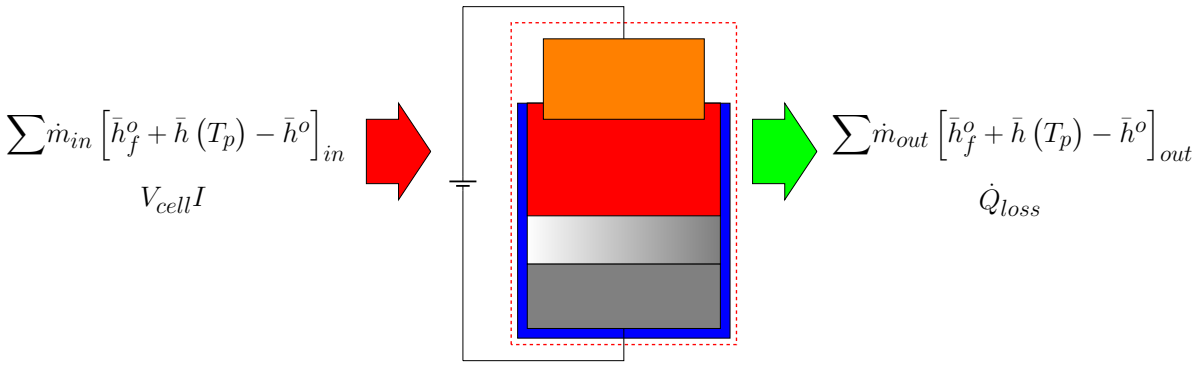

Figure 2.3 Relevant energy flows through the cell control volume.

where $\frac{\mathrm{d}E}{\mathrm{d}t}\big|_{CV}$ is the rate of accumulated energy within the control volume (W), V_{cell} is the cell electrical-potential difference (V), I is the current intensity (A), $\dot{m}$ is the mass flow rate ($\mathrm{kg\,s^{-1}}$), $\overline{h}_f^o$ is the formation enthalpy of the chemical compound ($\mathrm{J\,kg^{-1}}$), $\overline{h}\,(T_p) - \overline{h}^o$ is the enthalpy contribution due to the temperature T_p (which is null when T_p is equal to the ambient temperature) and $\dot{Q}_{loss}$ represents the thermal-power losses (W) [28, 31]. Each term of Equation 1 should be studied.

The power required to perform the reactions listed in the previous section enters the cell under the form of electricity. Modern cells work with a potential difference V_{cell} of 4-4.5 V and an electrical current I ranging from 300 to 600 kA [24]. Therefore, each cell requires around 2 $\mathrm{MW_{el}}$. Thus, as already said elsewhere in this document, the input energy is about 11 to 15 $\mathrm{MWh/t_{Al}}$.

For the sake of clarity, both input and output enthalpies in Equation 1 will be analyzed together; this is done by introducing the rate of enthalpy contribution $\Delta\dot{H}$, defined as [28]:

$$\Delta\dot{H} = \sum \dot{m}_{in}\left[\overline{h}_f^o + \overline{h}\,(T_p) - \overline{h}^o\right]_{in} - \sum \dot{m}_{out}\left[\overline{h}_f^o + \overline{h}\,(T_p) - \overline{h}^o\right]_{out} \tag{2}$$

The rate of enthalpy contribution (W) represents the net power to perform both endothermic and exothermic reactions. This term could be assumed approximately constant (even though the flow rates $\dot{m}$ are not constant). Then, the energy required to heat the reactants (alumina and the cathode graphite) and to perform Reaction R 1 is accordingly 6 $\mathrm{MWh/t_{Al}}$, while the secondary reactions absorb between 0.6 and 3 $\mathrm{MWh/t_{Al}}$ [28, 32].

The term $\dot{Q}_{loss}$ in Equation 1 takes into account all the heat losses due to the operation of the cell. This term depends on four procedures required to assure the sustaining of the industrial Hell-Héroult process.

1. Aluminum tapping (that is, collection of produced aluminum);
2. Bath correction (that is, introduction of all those chemical species listed in Section 2.1.2 causing the occurrence of reactions not producing aluminum, see Figure 2.4a);
3. Anode and cathode replacement (that is, substitution of consumed anodes and/or cathodes, see Figure 2.4b);
4. Bath cleaning.

These operations are the main cause of heat losses. Moreover, they do not occur simultaneously[3], making the overall heat lost by the cell time-dependent. However, why this heat

[3]For instance, aluminum tapping is performed daily, while anode change occurs once each 25-30 days.

(a) (b)

Figure 2.4 Photos of typical cell operations: (a) introduction of bath corrections; (b) anode change.

loss occurs? Most of these operations can be accomplished only by opening the cell. Then, on the one hand, during these operation, it is mandatory to keep the cell at the operation temperature (in order to do that, 0.38 MWh/t_{Al} are needed). On the other, it should be recalled that the pressure in the cell is lower than the atmospheric one; therefore, when the cell is open, ambient air enters into it. Once the cell is closed, the air is trapped into the gas collection cover (which is usually called hooding, Figure 2.5a). As a consequence, the inert air is responsible for absorbing about 2-3 MWh/t_{Al}. Moreover, two other phenomena of thermal loss should be included in the $\dot{Q}_{loss}$ term.

- The thermal dissipation due to the Joule effect in the the electrical connections of the electrodes (bus bars in Figure 2.5a), and
- The heat transfer phenomena that occur at shell walls and superstructure (that is, the gas collection cover).

The bus bars are responsible of the loss of 0.5-1 MWh/t_{Al}. The heat transfer phenomena are more difficult to estimate as the three transfer modes, that is, conduction, convection and radiation, occurs simultaneously on the cell shell. Amongst these modes, convection is particularly important; in order to avoid too-high temperatures in the electrolytic bath, a convective flux of ambient air flows along the cell walls [33].
According to Gusberti et al. [28] and to Zhao [34], the shell heat transfer losses ($\dot{Q}_{loss\,ht}$) can be expressed as the ratio between the temperature difference of the cell bath and the outer air and a thermal resistance R_{th}:

$$\dot{Q}_{loss\,ht} = \frac{T_{bath} - T_{room}}{R_{th}} \tag{3}$$

To evaluate this thermal resistance, it is necessary to know the geometry of the cell and the thermophysical properties of the materials. A sketch representing a modern cell geometry is shown in Figure 2.5a [27]. The thermal resistance can be estimated either by developing simple (but approximated) analytical models, such as proposed by Gusberti et al. [28] and by Zhao [34], or by carrying time-consuming (but more reliable) CFD simulations, as shown in Figure 2.5b [35]. Therefore, the selection of such methods helps to predict the thermal losses. They can be applied to the hooding (i.e. superstructure) of the cell (0.5-1 MW/t_{Al}) [28], where the difference between the cell temperature and that of the air is small. However, at the level of the cathode block, the temperature may reach values as high as 400°C [12]. It is obvious that at these locations of the cell, the heat transfer phenomena are so important that some form of external cooling is required; then, the consequent thermal losses amount to about 2 to 3 MWh/t_{Al} [28, 32].

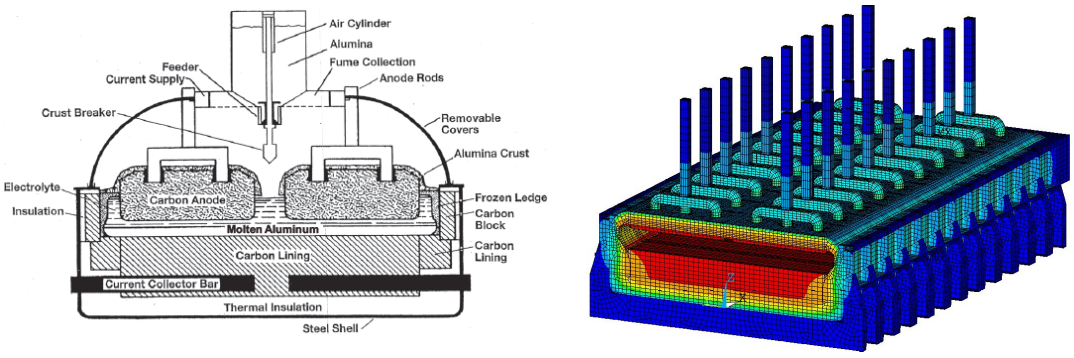

(a) (b)

Figure 2.5 (a) Inner geometry of a modern electrolysis cell [27] and (b) thermal simulation of a 500 kA cell [35].

2.2 Recovery of the thermal wastes in the aluminum production industry

The data mentioned in the previous section come from the pot energy balances available in the open literature; therefore, it is interesting to present and mostly to compare the results given in these studies. That being said, three works [4, 28, 32] are discussed. In these works, the energy balance has been performed for the following cell technologies:

- Gusberti et al. [28] have analyzed two cells having different efficiency[4], the first one absorbing 14.88 MWh/t_{Al}, and the second requiring 12.96 MWh/t_{Al};

[4]The efficiency of the cell is defined as the ratio of the energy used to produce aluminum and that required to operate the cell.

- Nowicki et al. [32] have applied the energy balance to a 13 MWh/t_{Al} cell;
- Fleer et al. [4] have presented an analysis of the thermal losses for a 14.7 MWh/t_{Al} cell.

The results of these studies are presented under the form of pie chart in Figure 2.6. It can be observed that almost half of the input energy is required to produce aluminum. However, notable differences between these studies can be observed. For instance, according to Nowicki et al. [32], the energy absorbed by secondary reactions is four times higher than those given in other studies. The energy demand to heat the cell gases varies between 10 and 23% of the input energy. The electrical bus bar and gas collection cover losses differ slightly in the these works. The shell heat losses are remarkable in all studies (24-27%), expect for Nowicki et al. [32], where these losses are estimated to be only the 8% of the input energy.
From Figure 2.6, one can investigate if it is possible to decrease the aluminum-production energy demand. In order to provide a satisfactory answer to this question, the approach followed by Gusberti et al. is vey useful. According to this work, three types of energy contribution should be defined [28].

- The energy required to produce aluminum: it is the electrochemical energy required by the endothermic Reaction R 1. Therefore, it is assumed to be **unavoidable**.
- The energy required to perform the secondary reactions: this contribution is considered **variable**. The occurrence of secondary reactions depends on random variables, as the degree of purity of the input materials and the effectiveness of the bath operations (e.g. addition of fluorides compounds and alumina in the bath). This contribution takes into account not only the enthalpy of reaction of the secondary reactions, but also (i) the thermal energy needed to heat the reactants of the sec-

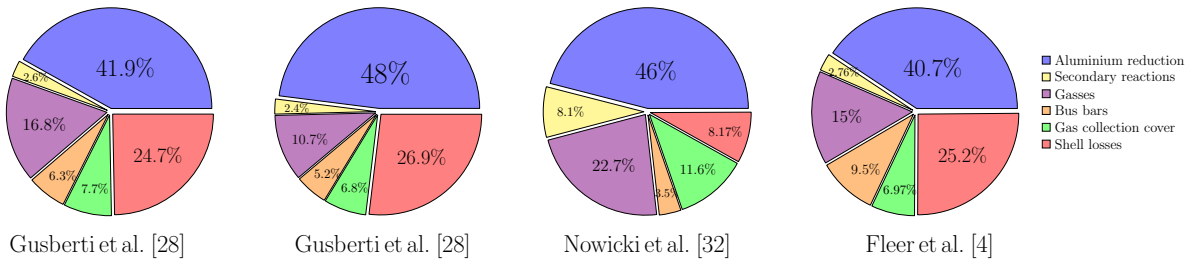

Figure 2.6 Electrolysis cell energy balances from three studies found in the scientific literature.

ondary reactions and (ii) the thermal losses due to the heating of the gases entering the cell when these operations are performed (Figure 2.4a).

- The energy losses of the process: as previously mentioned, thermal wastes occur due to the dissipation of energy by Joule effect in the electrical busbar and by the heat transferred across the cell sidewall; this energy contribution is completely **dissipated**.

It is obvious that decreasing the unavoidable contribution has the effect of reducing the aluminum production. The reduction of the variable energy contribution can be achieved by improving the effectiveness of the bath corrections and by decreasing the time spent during open-cell practices (e.g. anode change). Nonetheless, the thermal losses due to these mandatory operations cannot be reduced to zero[5]. Then, the contribution of dissipated energy should be studied. Since it is difficult to avoid the electrical bus bars losses, one could think of insulating the cell so that the heat transfer losses decrease. Even though this solution seems logical, it cannot be considered. It should be recalled that a layer of cryolite (called side or frozen ledge, see Figure 2.5a) is solidified at the inner walls of the cell. This layer is fundamental as it protects the refractory materials of the cell. Then, its thickness is a parameter to be controlled; when this layer becomes too thin or even absent (that is, when the cell is thermally insulated), liquid cryolite can attack the refractory materials of which the inner walls of the pot are made, causing its failure [33]. However, if this layer becomes too thick (that is, when the cell is excessively cooled), the chemical reduction of aluminum is affected [16].
The considerations listed above clarify how hard is to decrease the pot energy demand. Even though, it seems quite difficult to lower this demand, two aspects should be highlighted.

- As previously mentioned, the variable energy contribution is impossible to cancel. This is mainly due to the cell mandatory correcting operations which are responsible for the production of hot gases. Nowadays, these gases are released to the environment at relatively high temperature [4, 5].

- An adequate cooling of the cell is essential for its operation (recall that the cell wall temperature ranges between 200°C and 400°C) [24, 37]. In modern cells, this cooling is performed by forced convection; a stream of cold air flows alongside the pot sidewall in order to reduce its temperature [33].

[5]Unless inert anodes are introduced in the cell [36].

Hence, the production of aluminum causes the creation of thermal wastes; these are the release of gases heated in the cell and the thermal power due to convective cooling. These outputs cannot be canceled out, since they are the result of practices preserving the cell operation. However, these losses represent a large part of the input energy, as it is shown in Figure 2.6. This is further outlined in Table 2.1, which lists the mean and the standard error deviation of of the data found in the aforementioned four studies. Even though the standard error deviation of some energy distributions is considerably high (i.e. secondary reactions or shell losses), this table shows that almost 47% of input power is lost under the form of heat. These losses must be investigated to determine if it is possible to recover them and consequently convert them into useful power. Consequently, the most suitable heat exchangers to recover (i) the exhaust heat losses (Section 2.2.1) and (ii) the surface heat flux through the cell walls (Section 2.2.2) will be considered in the following sections.

Table 2.1 Statistical analysis of energy distributions (data from Figure 2.6).

	Mean of input energy [%]	Standard error deviation [%]
Aluminum reduction	44.2	± 3.4
Secondary reactions	4.0	±2.8
Gases	16.3	±5.0
Bus bar	6.1	±2.5
Gas collection cover	8.3	±2.3
Shell losses	21.2	±8.8

2.2.1 Recovery of exhaust heat loss

Fleer et al. [4] and Lostec and Nasreddine [5] have analyzed the solutions to recover the thermal loss of the exhausts produced in the pot. Their main idea is to use a heat exchanger so that the gases transfer heat to a secondary fluid. Depending on the phase of this fluid, two exchanger configurations are available. The exhausts can transfer heat to a liquid without phase change; this fluid could be water to be sent to other locations whereby thermal energy is needed (i.e. for space or district heating). Another solution consists in transferring heat from the gases to a phase-changing working fluid; because of the low evaporation temperatures, organic fluids are employed for this task. These fluids can be used to store thermal energy; furthermore, the produced vapour could be sent to the turbine of an organic Rankine or a Kalina engine in order to generate electrical power [8].

It is interesting to provide some examples where the smelter exhausts are used for district heating (the ORC engine technology will be discussed in Section 2.3.1). In Norway, the

exhaust waste heat of the Norsk Hydro® Sundal smelter is currently used to cover the heating needs of the nearby town of Sunndalsøra. This technology is also implemented in the municipality of Høyanger, 400 km south of Sunndalsøra, where the Norsk Hydro® Høyanger smelter is present [4]. The residual exhaust heat for the plant in Sunndalsøra is 340 MW_{th}, while this value for the Høyanger plant is 87 MW_{th} [38]; then, two water loops are currently bringing 6 MW_{th} and 4.2 MW_{th} to the citizens of Sunndalsøra (4,030 habitants) and Høyanger (4,190 habitants), respectively. This technology has been considered by Fleer et al. [4], who analyzed the town of Akranes, in Iceland. Nowadays, hot water is brought to the 7,000 habitants of this town by means of the Deildartunguhver hot springs, located 62 km north of Akranes. Nonetheless, the Nordural® aluminum smelting plant is only 17 km away from Akranes; the exhaust thermal wastes account for about 90 MW_{th}. Afterwards, this source is more than sufficient to stock energy at 77°C and to provide water at 72°C to the inhabitants of Akranes [4]. In addition, for this case, district heating becomes particularly interesting as the required storage tank is already available in this town. Figure 2.7 shows the scheme proposed by Fleer et al. [4].

According to the author, the district heating could be implemented to a smaller extent in Alma, QC; the mass flow rate of the exhausts of the nearby Rio Tinto plant (Figure 1.1) is 450 $kg\,s^{-1}$ and the mean gas temperature over the year is 110°C. Then, 11.36 MW_{th}

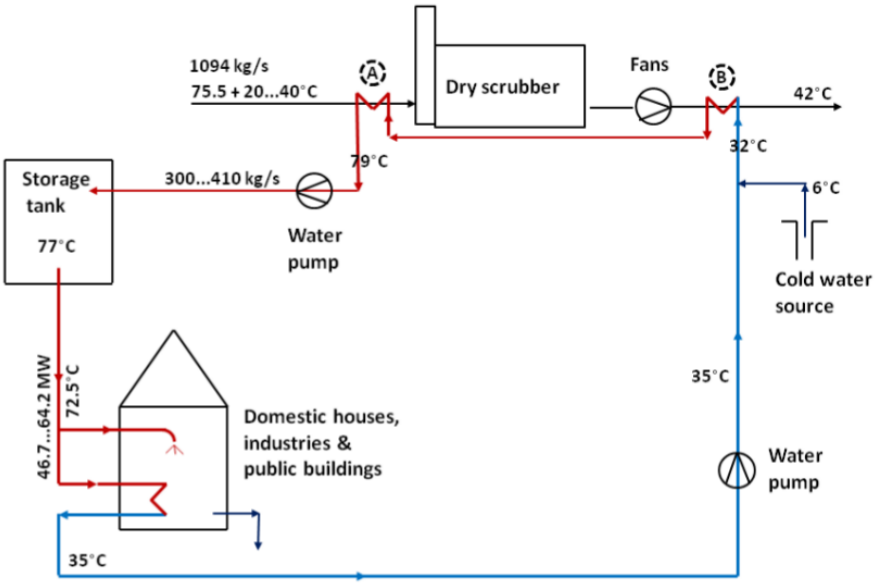

Figure 2.7 District heating scheme for the town of Akranes, proposed by Fleer et al. [4].

® Norsk Hydro is a registered trademark.
® Nordural Hydro is a registered trademark.

could be recovered [5]; comparing this value to those of the aforementioned plants and recalling that the population of Alma is of 30,000 habitants, the exhaust wastes could be used to supply heat only to a small part of the town. Thus, the recovered heat should be used for other purposes, such as greenhouse heating, fish farming, soil heating, snow melting or power generation by means of ORC engines [4, 5].

2.2.2 Thermal recovery of heat flux through the walls of electrolytic cells

A detailed analysis of the thermal losses occurring in the aluminum production line cannot neglect the temperature difference that exists between the cell walls and the surrounding (i.e. air). As previously said, the wall surface can reach a temperature ranging between 200°C and 400°C [12], while the surrounding air is at about 20°C. If the pot wall reaches too-high temperatures, forced convection is used to cool down the walls to preserve the electrolysis process. Moreover, other heat transfer modes can be considered, such as thermal radiation [6, 28]. Both convection and radiation can be studied in the context of thermal waste recovery and depending on the specific transfer mode, a proper analysis of the heat exchanger design must be implemented. Despite the importance of these heat transfer processes, there is a lack of works about heat recovery either by convection or radiation.

a) Convection heat transfer

As it has been previously mentioned, the necessary cell cooling process is performed by means of a stream of cold air. The external air enters into the pot room by opening the windows of the aluminum smelter. In this way, the cell walls transfer heat to the air by convection. Once the air is heated, buoyancy forces let it go to the top of the pot room and finally leave the smelter. This is clearly shown in Figure 2.8a, where the cooling-air flow in a pot room was predicted by means of a CFD study found in the literature [34]. Implementing such methodology may not allow a proper and precise control of the thickness of the solified cryolite (commonly called frozen or side ledge, see Figure 2.5a) when it gets too thick (see Figure 2.5a). In this case, localized cooling is required. It is possible to use air-jet nozzles in order to perform this task, as proposed by Bos et al. [33]. This technology is presented in Figure 2.8b. A pipe system (denoted by the numbers 20 to 24 in Figure 2.8b) is installed under the pot to cool the sidewall by means of the jets (denoted by the number 27 in Figure 2.8b). Then, the cooling can be easily controlled by either regulating the valves (denoted by the number 14 in Figure 2.8b) or by varying the jet inclination [33]. Similarly to the previous cooling strategy, once the cooling air is heated,

it is simply released to the environment.

It is obvious that these procedures are not energy-efficient because these are responsible of the important thermal energy waste. For this reason, Namboothiri et al. [37] have proposed to control these thermal losses by designing a heat exchanger to be attached on the sidewalls. A simplified sketch of this exchanger is presented in Figure 2.9, where a flow of compressed air is used to cool the walls. This system has been designed not necessarily to recover wasted heat but to assure the proper temperature of the refractory materials of the electrolytic cell. However, as shown in Figure 2.9, the hot air could be collected at the outlet of the heat exchanger so that it can be used for other purposes. Namboothiri et al. [37] did not only to verify the effectiveness of this technique, but also performed an economic analysis. The benefits are evident, since the payback time due to the introduction of these heat exchangers does not exceed two years. Moreover, the use of these systems can increase the effectiveness of the cell (which is strongly dependent on the bath temperature), which turns into an increment of the rate of produced aluminum and, consequently, of the incomes for aluminum producers (it is estimated that an improved control of the cell by means of the sidewall heat exchangers can increase the profits of a smelter of abaut 276,000 US$ per year) [37].

Further works describing this kind of heat exchangers have not been found in the scientific literature. As a matter of fact, their implementation and operation can be difficult. These systems may be responsible of an excessive reduction of the wall temperature; then, under these conditions, the layer of the frozen cryolite in the cell may increase its thickness, affecting the electrolysis process. As previously mentioned, this scenario is highly dangerous, not only for the operation of one cell, but also for the entire potline. Indeed, as in a typical aluminium smelter, between 100 and 400 cells are interconnected in series. According to the author, this is the main reason explaining the lack of works similar to

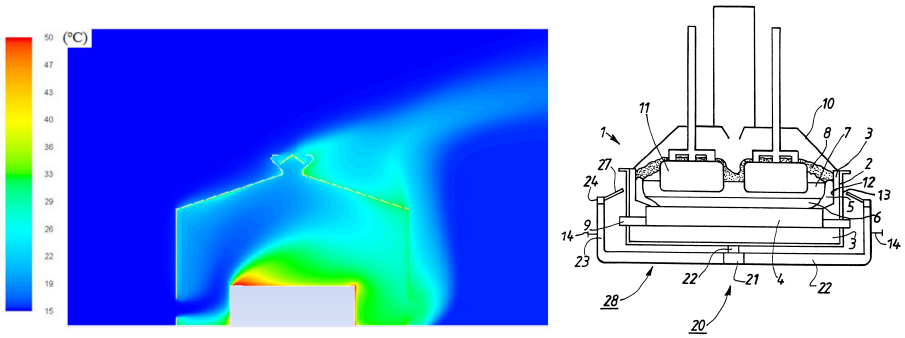

(a) (b)

Figure 2.8 Pot cooling strategies: (a) flow of external air cooling the pot evaluated by means of CFD [34]; (b) scheme of localized jet cooling [33].

the one published by Namboothiri et al. [37] in the scientific literature.
Finally, we mention that estimating the heat that is actually transferred from the cell sidewalls by convection is not an easy task; in fact, convective cooling strongly depends on the operation of the cell and on the cooling strategy (i.e. air nozzles rather than sidewall heat exchangers). In order to provide such an estimation, the measured data found in the literature could be useful. However, as it is shown in Figure 2.6, they do not provide a unequivocal answer to this problem. Moreover, the available data of the heat rejected by the sidewalls are not a measure of the cooling due to convection alone, but rather to a more complex combination of convection and radiation. To date, the role of radiation heat transfer from the pot has not been studied yet. This is the reason why, the topic of thermal radiation from the pot sidewall will be addressed in the following section.

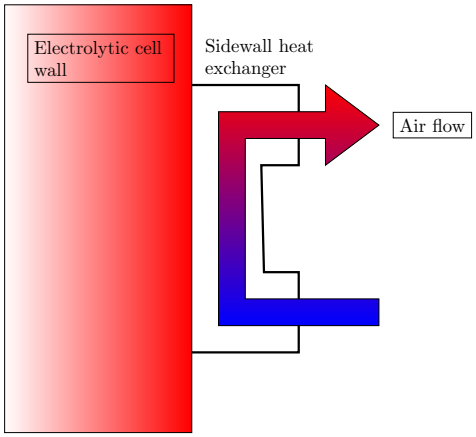

Figure 2.9 Sketch of a sidewall heat exchanger.

b) Radiation heat transfer

An important heat transfer mechanism which takes place at the cell walls is radiation heat transfer. Hence, the cell walls do not only transfer thermal power to the surrounding air by convection, but also towards the pot room walls by radiation. From the theory, it is well known that the heat flux exchanged due to this mode is a function of several variables, including the difference of the forth powers of the wall temperatures [39, 40]. Therefore, due to the temperature difference between the pot and the environment, this heat transfer mode should be taken into account as well.
Even though convection heat transfer from the walls of the cell has been slightly analyzed in the open literature, the thermal radiation heat transfer in aluminum production facilities has not been considered at all. Only few researchers have recently started to investigate heat waste by radiation in aluminum plants. For instance, Zhao [34] has recently proposed a modelling approach to compare the importance of natural convection and

thermal radiation heat transfer in aluminum plants; however, the possibility of recovering thermal radiation was not considered in this study [34]. Johansson and Söderström [41] have performed a similar study for the steel production industry. They have assumed that the heat radiated by a steel furnace (or from steel casting) could be recovered by using thermophotovoltaic diodes in order to produce electricity. In spite of that, this technology is not described in detail, since it is "still under development and not yet commercially available" [41]. Nonetheless, they have suggested that this is a promising technology, since at least 4% of the thermal energy needed to produce steel could be recovered by means of these conversion systems [41].

Johansson and Söderström have analyzed radiative energy losses in the steel production factories. One could investigate if the solution they have proposed (i.e. the installation of thermophotovoltaic diodes to recover radiative losses from casting iron) could be implemented in an aluminum smelter as well. In this section, this analysis is performed by evaluating the radiative power that could be recovered from the sidewalls of the pot. Let us consider an infinitesimal pot-wall surface denoted by $\mathrm{d}\sigma$ (Figure 2.10a) whose temperature is T_σ. From this surface, an infinite number of light rays in likewise infinite directions are emitted. A generic light ray travels through an infinitesimal conical (or solid angle) element $\mathrm{d}\Omega$, having its vertex in $\mathrm{d}\sigma$ and whose direction is (θ, ϕ) (Figure 2.10a). Then, the spectral intensity i'_λ due to this light ray is defined as the rate at which energy is emitted in the direction (θ, ϕ) per unit of projected area normal to the direction $\mathrm{d}\sigma \cos\theta$ per unit of solid angle $\mathrm{d}\Omega$ and per unit of small interval around the wavelength λ[6]. The prime in i'_λ is used to define an intensity emitted in a single direction, while the subscript denotes

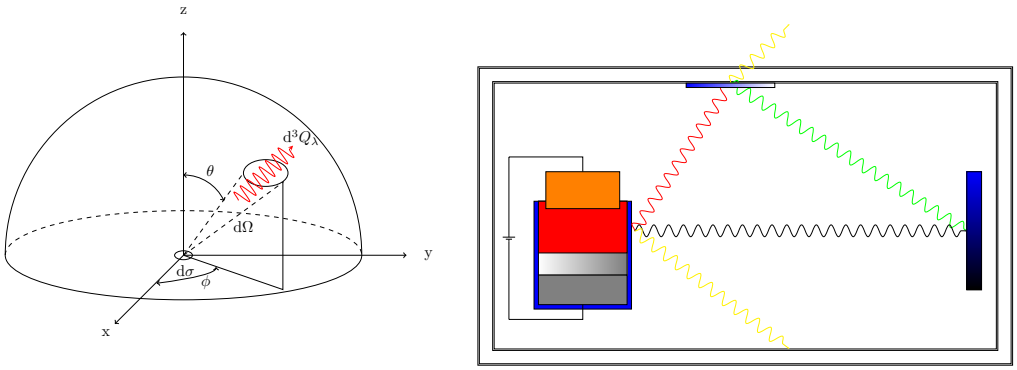

(a) (b)

Figure 2.10 (a) Radiation from an infinitesimal surface $\mathrm{d}\sigma$ in the direction of the conical element $\mathrm{d}\Omega$; (b) infrared light radiation from the walls of a pot (b).

[6]The relationship between wavelength λ and frequency ν for electromagnetic waves is [42]:

$$\lambda \nu = c$$

a spectral quantity; i'_λ is measured in $\mathrm{W\,m^{-3}}$. Then, power $\mathrm{d}^3Q'_\lambda$ (W) leaving the surface $\mathrm{d}\sigma$ at a temperature T_σ in the wavelength interval $\mathrm{d}\lambda$ and reaching the base of the conical element $\mathrm{d}\Omega$ is given by [40]:

$$\mathrm{d}^3Q'_\lambda\left(\lambda,\theta,\phi,T_\sigma\right) = i'_\lambda\left(\lambda,\theta,\phi,T_\sigma\right)\mathrm{d}\sigma\cos\theta\,\mathrm{d}\lambda\,\mathrm{d}\Omega \tag{4}$$

The third differential in $\mathrm{d}^3Q'_\lambda\left(\lambda,\theta,\phi,T_\sigma\right)$ is used to specify that the radiative power is of differential order in wavelength, solid angle and projected area. If the pot wall surface behaves as a black body (i.e. the perfect emitter), its emitted radiative power does not depend on the direction (θ, ϕ). Then, the ratio between the spectral intensity of a real surface i'_λ and that of a black-body $i'_{\lambda,b}$ is called coefficient of *emission* [40]:

$$\varepsilon'_\lambda\left(\lambda,\theta,\phi,T_\sigma\right) = \frac{i'_\lambda\left(\lambda,\theta,\phi,T_\sigma\right)}{i'_{\lambda,b}\left(\lambda,T_\sigma\right)} \tag{5}$$

where $\varepsilon'_\lambda\left(\lambda,\theta,\phi,T_\sigma\right)$ is a function of the wavelength λ (m), direction of Ω (θ and ϕ, rad) and surface temperature T_σ (K). ε'_λ is also called *directional spectral emissivity*; this coefficient is always positive and smaller than one (it is exactly 1 for the black body).
Consider the electrolytic cell in Figure 2.10b; as we can see, the cell radiates a finite quantity of energy through its surface by emitting light rays. So, the total power emitted by the pot walls will be the sum of all energies radiated in every direction given by Equation 4. One can think of introducing a collector, such as the black-and-blue shaded rectangle in Figure 2.10b, to recover this energy. The main question is to evaluate how much energy releaseb by the cell wall will be collected by this surface (i.e. a thermal collector).
A part of the radiation emitted from an infinitesimal area $\mathrm{d}\sigma$ of the electrolytic cell (Figure 2.10b) can hit the collector surface, be recovered and eventually be converted into electricity. However, the amount of thermal power absorbed by the collector is not necessarily equal to the total emitted power (which is given by integrating Equation 4). Indeed, part of this radiation will be also absorbed by the medium through which it passes through. Thus, it can be assumed that the absorbed radiation A is proportional to the path s travelled by the light rays, hence [39]:

$$A \propto s\,\alpha'_\lambda\left(\lambda,\Omega,T\right) \tag{6}$$

where $\alpha'_\lambda\left(\lambda,\Omega,T\right)$ is the coefficient of *absorption* which is also a function of the wavelength λ, direction of Ω and medium temperature T. Similarly to the emission coefficient,

where c is the speed of light ($c = 2.99 \times 10^8\ \mathrm{m\,s^{-1}}$). The range of wavelength where thermal radiation occurs is $10^{-1}\mu\mathrm{m} < \lambda < 10^2\ \mu\mathrm{m}$ [43].

$0 < \alpha'_\lambda < 1$. This contribution is neglected if the medium does not affect the light rays; under these conditions, it is assumed that the medium is not-participating to the radiation phenomenon. For instance, air is a non-participating medium if the concentration of some chemical compounds, including water and carbon dioxide, is low. Another chemical compound that could affect the radiation in the pot room is alumina (Al_2O_3) [40]. However, the concentration of this compound in the aluminum plant shown in Figure 2.10b is lower than 10 ppm. Therefore, it is assumed that the these particles do not participate to the radiation heat transfer in the aluminum plant environment.

The collector under analysis can recover not only direct radiation (i.e. the black rays shown in Figure 2.10b) but also those reflected by the pot room walls. In fact, some radiation emitted by the cell surface could hit the walls of the pot room, as well as its roof and floor. These rays can be absorbed, as well as reflected by (green rays shown in Figure 2.10b) or transmitted to (yellow rays) other surfaces. The percentage of the energy that is reflected by a surface is defined by the coefficient of reflection $\rho'_\lambda(\lambda, \Omega, T)$, while the coefficient of transmission $\tau'_\lambda(\lambda, \Omega, T)$ defines the portion that is transmitted; then, applying an energy balance to the reflecting surface, it can be demonstrated that:

$$[\rho + \tau + \alpha]'_\lambda(\lambda, \Omega, T) = 1 \tag{7}$$

The reflected radiation can hit the thermal collector. The amount of energy absorbed from the reflected radiation and reaching the collector can be enhanced by introducing highly reflecting surfaces (as shown by the white-and-blue shaded rectangle in Figure 2.10b).

The considerations listed above have emphasized that only a part of the radiation leaving the cell walls reaches the collector surface. Furthermore, it has been shown that the rate of transferred heat depends on the coefficients defined by Equations 5, 6 and 7. However, these coefficients are characteristics of the materials under analysis (the coefficients of emission and of absorption should be evaluated for the cell walls and for the collector surfaces as well). This is not sufficient to analyze the radiative phenomena; in fact, it is reasonable to expect an increase of the thermal energy absorbed by the collector if this system has a larger surface, or if it is placed closer to the emitting walls. The introduction of the view factors helps to understand the dependency between the transferred heat and the surface geometry. The view factor F_{ij} is defined as the ratio between the radiation leaving a surface A_i and the radiation intercepted by a surface A_j. It can be shown that [40]:

$$F_{ij} = \frac{1}{A_j} \int_{A_j} \int_{A_i} \frac{\cos\theta_j \cos\theta_i}{\pi R^2} \mathrm{d}A_i \mathrm{d}A_j \tag{8}$$

where θ_j and θ_i represent the angles between the direction of the light ray and the vector normal to the surface A_j and A_i, respectively; R is the distance between the two surfaces A_j and A_i.

The rough description of the thermal radiation phenomena outlined in the previous paragraphs has listed the main variables required to calculate the heat flux in a cavity containing N surfaces. By assuming that the medium in the cavity is non-participating, either the net radiative power of the j-surface $\dot{Q}_j$ or the fourth power of the j-surface temperature T_j^4 can be evaluated by solving the following system of linear equations[7] [40]:

$$\sum_{j=1}^{N} \left(\frac{\delta_{ij}}{\varepsilon_j} - F_{ij} \frac{1-\varepsilon_j}{\varepsilon_j} \right) \frac{\dot{Q}_j}{A_j} = \sum_{j=1}^{N} F_{ij} \sigma \left(T_i^4 - T_j^4 \right) \tag{9}$$

where δ_{ij} is the Kronecker delta defined as $\delta_{ij} = \begin{cases} 1, & \text{if } i = j \\ 0, & \text{if } i \neq j \end{cases}$ and σ is the Stefan-Boltzmann constant ($\sigma = 5.67 \times 10^{-8}\ \mathrm{W\,m^{-2}\,K^{-4}}$). Note that subscript λ and the primes for the coefficient of emission ε have been dropped as these quantities are neither spectral nor directional.

It would be interesting to use Equation 9 to estimate the radiative heat flux from the pot sidewall. To do that a description of the sidewall is required to define a closed cavity (that is, the control volume to which Equation 9 is applied). The left side of Figure 2.11 shows a sketch of an electrolysis cell used to produce aluminum; it can be seen that the pot stands on several supporting beams. Then, an open cavity can be found between each of these two beams and the pot wall. This cavity is indicated by the red ellipse shown in

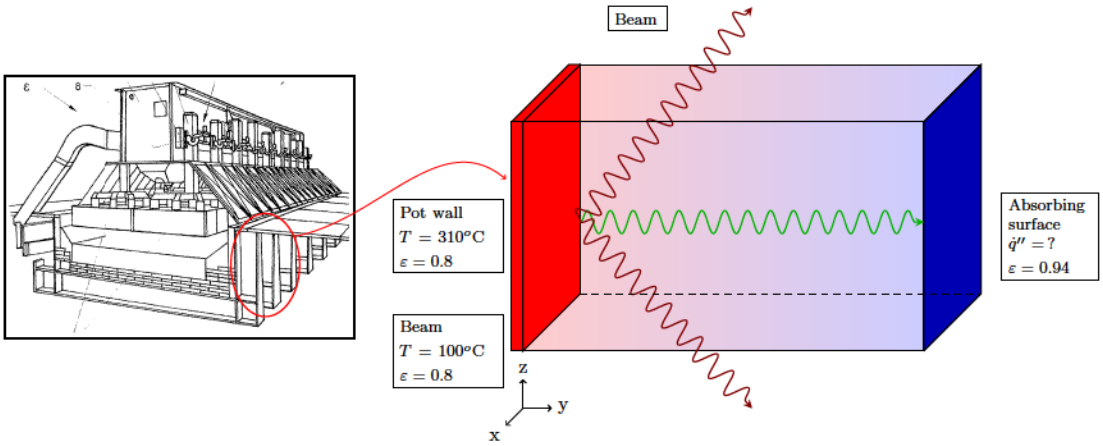

Figure 2.11 Schematic description of the control volume used in Equation 9.

[7] Note that the system of Eqation 9 is linear with respect to either $\dot{Q}_j$ or T_j^4

Figure 2.11 and enlarged in the right side of the same figure. Here, the red surface standing on the xz plane represents the sidewall of the pot, while the violet surfaces represent the inner sides of the supporting beams (these surfaces stand on planes parallel to yz). Then, since our objective is to estimate how much radiative power could be collected, a flat collector (the blue surface shown in Figure 2.11) is introduced. Moreover, the top and bottom surfaces (parallel to the plane xy in Figure 2.11) can be considered as imaginary surfaces required to obtain a closed cavity (it can be assumed that the radiation passing through these surfaces is completely lost).

Equation 9 is applied to the control volume described in the previous paragraph. The dimensions of the different surfaces shown in the sketch in Figure 2.11 are those of a real pot. The view factors are calculated from the formulae available in the literature[8]. It is supposed that the emissivities of the different surfaces is known (the emissivity of the imaginary surfaces is assumed to be 1; in other words, they behave as black surfaces). Moreover, the temperatures of the pot wall and that of the beams are 300°C and 100°C, respectively. The thermodynamic conditions of the collector are not known *a priori*; effectively, either the temperature or the heat flux need to be specified (otherwise, the system of equations is undetermined). For this reason, a parametric study is carried; the heat flux on the collector is determined for different values of its exposed-surface temperatures. The results of this study are plotted in Figure 2.12, where the dependency of the distance between the collector and the sidewall is presented as well.

Figure 2.12 clearly states that as the collector is approached to the sidewall, the radiative heat flux increases; moreover, as the collector temperature increases, the collected heat flux decreases. These results are in agreement with the theory of thermal radiation and with the 1st law of Thermodynamics. Furthermore, this figure shows that a heat flux of at least 1 kWm^{-2} could be recovered by radiation; such a flux is interesting in term of energy conversion, as its temperature is about 100°C. Then, an ideal Carnot engine would convert this heat with a maximal efficiency of about 27%.

Before concluding this section, some limits of the presented parametric study must be recalled. Firstly, the geometry presented in the right side of Figure 2.11 is a simplification of the actual sidewall. Therefore, by using a more realistic geometry, the view factors and consequently the radiative heat flux will change accordingly. Secondly, it is assumed that the temperatures of all the exposed surfaces are constant (which is not necessarily true). Thirdly (and most importantly), the effects due to the air in the control volume have been neglected. On the one hand, it has been assumed that the air behaves as a

[8]The interested reader is referred to Appendix B of reference [40] or to the website http://www.thermalradiation.net/tablecon.html.

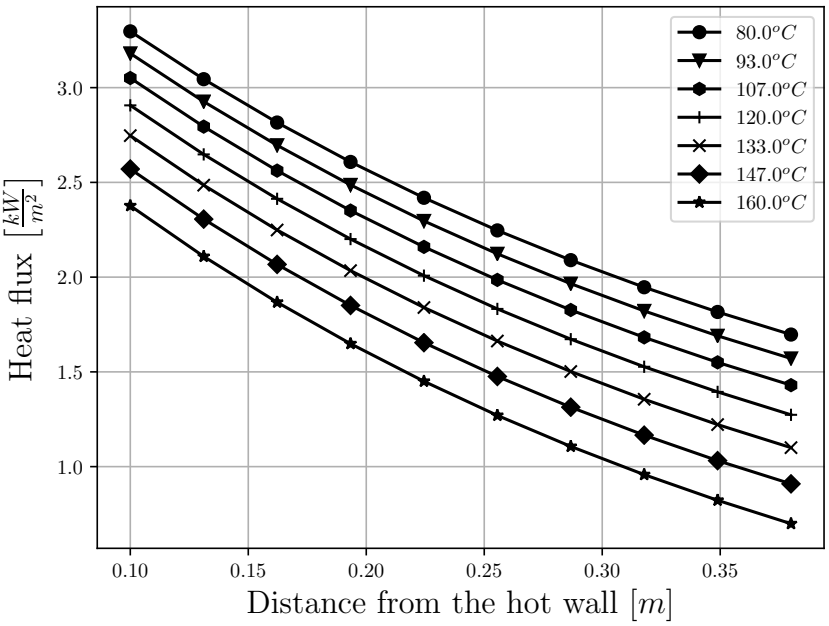

Figure 2.12 Heat flux at the collector as a function of its temperature and distance estimated by Equation 9.

non-participating fluid, that is, the variation of emission, absorption, reflection and transmission coefficients are neglected (which can be considered as an acceptable hypothesis). On the other hand, convective heat transfer cooling is not considered in this study. It is expected that forced convection will affect the temperature of the pot walls and consequently the thermal radiation exchange (and *vice versa*). This means that, in order to estimate the actual radiative energy transport, a different (and more complex) theoretical approach needs to be applied. This topic will be the main subject discussed in Chapter 3. Herewith, it will be described how the CFD theory becomes a necessary tool to estimate the radiative heat flux acting upon a flat thermal collector.

2.3 Conversion of thermal wastes into useful work

The experimental results found in the open literature permitted us to have a rough estimate about the amount of the thermal wastes. The data presented in Table 2.1 compare the different sources of thermal wastes in the aluminum production line; however, it is useless to judge which transport mechanism is most appropriate for their recovery. In order to find a satisfactory answer to this question, the second-principle theory become useful, as it introduces the Carnot factor [31]:

$$\eta_C = 1 - \frac{T_o}{T_s} \tag{10}$$

where T_o is the ambient temperature and T_s is the temperature at which the thermal waste is available. The Carnot factor corresponds to the efficiency of an ideal (i.e. completely reversible) engine working between two sources whose temperature are T_s and T_o[9]; then, from Equation 10, it is possible to evaluate the exergy Ex (J) of a thermal source Q_s (J), which is defined as the energy that can be converted into useful work by means of an ideal system:

$$Ex = \eta_C Q_s \tag{11}$$

Table 2.2 compares the exergies of the various thermal losses shown in Figure 2.6. In order to evaluate the Carnot factor, it will be assumed that the temperature of the gases is equal to 110°C, while that of the pot walls is 300°C; thus, for both cases, $T_o = 20$°C. In Table 2.2, the Carnot factors for both thermal wastes are calculated according to Equation 10; this factor is considerably higher for the cell-wall thermal wastes, since it is almost twice that of the thermal gas wastes. Consequently, according to the data pubblished by Gusberti et al. [28] and Fleer et al. [4], the exergy of the sidewall thermal wastes is more than three times that of the exhausts (see Equation 11). This aspect is relevant. Figure 2.6 shows which one of these two transport phenomena is responsible of the highest thermal losses. In addition, Table 2.2 also shows that the most suitable source for conversion purposes is the thermal loss of the cell walls; actually, the exergy estimated for this loss is higher than that of the gases[10].

Table 2.2 Second-principle analysis of the thermal wastes.

	Gas losses MWh/t_{Al}	$\eta_{C,gas}$	Ex_{gas} MWh/t_{Al}	Shell losses MWh/t_{Al}	$\eta_{C,walls}$	Ex_{walls} MWh/t_{Al}
Gusberti et al. [28]	2.49	0.235	**0.58**	3.67	0.490	**1.80**
Gusberti et al. [28]	1.39		**0.33**	3.49		**2.20**
Nowicki et al. [32]	2.95		**0.69**	1.62		**0.79**
Fleer et al. [4]	2.20		**0.52**	3.70		**1.81**

The efficiency η_C in Table 2.2 are attainable only by an ideal machine. It would be more interesting to investigate some technologies that could effectively generate useful power from the thermal wastes. In the following sections, three systems will be presented. Even

[9]The introduction of the Carnot factor is justified by the Kelvin-Plank statement [44]:

"It is impossible to devise a cyclically operating device, the sole effect of which is to absorb energy in the form of heat from a single thermal reservoir and to deliver an equivalent amount of work."

Hence, it does not exist (not even ideally) a heat engine whose efficiency is 100%; rather, the rate of conversion of any thermodynamic machine has an upper limit defined by the Carnot factor.

[10]It should be noted that according to the data pubblished by Nowicki et al. [32], an ideal engine is able to produce a quantity of useful work, from the same source, that is of the same order of the one produced from the exhausts. This is possibly due to the underestimation of the sidewall heat losses in their work (See Figure 2.6).

though it is not very efficient to convert the energy available from the exhaust gases, the ORC technology has been proposed as it has been widely analysed in the literature. Nevertheless, the conversion of energy lost from the pot walls is a problem that has not found a satisfactory solution yet. Thermoelectric modules could be used; however, they present a very low conversion efficiency [17]. Thus, a more efficient (but not yet tested) technology will be discussed in the following sections.

2.3.1 Conversion of exhaust low-grade heat wastes by means of ORC engines

Most of the works about the recovery of aluminum-industry wastes are focused on the conversion of the exhaust thermal energy into useful work. In fact, it is relatively easy to collect the thermal power from the gases and use them as a hot thermal source. Eventually, this source, whose temperature varies between 90°C and 120°C [5], can be converted into useful work outside the smelter; this means that the operation of the conversion system will not affect the aluminum production line.

A conversion system well suited to convert such a low-temperature thermal source into useful work is the ORC engine. In these systems, the available heat is transferred to a phase-changing fluid through an evaporator; therefore, the vapor expands in a turbine in order to produce mechanical work; the working fluid is then condensed in a heat exchanger and finally pumped back to the evaporator to close the cycle [17]. A schematic sketch of a typical engine of this kind is shown in Figure 2.13a.

Several collaborations between aluminum producers and researchers have been established

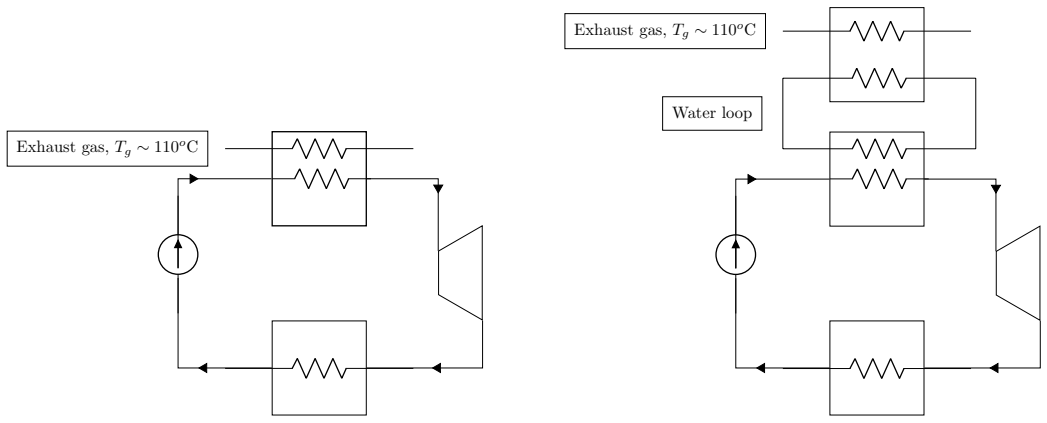

(a) (b)

Figure 2.13 ORC engine configurations: (a) the exhausts heat is transferred to the organic working fluid of the ORC; (b) a water loopp is used to transfer heat of the exhausts to the organic working fluid.

to study the conversion of the exhausts heat into useful power by means of the ORC (or Kalina) engines. Among these, the collaboration between Rio Tinto and the HydroQuebéc Energy Technology Laboratory [5] should be mentioned. In the framework of this research, the ORC configurations shown in Figure 2.13 have been investigated. In Figure 2.13a, the gases of the smelter exchange heat with the organic working fluid; in Figure 2.13b, a water loop is used to recover the exhaust heat to be transferred to the ORC evaporator. Thus, the rate of conversion of the thermal wastes as well as the investments related to the introduction of each of these ORC configurations have been studied. It is demonstrated that the ORC shown in Figure 2.13a could be used to generate up to 800 kW_{el}, while lower useful powers are achieved by the engine shown in Figure 2.13b. Nonetheless, the economic analysis has shown that the choice of the latter configuration turns into lower capital costs [5].

The data collected by Lostec and Nasreddine [5] can be used to emphasize further considerations regarding the ORC technology. According to these authors, the available heat of the exhausts is about 11 MW_{th}; then, the best case scenario would predict a conversion of 800 kW_{el} [5]. Thus, the efficiency of such a system should be

$$\eta_{\mathrm{ORC}} = \frac{\dot{W}_{\mathrm{ORC}}}{\dot{Q}_{gas}} = \frac{0.8\,\mathrm{MW}}{11\,\mathrm{MW}} = 0.07 \tag{12}$$

Furthermore, the Carnot factor for the exhaust thermal wastes, $\eta_{\mathrm{C,gas}}$, is 0.235 (see the Table 2.2). To a first approximation, the exergy efficiency of the conversion system can be estimated as the ratio between the engine efficiency and the Carnot factor, hence:

$$\eta_{\mathrm{Ex,\ ORC}} = \frac{\eta_{\mathrm{ORC}}}{\eta_{\mathrm{C,gas}}} = \frac{0.07}{0.235} = 0.3 \tag{13}$$

The exergetic efficiency (or second-law efficiency) is a measure of the system departure from a thermodynamically-perfect Carnot engine operating under the same conditions [45]. Then, the ORC engine is able to convert up to 30% of the useful power that could be delivered by an ideal engine. Here, we will not consider if it is possible to improve the exergetic efficiency; rather, in the following sections, this parameter will be estimated for other conversion systems and their values will be finally compared.

Before introducing the thermoelectric module and the Stirling technology, it should be mentioned that aluminum producers have never found the use of ORC engines to be economically interesting. Even though it is possible to recover heat from the gases to generate power, the financial investment related to the introduction of these solutions is

still too high (even for the configuration shown in Figure 2.13b) and represents an obstacle for the aluminum production industry [6].

2.3.2 Conversion of low-grade sidewall heat flux

Because of the high capital costs associated to the use of ORC units, the aluminum producers have lately launched some research projects aimed to investigate the conversion of the second source of thermal waste (i.e. the heat flux through the walls of the electrolytic cells) into useful work. In the following paragraphs, two technologies are described, namely, the thermoelectric generator and the Stirling engines.

a) Thermoelectric generators

The physical principle of thermoelectric generators (or modules) is the Seebeck effect. This phenomenon was discovered by a German physicist, Thomas Johann Seebeck, in 1821, when he realized that a voltage difference is produced when a thermal gradient occurs in a junction of two different conductors [46]. Therefore, this difference of potential can be used to generate an electric current.

The rough description of this phenomenon helps to understand how this technology can be used in aluminum plants. These generators can be simply installed on the electrolytic cell walls which are actually cooled by forced convection (see Section 2.2.2). Therefore, in these systems a temperature gradient is applied to transform heat into electrical energy. These systems do not have any moving parts, thus they do not require any complex maintenance; this aspect makes this technology quite suitable to find application in the industry.

Thermoelectric modules have been considered only recently by the aluminum producers, who are reticent to publish their results. For this reason, the open literature lacks of works about this topic. In spite of that, we can mention the patent proposed by Bayer and Olmstead [16], where the thermoelectric generator shown in Figure 2.14 is designed for pyrometallurgic applications (as the electrolysis process used for aluminum production). These thermoelectric generators can be installed directly on the cell wall, as shown in the figure. The physical orientation of these systems was studied to generate power not only from the aforementioned Seebeck effect, but also by the Nernst one[11] (recall that the considerable electrolytic currents in the cell cause strong magnetic fields in the pot room). Thus, according to Bayer and Olmstead [16], an increase of the generator efficiency is achieved by combining these two effects. It should be mentioned that this technology

[11]The Nernst effect describes the electric current due to the presence of both a temperature gradient and a magnetic field in a conductor.

is proposed with the purpose of controlling the electrolytic bath temperature and, consequently, the rate of produced aluminum.

The main drawback of thermoelectric converters is their low efficiency (and, to a lesser extent, their costs). It can be estimated as [17]:

$$\eta_{\mathrm{tm}} = \frac{T_h - T_l}{T_h}\left[\frac{M-1}{M+T_l/T_h}\right] = \eta_{\mathrm{C}}\left[\frac{M-1}{M+T_l/T_h}\right] \tag{14}$$

where the Carnot factor has been noted. In this equation, T_h and T_l are the high and the low temperatures of the junction and M is a characteristic of the operation of the generator:

$$M = \sqrt{1+\frac{Z}{2}\left(T_h+T_l\right)} \quad \text{with} \quad Z = \frac{S}{\rho k_t} \tag{15}$$

In the literature, Z is called the figure of merit (K^{-1}), S is the Seebeck coefficient (a physical variable dependent on the specific material, $\mathrm{V\,K}^{-1}$), ρ is the electrical resistivity ($\Omega\,\mathrm{m}$) and k_t is the thermal conductivity ($\mathrm{Wm}^{-1}\mathrm{K}^{-1}$). The typical values that have been measured for Z are between $1\times10^{-3}\mathrm{K}^{-1}$ and $3\times10^{-3}\ \mathrm{K}^{-1}$ [17]. Then, according to these values, it is almost impossible to attain conversion efficiencies higher than 15%. This can be further explained by recalling that the optimal operation of thermoelectric modules is achieved by using materials with small electrical resistivity and small thermal conductivity (in this way, the figure of merit increases). However, it is well known that good electrical conductors are also good thermal conductors.

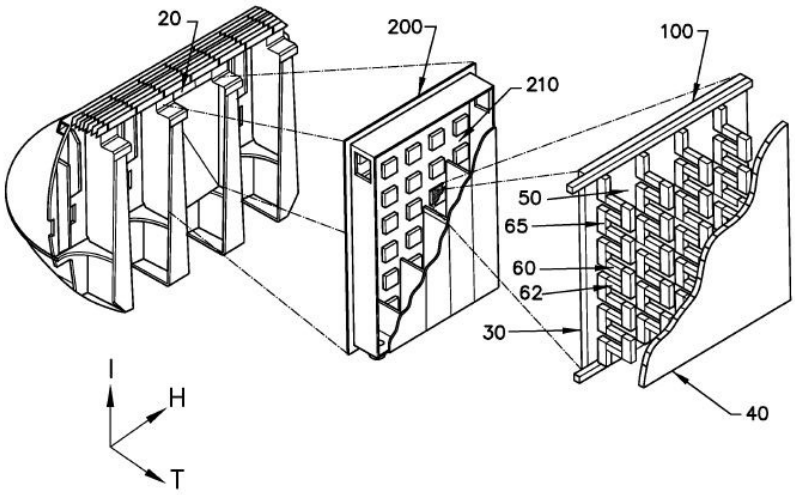

Figure 2.14 Design and exploded view of the proposed thermoelectric generator.

Finally, we notice from Equation 14 that the expression for the exergetic efficiency can be written as:

$$\eta_{\mathrm{Ex,tm}} = \frac{M-1}{M+T_l/T_h} = \frac{\eta_{\mathrm{tm}}}{\eta_{\mathrm{C}}} \tag{16}$$

Then, according to the aforementioned values, $0.12 \leq \eta_{\mathrm{Ex,tm}} \leq 0.25$. Even in this case, we will not discuss if it is possible to increase the second-principle efficiency defined by Equation 16; rather, we limit to remark that these values are lower than those estimated for the ORC engine in Section 2.3.1.

b) Stirling engines

Since its invention in 1816, the Stirling heat engine has always caught the interest of researchers and engineers [14, 15, 47, 48]. These systems present several interesting features. One advantage is their ability to convert heat into work by using any kind of sources. The open literature offers a wide range of Stirling movers driven by electrical resistances [13, 49], solar radiation [50, 51], nuclear power [52] and heat from the combustion of fossil fuels [13, 14]. Furthermore, these engines come in several configurations and dimensions. Therefore, Stirling systems are very flexible to find application in several fields, from solar power [13, 22] to both the automotive and the propulsion systems [14, 15].
Another interesting aspect of Stirling engines is their efficiency. According to Martini, "the Stirling engine is potentially a better cycle than other cycles because it has a potential for higher efficiency" [14]. This statement is justified by thermodynamic considerations. In the Stirling cycle, a working fluid undergoes four thermodynamic transformations, two of which are at constant temperature and the remaining two at constant volume (Figures 2.15a and 2.15b) [53]. Since heating and cooling processes undergo at isothermal conditions, the ideal-cycle efficiency is expressed as:

$$\eta_S = 1 - \frac{Q_{12}}{Q_{34}} = 1 - \frac{T_2\,(s_1 - s_2)}{T_3\,(s_4 - s_3)} = 1 - \frac{T_2}{T_3} = \eta_C \tag{17}$$

where Q_{12} and Q_{34} are the thermal energies exchanged during the cooling and heating processes (J), respectively; T is the temperature (K) and s is the massic entropy ($\mathrm{J\,kg^{-1}\,K^{-1}}$). In Equation 17, it is assumed that $s_4 - s_3 = s_1 - s_2$ [12] (see Figure 2.15b). The efficiency just found is nothing else but the Carnot efficiency. This means that the ideal Stirling engine is as efficient as the Carnot one. This feature cannot be shared by any other ideal

[12] This can be easily demonstrated by recalling that Stirling engines use air, argon or helium as working fluid. Then, assuming that the working fluid behaves as an ideal gas, the entropy variation Δs can be estimated by integrating the following expression [54]:

$$\mathrm{d}s = c_v \frac{\mathrm{d}T}{T} + R^* \frac{\mathrm{d}V}{V}$$

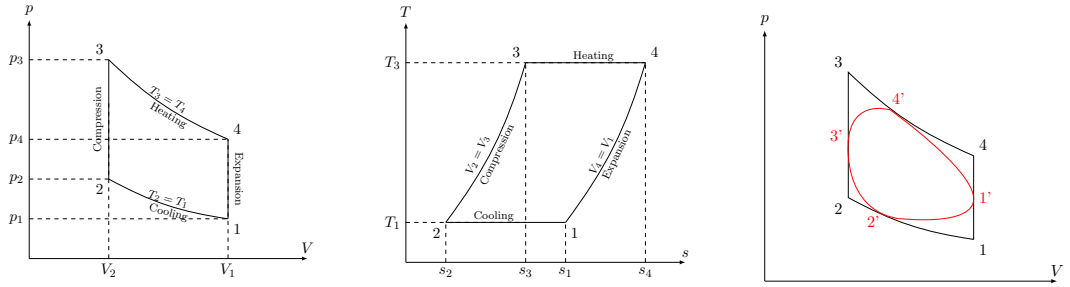

(a) (b) (c)

Figure 2.15 Thermodynamic diagrams describing a Stirling cycle: ideal Stirling cycle in the pV (a) and Ts (b) diagram and real versus ideal Stirling cycle (c).

machines (e.g. Otto, Diesel, etc.), because their cycles do not undergo isothermal heating or cooling [31]. Obviously, engineers do not deal with ideal machines. Thus, Figure 2.15c compares an ideal (black path) and a real (red path) Stirling cycle; the actual thermodynamic transformations of the working fluid are neither isothermal nor isochoric. Then, the real Stirling engine will convert less work than the ideal one.

The interest for Stirling engines has increased over the past 20 years, because they are able to work under relatively Low Temperature Differences (LTD) between the hot and the cold sources. Since these systems are considered to produce useful work from low-temperature sources (i.e. from Figure 2.15c $T_{4'} \leq 200°C$), they may be easily adapted to the thermal wastes of several industrial process. Many research works have been undertaken to study the most appropriate design for these machines [55–61]. An interesting example of these studies has been published by Formosa et al. [13], who has manufactured a Stirling mover generating useful power from a heat source at 150°C. Some researchers have come to the conclusion that among the engine configurations under analysis, LTD Free-Piston Stirling Engines (FPSE) are well suited for industrial applications. These units present several advantages indeed: they have a design which is simpler than other Stirling configurations, such as α or β type (usually called kinematic engines); their useful life can be as high as 10 years; FPSEs rarely require maintenance; the leakage of the pressurize working fluid is not encountered during the operation of these engines as these can be easily sealed [62]. Different theoretical models describing the operation of FPSEs have been proposed in the literature; in fact, these models can be used as a tool not only to predict the operation

where c_v is the constant volume heat capacity ($\mathrm{J\,kg^{-1}\,K^{-1}}$), T is the temperature, $R^* = \frac{R}{M_m}$, where R is the universal gas constant ($R = 8.314\ \mathrm{J\,mol^{-1}\,K^{-1}}$), M_m is the molar mass of the gas ($\mathrm{mol\,kg^{-1}}$) and V is the volume ($\mathrm{m^3}$). Then, recalling that both heating and cooling processes are isothermal and that both expansion and compression are isochoric, it can be shown that:

$$\Delta s_{43} = s_4 - s_3 = R \log \frac{V_4}{V_3} = R \log \frac{V_1}{V_2} = s_1 - s_2 = \Delta s_{12}$$

of these systems, but also to design them. Nonetheless, the development of such a model may be difficult because the operation of FPSE relies on many nonlinear phenomena [63]. Therefore, models taking these effects into account are usually cumbersome. A widely-used nonlinear model for Stirling engines is the isothermal analysis illustrated by Urieli and Berchowitz [47]. Starting from the equations of motion for the engine moving parts, a dynamical system is obtained and written in matrix form as follows:

$$\dot{\mathbf{x}} = A\mathbf{x} \tag{18}$$

where $\mathbf{x} = [x_1(t), x_2(t), \dots x_n(t)]^T$, $\dot{\mathbf{x}} = \left[\frac{\mathrm{d}x_1(t)}{\mathrm{d}t}, \frac{\mathrm{d}x_2(t)}{\mathrm{d}t}, \dots \frac{\mathrm{d}x_n(t)}{\mathrm{d}t}\right]^T$ and A is the $n \times n$ transfer matrix. A is usually non-linear (the coefficients $a_{i,j}$ of the matrix A are a function of $\dot{\mathbf{x}}$). Thus, attempts to linearize A by means of a Taylor expansion around a steady-state operation point have been proposed. This means that a new dynamical system based on the linearized matrix A_{lin} is obtained; hence:

$$\dot{\mathbf{x}} = A_{lin}\mathbf{x} \tag{19}$$

The stability of the dynamical system in this equation can be studied to propose an approximative design for Stirling engines. Chen and Griffin [64] and Redlich and Berchowitz [62] have noted that Equation 19 has non-trivial solutions only if $\det(A_{lin}) \neq 0$ [62, 64]. However, this criterion may not assure the stability of the solution for $\mathbf{x}$. Then, a more stringent analysis is performed by evaluating the eigenvalues of A_{lin}; if λ_i are the eigenvalues of A_{lin} and $\lambda_i \in \mathbb{C}$, stability is assured when $\Re[\lambda_i] \leq 0$ (the engine steady-state operation is achieved when $\Re[\lambda_i] = 0$). This approach has been followed amongst other by Kankam et al. and Bégot et al. [63, 65].

The problem of this modelling approach is that the results are strongly dependent on the operating point used to linearize the matrix of Equation 18. This means that these models are not reliable to predict the engine operation for conditions different from those chosen to perform the linearisation. For instance, Bégot et al. [65] have tested their model by comparing the predictions with the data collected for the RE-1000 unit [49], a Stirling engine tested under a wide range of working conditions; they noticed that their model was not able to predict the power of the RE-1000 machine for the operating conditions for which data were available. For these reasons, other modelling strategies, such as the use of non-linear analysis have been proposed. Iterative procedures have been considered by Chen and Griffin [64] and Formosa [66]. An alternative to this approach is the analysis proposed by Ulusoy [67]; starting form the non-linear isothermal model by Urieli and Berchowitz [47], Ulusoy applied the centre manifold theory and the normal analysis in

order to study the stability of Stirling engines operation[13] [67]. Another modelling approach has been proposed by Formosa et al. [13]. Their model is based on the mass and momentum conservation equations applied to each component of the system; then, from the thermoacoustic theory of Swift, they have demonstrated that an electrical analogy can be established between the characteristic variables of the engine (i.e. pressure and volumetric flow rate) and those of a electrical circuit (i.e. electrical potential and current intensity). Thus, an equivalent electrical circuit is derived and it can be used to predict the operation of the engine [13, 68]. Following this approach, the analysis of FPSEs is simplified (as it is reduced to the study of the equivalent electrical circuit). However, by following the theory proposed in the literature, some thermal aspects (i.e. the operation of the heat exchanger) can be introduced only indirectly; for instance, Formosa et al. [13] do not take into account the energy conservation equation into their modeling.

Finally, as it has been done for ORC machines and thermoelectric generators, an estimation of the second-principle efficiency for Stirling engines is provided. In order to do that, the Formosa et al.'s engine, which is shown in Figure 2.16, will be considered as case study [13]. This machine consists of three FPSE-type Stirling engines mechanically connected in series. Each engine has an expansion chamber, a heater, a regenerator, a cooler and a compression chamber (see Figure 2.16). Also, the compression and expansion chambers have moving membranes that replace the pistons. The engine requires a heat input of 2255.1 mW to produce 281 mW of electric power. Therefore, the thermodynamic efficiency is $\eta_F = 0.1246$; however, this machine works with a heat source at approximately 120°C and discharges heat at 40°C. Then, the efficiency of the Carnot machine working under this temperature difference is $\eta_C = 0.2035$. To a first approximation, the exergetic

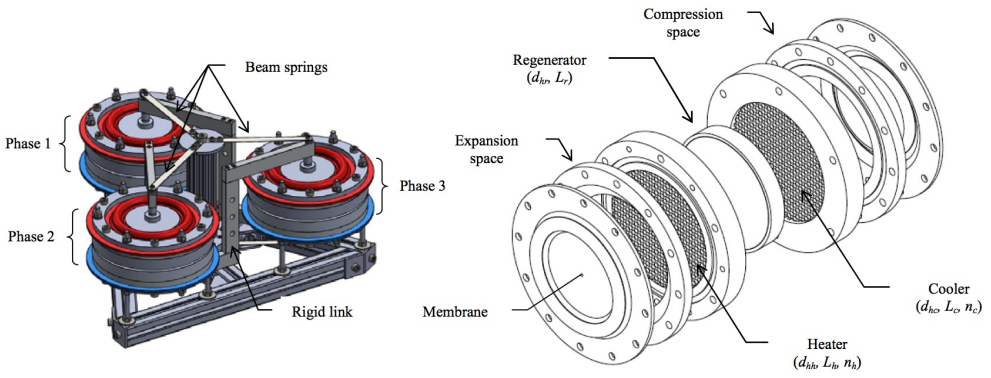

Figure 2.16 Design and exploded Stirling machine under analysis [13].

[13]Moreover, Ulusoy has also applied this theory to a non-isothermal model for Stirling engines [67].

efficiency of the engine can be calculated as the ratio of the actual and ideal yields; thus:

$$\eta_{Ex,s} = \frac{\eta_F}{\eta_C} = \frac{0.1246}{0.2035} = 0.6092 \tag{20}$$

From this equation, it can be stated that the Stirling engine under analysis is able to produce more then 60% of the work converted by an ideal Carnot machine. The exergetic efficiency in Equation 20 is considerably higher than those estimated for both ORC machines (Equation 13) and thermoelectric modules (Equation 16).

2.4 Specific objectives of the research

The production of thermal wastes in aluminum smelters, as well as the most suited solutions to recover and convert heat losses into useful work have been discussed in the previous sections. The aim of this thesis is to improve the energy efficiency of aluminum plants. In order to do that, both thermodynamic aspects (such as the efficiency of conversion of the wastes) and safety ones (i.e. the possible risks due to the operation of the proposed solution) must be considered.

2.4.1 Waste-heat recovery by thermal radiation and conversion using Stirling engines

We have already demonstrated that among the two principal transfer mechanisms of thermal wastes, the release of heat due to the high temperature of the pot sidewall seems to be more attractive than that of the hot gases. In fact, Table 2.2 clearly indicates that it is theoretically possible to conceive a high-conversion efficiency system to be coupled to the sidewall losses. Such a system must accomplish two fundamental tasks, that is, the recovery and the conversion of the thermal wastes into useful energy. The recovery of the sidewall thermal wastes can be accomplished by using an appropriate heat exchanger. It is then obvious that the design of such a system will depend on the heat transfer mode (i.e. conduction, convection or radiation) used to recover the thermal losses.

If the heat exchanger is designed to recover heat by conduction, this equipment must be in thermal contact with the sidewall. Such a recovery system already exists; in fact, the thermoelectric modules discussed in Section 2.3.2 can be thought as cooling systems to be attached upon the pot sidewall. The effects of these devices on the pot operation is almost negligible because they are able to recover only a little portion of the sidewall thermal wastes. Therefore, a different system that can collect a greater amount of heat losses should be designed. However, implementing such a design is difficult, because aluminum

producers fear that these systems may affect the electrolysis process. Moreover, as it has been already mentioned in this document, the cooling requirements of the pot are not constant; consequently, the operation of a conduction heat exchanger should be adapted to all the pot working conditions.

A convective heat exchanger, such as the one sketched in Figure 2.9, could be considered to overcome the controlling issues mentioned above. In fact, the working conditions of these systems depend on the working fluid, which does not need to be in thermal contact with the sidewall. Then, the amount of heat to be recovered can be easily controlled by varying the fluid mass-flow rate (or its inlet temperature). In spite of that, the choice of the working fluid is a challenging for aluminum producers. The only fluids that can be used are those not hazardous for the smelter. This requirement is fundamental because the environment of the smelter is characterized by the presence of both aluminum and alumina (Al_2O_3) particles. These chemical compounds are highly reactive. Therefore, if a leakage of the fluid occurs, it must be completely inert in the smelter environment. Even though water and organic fluids are usually desirable for heat transfer purposes, they cannot be used, since they react with the aforementioned chemical compounds. Hence, other less-efficient but safer fluids, such as air, should be considered to design the heat exchanger.

The radiative heat exchanger (reviewed is given in Appendix B) can be considered as a system able to vary the amount of heat to be recovered (meaning that it can be regulated according to the pot cooling needs). Moreover, its operation respects the safety requirements of the plant. These statements can be easily demonstrated by recalling the theory of thermal radiation heat transfer. To a first approximation, the radiative heat flux in an enclosure (either empty or filled with non-participating medium) are governed by Equation 9 (it is assumed that both conduction and convection heat transfer are negligible); this equation states that the radiative heat flux are proportional to the emissivity of the surfaces, the difference of the fourth powers of the surface temperatures and the view factors. Furthermore, from Equation 8, the view factors are inversely proportional to the square of the distance between the surfaces that are exchanging heat by radiation [40, 43]. Thus, it can be expected that the distance between the pot sidewall and a flat collector (that is, the radiative heat exchanger studied in this research) will have a deep influence on the exchanged flux; then, the distance between these systems can be the variable controlling the cooling of the pot. Moreover, this is not the only interesting aspect of these exchangers. Since radiation transports heat by electromagnetic waves, a medium is not

required for the exchange of thermal energy to occur[14]. These considerations permit us to consider a simple flat collector that will be inherently safe to cool the pot (when needed) and to recover the thermal wastes of aluminum smelters.

Once the thermal wastes have been recovered by radiation heat transfer, those need to be converted into useful power. In the previous sections, some LTD conversion systems have been presented, that is, ORC machines, thermoelectric generators and Stirling engines. The ORC technology has been mentioned to describe the conversion of the heat wasted by the gas; this technology cannot be used to recover the sidewall losses because of the aforementioned safety considerations (ORCs use organic working fluids). So, the choice is limited to thermoelectric modules and Stirling engines. The use of the former systems has already been studied, nevertheless such an analysis has not been performed yet for the latter ones. Stirling engines present interesting aspects: the working fluid of these engines is usually a gas (e.g. air, argon, nitrogen...), thus, their use in the smelter is not dangerous; a LTD configuration for these engines has already been well proven in the open literature [69]; they can convert any forms of heat (conduction, convection or radiation) into useful work [14]; and finally, their dimension can vary from some millimetres [70, 71] to some meters [49].

The characteristics mentioned above make Stirling engine worthy of being studied as an alternative to thermoelectric modules. Figure 2.17 compares the performances of both energy conversion systems. Figure 2.17a shows the thermoelectric generator efficiency evaluated from Equations 14 and 15 and the experimentally-measured efficiency of several Stirling engines found in the open literature [13, 69, 72–74]. It is interesting to note that for all but only one Stirling engine, the measured efficiency is greater than the ideal efficiency of thermoelectric generators. Furthermore, the gap between the Stirling-engine and thermoelectric-module efficiencies seems to increases as the hot-source temperature increases and by keeping the cool temperature constant and the same for both cases. Thus, Stirling engines are superior in terms of efficiency of energy conversion.

Figure 2.17a shows results that can be easily found on textbooks [17], i.e. the efficiency of Stirling engine is usually higher than that of thermoelectric modules. This statement is not strong enough to justify the choice of one technology with respect to the other because a further aspect need to be noted. Thermoelectric generators can convert sidewall thermal wastes by conduction heat transfer (these systems must be attached to the sidewalls). Therefore, the aim of this thesis is to study the possibility of using Stirling engines to collect and convert thermal wastes by radiation (i.e. without mechanical contact with

[14]However, thermal radiation can be affected by the nature of the medium in which these electromagnetic waves travel. The interested reader is addressed to Chapters 9 to 13 of reference [40].

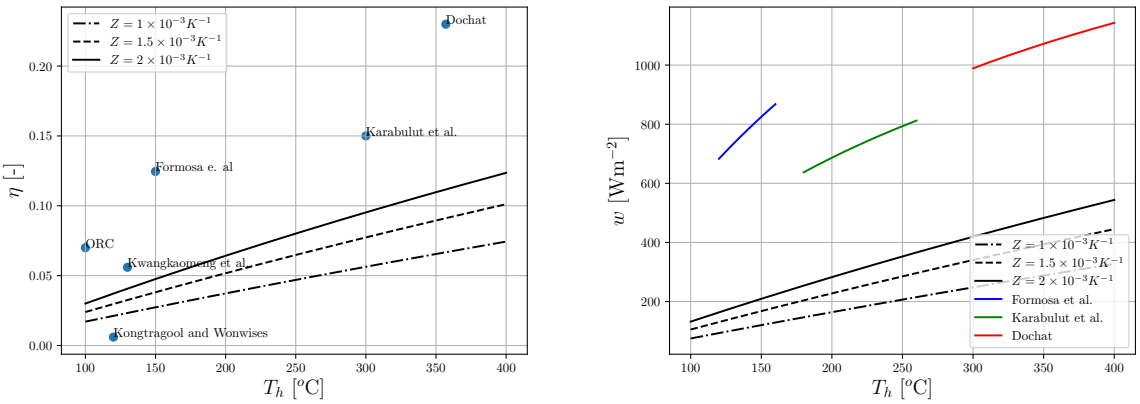

(a) (b)

Figure 2.17 Comparison of the performance of Stirling engines with thermoelectric generators: (a) comparison of measured thermodynamic efficiencies of various Stirling engines proposed in the literature [13, 69, 72-74] with thermoelectric-module as a function of the hot-source temperature for the same cool temperature ($T_k = 20°C$); (b) comparison of the useful work converted by Stirling engines proposed in the literature with the work obtained by thermoelectric modules as a function of the hot-source temperature for the same cool temperature ($T_k = 20°C$).

the pot sidewall). Then, it is fundamental to show that the configuration under analysis is superior to the use of thermoelectric modules (that is, Stirling engines coupled with a simple radiative collector can generate more work then thermoelectric modules attached to the sidewalls). Figure 2.17b shows a comparison of the conversion rates of the systems under analysis. In this figure, it is assumed that the amount of the sidewall losses is 4.4 kW m^{-2} and that this power density can be completely recovered either by conduction (such as the case of thermelectric modules) or by radiation (such as the case of Stirling engines with a radiative collector); thus, Figure 2.17b shows that the real Stirling engines working at low temperature, such as that studied by Formosa et al., Karabulut et al. and Dochat [13, 73, 74], are able to produce more work than ideal thermoelectric generators working at high temperature. Hence, according to Figure 2.17, we can justify the choice of Stirling engines for recovering thermal losses by radiation instead of using thermoelectric modules.

2.4.2 Principal contributions of the present work

In the previous section it has been highlighted that the recovery of the sidewall thermal wastes by means of a radiative collector and their conversion using a Stirling engine could be a safe and efficient solution to improve the energy efficiency of aluminum smelters. In

order to prove this statement, a research has been undertaken and its main results are outlined in this document. This research focuses on two main topics, that is (i) the recovery of the thermal wastes and (ii) their conversion into useful power.

In this work, it is assumed that a flat collector placed parallel to the sidewall can recover the heat losses by radiation. Afterwards, both the temperature of this system and the amount of the collected thermal power need to be estimated to predict the operation of an appropriate Stirling engine. Such an evaluation is complex because the radiation heat transfer is not the only mode occurring between the sidewall and the collector; in fact, conduction through the pot and convection due to the air-nozzle cooling system (see Section 2.2.2) must be considered because they will deeply affect the heat recovered by radiation. This is to say that a problem of conduction coupled with mixed convection and radiation must be solved to obtain an acceptable estimation of the collector temperature and heat flux. In this work, it is chosen to solve such a problem by using a CFD tool (i.e. OpenFOAM 5.0). Then, this methodology is followed to simulate different sidewall cooling scenarios and their effects on the thermal collector behavior. This study is the main topic of a journal paper written in the framework of this research project and published to "Energy Conversion and Management"; this scientific article is reported in Chapter 3.

The knowledge of the characteristics of the plate collector is essential to predict the operation of the Stirling engine; in spite of that, it is not a sufficient information to select the most suitable engine to recover the thermal wastes. In fact, other variables must be accounted for (these variables are mainly constraints imposed by the industrial plant, such as the space available to install the units). Since the Stirling engine satisfying the smelter needs does not exist yet, a preliminary design is mandatory; this could be implemented by using the models available in the open literature. However, it seems that these models are not suitable for these pupuses, as they overpredict the power converted by the engine [65]. It is for these reasons that it is chosen to develop a new model, starting from the considerations described by Formosa et al. [13]; they proposed a theoretical approach based on the electrical analogy between the characteristic variables of a Stirling engine and those of an electrical circuit [13]. Following this theory, it is possible to couple both dynamic aspects (such as the motion of the power piston) and thermodynamic ones (e.g. the operation of the heat exchangers); thereafter, an electrical circuit whose behavior is equivalent to that of the machine is derived from the electrical analogy theory. It is interesting to note that the obtained equivalent circuit can be applied to predict the operation of FPSEs, independently on their dimensions. It should be mentioned that the Formosa et al.'s modeling approach [13] did not seem to be satisfactory, as not all the conservation equations were used in that work; it is for this reason that a more rigorous approach is proposed in this

document. The electrical analogy theory developed during this research is the subject of a peer-reviewed article published on "Energy Conversion and Management" journal; this article is reported in Chapter 4.

2.4.3 Release of residual cooling heat

Before concluding this chapter, it is mandatory to highlight one more aspect of this research. It is well known from thermodynamic principles that "it is impossible to construct an engine which will work in a complete cycle, and produce no effect except the raising of a weight and cooling of a heat reservoir" [75]. This is nothing but the Kelvin-Planck's statement of the second law of Thermodynamics. Therefore, a proper analysis of the solution presented above cannot neglect the study of a cold reservoir, otherwise, the second law of Thermodynamic will be violated.

The conversion of thermal wastes into useful power by means of a Stirling engine necessitates a cooling system to be designed. Despite its importance, this topic will not be covered in this thesis. This choice is justified by the fact that there already exists an hypothetical cooling heat exchanger for the conversion system. It consists of a set of the air nozzles currently used to cool the pot sidewall. Thus, it is assumed that this system could be used to cool the bottom side of the Stirling engine. Such a system is chosen because its operation is already tested in the aluminum plants. It should be also recalled that it is not possible to consider other heat working fluids (e.g. water or any organic fluid) because its operation may be responsible dangerous reactions. For instance, the leakage of water may cause the production of hydrogen, according to the following reaction:

$$2\,\mathrm{Al} + 3\,\mathrm{H_2O} \longrightarrow \mathrm{Al_2O_3} + 3\,\mathrm{H_2} \qquad (\mathrm{R}\,17)$$

It is obvious that the production of hydrogen is undesired. For this reason, cooling must be performed by other working fluids (e.g. air, as is the case of air nozzles, or molten salts) or it has to be designed to reject heat by a different transfer mode, such as by radiation as well.

CHAPTER 3

PROOF OF CONCEPT TO RECOVER THERMAL WASTES FROM ALUMINUM ELECTROLYSIS CELLS USING STIRLING ENGINES

Avant-propos

Auteurs et affiliation :

- Franco Cascella, étudiant au doctorat, Département de génie mécanique, Université de Sherbrooke ;
- Simon Gaboury, chercheur en efficacité énergétique, Centre de Recherche et de Développement Arvida (CRDA) ;
- Mikhail Sorin, professeur, Département de génie mécanique, Université de Sherbrooke ;
- Alberto Teyssedou, professeur, Institut de génie nucléaire, Département de génie physique, Polytechnique Montréal.

Date de soumission : 18 mai 2018.
État de l'acceptation : version finale publiée.
Référence : Cascella, F., et al. "Proof of concept to recover thermal wastes from aluminum electrolysis cells using Stirling engines." Energy Conversion and Management 172 (2018) : 497-506.
Revue : Energy Conversion and Management.
Titre français : Conception de la récupération les déchets thermiques des cuves d'électrolyse produisant aluminium à l'aide de moteurs Stirling.
Titre anglais : Proof of concept to recover thermal wastes from aluminum electrolysis cells using Stirling engines.
Contribution au document : Dans ce chapitre, la première contribution scientifique de cette recherche doctorale est présentée. Il s'agit d'un deuxième article rédigé dans le cadre de cette recherche et qui est présente en premier pour garder la cohérence du document. Dans cet article, le sujet de la récupération des déchets thermiques d'une cuve d'électrolyse

à l'aide d'un collecteur plat est traité. La nouveauté de la recherche présentée dans cet article est l'approche CFD utilisé pour estimer les pertes thermiques de la paroi de la cuve. Cette approche se base sur l'utilisation du logiciel OpenFOAM 5.0, pour lequel une validation est implémentée.

Résumé français : La production d'aluminium est l'un des procédés industriels les moins efficaces du point de vue énergétique. En effet, près de la moitié de son besoin énergétique est perdu sous forme de chaleur lors de la production de ce métal. Pour cette raison, les producteurs d'aluminium sont intéressés à améliorer l'efficacité énergétique de leurs fonderies en récupérant les pertes thermiques. Il est bien connu qu'une perte d'énergie importante se produit à travers les parois latérales des cuves d'électrolyse. Cet article démontre la faisabilité d'une solution pour augmenter l'efficacité énergétique des fonderies d'aluminium ; dans cette solution, les déchets thermiques des parois latérales sont utilisés pour entraîner les moteurs Stirling à basse température. Pour estimer les pertes, une étude de transfert thermique est accomplie. La conduction thermique couplée à la convection mixte et au rayonnement est évaluée au moyen du logiciel OpenFOAM. Ensuite, une étude paramétrique est effectuée pour analyser les conditions de travail des cellules selon lesquelles les déchets thermiques pourraient être récupérés. Le flux de chaleur et la température des déchets thermiques sont utilisés pour juger de l'utilisation de la technologie du moteur Stirling. Deux scénarios sont étudiés : i) un collecteur de chaleur plan couplé à la paroi latérale rayonnante et ii) un collecteur de chaleur plan en contact thermique avec la paroi latérale de la cuve. Puisque le fonctionnement du collecteur n'est pas connu a priori, une très faible valeur pour le coefficient d'émission est choisie pour ce système. Il est démontré que les déchets récupérés par rayonnement peuvent alimenter certains moteurs Stirling donnés dans la littérature scientifique. La puissance utile peut augmenter lorsque le collecteur est en contact thermique avec les parois latérales de la cellule ; mais, la configuration physique des parois des cuves ainsi que les restrictions de l'installation de sécurité ne permettent pas d'envisager cette configuration. Par conséquent, la récupération des déchets actuellement perdus par rayonnement et leur conversion ultérieure au moyen du moteur Stirling constituent une solution intéressante pour améliorer l'efficacité énergétique des fonderies d'aluminium.

3.1 Abstract

The production of aluminum is a low energy-efficient industrial process. In fact, almost half of its energy demand is lost under the form of heat along the production line. For this reason, aluminum producers are interested in improving energy efficiency of their smelters by recovering the thermal losses. It is well known that a significant loss of energy occurs across the sidewalls of the electrolysis cells. This paper proposes a proof of concepts where the sidewall thermal wastes are used to drive Low Temperature Differential (LTD) Stirling engines. To estimate the losses, a heat transfer study is implemented; heat conduction coupled with mixed convection and radiation is evaluated by using the OpenFOAM Computational Fluid Dynamic (CFD) software. Then, a parametric study is performed to analyze cell working conditions under which thermal wastes could be recovered. The heat flux and the temperature of the thermal wastes are used to judge the utilization of possible Stirling engine technologies. Two scenarios are studied: i) a plane heat collector coupled to the radiative sidewall and ii) a plane heat collector in direct thermal contact with the cell sidewall. It is demonstrated that the recovery of the wastes by radiation is technically feasible and it does not threaten the safety of the smelter; furthermore, the losses can power some Stirling engines given in the open literature. Therefore, the recovery of the radiative wastes and the further conversion by means of the Stirling engine is an interesting solution to improve the aluminum smelter energy efficiency.

Keywords: Stirling engine, thermal wastes, heat recovery, radiation, conduction, Computational Fluid Dynamic.

3.2 Introduction

The aluminum production is one of the most energy intensive industrial sectors. The only known-to-date method to produce primary aluminum is the Hall-Héroult process (independently discovered by Charles Martin Hall and by Paul Héroult in 1886), where alumina (Al_2O_3) is reduced to aluminum by electrolysis [76]. From a theoretical view point, such a process requires 6 MWh/t_{Al}; nevertheless, the actual energy demand in aluminum smelters is much higher, ranging between 11 and 15 MWh/t_{Al}.

To understand the differences between theoretical and real-plant energy demand, a detailed energy balance of the pot (i.e. the electrolysis cell producing aluminum) should be performed. According to the data found in the literature [4, 6, 28], about half of the energy demand ($\sim 44.2\%$) is effectively required to produce aluminum, while the remaining is lost

along the production line. Several mechanisms are responsible of these losses: secondary (endothermic) reactions occurring in the electrolysis bath, the production of hot gases in the pot, the electrical losses in the busbars (i.e. anode-cathode connectors), the frequent openings of the cells and the thermal losses across pot sidewalls [11, 28]. Among these losses, the most notable are those due to the high temperature of the gas ($\sim$ 16.3% of the energy demand) and those of the sidewalls ($\sim$ 21.2%).

It is apparent that the analyses of heat wastes are of primary importance for aluminum producers; they could be recovered and converted into useful work [77]. Although the most important are of the same order of magnitude, the majority of the works in the open literature is focused to recovering heat wastes from the hot gases [78]. Such a recovery is interesting. Since it is performed outside the smelter, it does not threaten the plant's safety. Moreover, the temperature of this source (90-120°C, depending on the season) is well suited to power Organic Rankine Cycle (ORC) engines [4, 6, 28]. Notwithstanding, ORCs are not often employed; the high costs and the low returns of investment make this technology economically unattractive for most aluminum producers [5]. In addition, the use of organic fluids in this type of industry is not welcomed.

The recovery of the heat losses from the sidewalls of the pots has been scarcely studied [11]. The temperature on the pot external surfaces varies between 200 and 400°C; therefore, these thermal potentials are important from both energetic and exegetic viewpoints [6]. However, the recovery is challenging, essentially amongst other because it is difficult to access at these locations as these portions of the pots are underneath the working operator area; the wall surfaces of interest are confined to a restricted space; the high concentration of both aluminum and alumina particles makes the smelter environment chemically reactive (thus, the choice of heat recovery systems must be limited to those using non-reactive fluids). In parallel to these drawbacks, the recovery and the conversion of the thermal wastes must not affect the electrolysis process, which is the main concern for aluminum producers. Few systems respecting these requirements have been proposed in the open literature. Namboothiri et al. [37] have designed an air heat exchanger to be installed directly onto the external pot walls; however, the main purpose of this work is not devoted to recover waste heat, but to control the delicate cell heat balance. The use of thermoelectric modules has been proposed too [16, 79]; however, their low thermodynamic efficiency (around 7%) makes their use a poor waste-heat recovery option.

Herewith, the evaluation of sidewall thermal losses and their conversion rate into mechanical power using Stirling engines is presented. To estimate heat losses by conduction, convection and radiation, a series of CFD simulations are carried out. To this aim, version 5.0 of OpenFOAM is used and the calculation schemes are validated. Electrolysis cell

conditions under which the heat recovery can be maximized are parametrically studied. As a proof of concept, the use of the Stirling engines as energy conversion systems is investigated. Several reasons justify the choice of these technologies: they can be driven by any form of heat transfer (conduction, convection and radiation); the working fluid is a gas, such as argon or helium, making their use safe in aluminum smelters; they can operate under relatively low thermal potential differences and they can be dimensioned to produce power levels ranging from few watts up to several kilowatts [13, 14, 22].

This work considers the following two scenarios: i) it is supposed that the engine has a plane heat collector that recovers energy from the sidewall only by radiation; ii) the same heat collector is placed in direct thermal contact with the pot sidewall. Due to the structure of the sidewalls and the presence of air ventilation nozzles, the CFD modeling approach must consider three modes of heat transfer (i.e. conduction, convection and radiation). Appropriate Stirling engines are then selected from the open literature and thus, their estimated efficiencies are used to determine the available mechanical power. It should be mentioned that the nozzle cooling system used to control the temperature of the pot sidewalls can be applied to cool the Stirling engines. Nevertheless, this system will not require major modifications other than a partial reduction on the air mass flow rate, because the Stirling engine will reject less heat than that collected by radiation from the whole sidewall. In this document, the changes of the actual cooling system are not addressed. The final choice of the most suitable scenario is discussed by considering the engine conversion rate and possible effects on the safe operation conditions of electrolysis cells.

3.3 Cooling the pots in aluminum smelters

The production of aluminum by electrolysis takes place in several reactor units, commonly called pots. The number of pots in a conventional smelter can reach few hundreds. The challenge for aluminum producers is to preserve the working conditions of all the pots simultaneously, since they are electrically connected in series through busbars. The temperature of the pot sidewalls constitutes a critical variable. To avoid high temperature concentration zones, it is controlled by means of several air cooling jets. To this aim, air flows at about 20°C to cool the sidewalls, whose temperatures may vary between 200 and 400°C. It is thus obvious that large amounts of thermal energy are lost by convection and radiation.

The aluminum smelter energy demand is about 11-15 MWh_{el}/t_{Al} and the aluminum production of the Canadian industry ranges between 100 and 600 kt/year. According to

the pot energy balances described in the open literature [4, 28, 32] around 21% of the consumed energy is lost through the sidewalls. Hence, heat losses occurring across the external wall of each cell represent approximately 0.36 MW_{th}. These losses are due not only to convective cooling, but also to radiation heat transfer because there are significant temperature differences between the pot walls and the surrounding surfaces. Under such conditions, convection and radiation heat transfer are coupled. Therefore, the estimation of the amount of these losses must be performed using CFD modelling approaches. This estimation represents one of the objectives of the present work that is discussed in the following sections.

3.4 The numerical model

In this section, the heat transfer process from the electrolysis cell walls is modeled. The control volume, the conservation equations as well as the turbulence models and boundary conditions are discussed in the following sections.

3.4.1 The integration domain

The length of a conventional pot is about 10 m and counts several equally-spaced vertical beams that can behave as thermal fins [29]. The present work is intended to model the heat transfer from the external walls therefore, the physical-chemical processes occurring inside the pots are not treated. In addition, the heat transfer from the upper portion of the electrolysis cells is neglected and thus, only the external lateral surfaces of the pots are considered.

As shown in the Figure 3.1, according to the geometry of a conventional electrolysis cell, the lower regions of the pots consist of equal regions bounded by two beams and the hot surface of the sidewall. The number 1 in this figure indicates the sidewall, while the numbers 2 and 3 specify the vertical beams. A complete cell contains several portions like Figure 3.1, which repeat with a given periodicity. Thus, the present study is focused on a single region of the pot and the cooling alongside the end-lateral surfaces is not considered. Since the objective consists in evaluating the heat that can be recovered by radiation, it is assumed that the Stirling engine thermal collector consists of simple planar surface, indicated by the number 4 in the Figure 3.1. The thermal conductivity as well as the emissivity of the surfaces used to perform the simulations are given in the Table 3.1. These values, taken from the open literature are considered as constants, independent of the local temperature. A very low value for the emissivity of the heat collector, to be coupled with the Stirling engine, is voluntarily selected to evaluate the performance of the

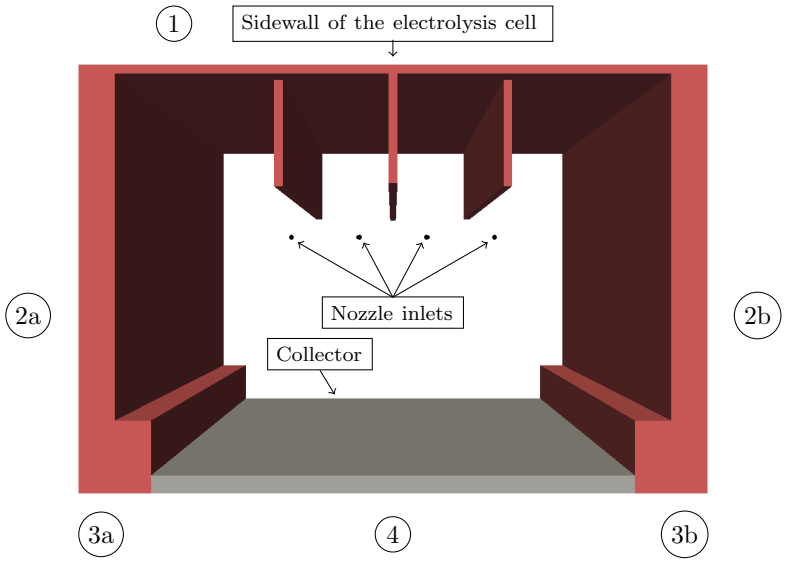

Figure 3.1 Top view of the control volume.

system under the worst conditions. In fact, there is no information about the effect that the deposit of alumina aerosols or other particles may have on the emissivity of exposed surfaces; in any case, according to the industrial partner, the concentration of this chemical compound never exceeds few ppm.

Moreover, to consider the effect of forced convection heat transfer on the surface temperature distribution upon the collector, four air-jet nozzles shown by the black dots in Figure 3.1, are numerically modeled. The geometry of the entire domain described above is treated using the version 8.3 of SALOME CAD software. Salome is an open source software developed by Électricité de France and the Commissariat à l'énergie atomique in 2001. It is used to model the geometry of a generic computational domain. It can also be applied for either pre- and post- processing of numerical simulations. Hence the Salome software can generate meshes having different geometries. In the present work, it is used to export the integration domain to the convenient form, required by the "snappyHexMesh" tool of OpenFOAM. In this way, we have generated a mesh containing 2×10^6 cells. The appropriate number of cells is estimated by performing previous dimensional studies which are not presented in this document. Due to the relatively simple geometry of the integration domain, a structured mesh is used to perform the computations.

The Figure 3.2a shows a bottom view of the air inlet region, where the meshes for both the sidewall and the heat collector are not shown. Note that in these figures only the central fin is visible, because the other two vertical ones shown in Figure 3.1, are shorter than the central one and consequently they do not touch the bottom of the pot integration domain. The effects that the air-jet flows may have in the heat recovery process are of

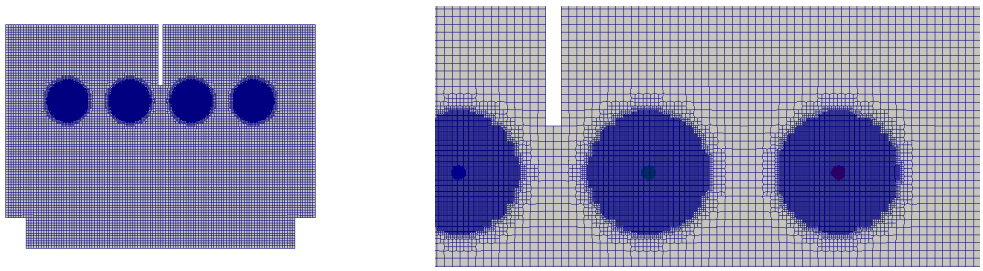

(a) (b)

Figure 3.2 Computational domain used to perform the simulations: (a) bottom surface of the fluid region; (b) mesh refinement around the air inlet nozzles.

great importance; therefore, the mesh is refined around these regions, as shown in the Figure 3.2b.

3.4.2 Conservation equations

The control volume described above contains both solid structures (i.e. the pot wall, the vertical beams and the heat collector) and air-flow regions. Therefore, different heat transfer modes occur. In the solid regions, only the Fourier equation's is applied and thus, the following equation needs to be solved:

$$\nabla \cdot (k_s \nabla T_s) = 0 \tag{1}$$

where k_s is the thermal conductivity (see Table 3.1) and T_s is the temperature in the solid regions (i.e. beams, walls and collector). The four jets in the fluid regions are the main source of turbulence; therefore, a turbulent flow needs to be computed. Several numerical methods to solve this type of problem are available in the literature; the most largely used are: the Reynolds Averaged Navier-Stokes (RANS) equations, the Large Eddy Simulations (LES) and the Direct Numerical Simulations (DNS) [18, 19]. To perform this work, the RANS modelling approach has been chosen because it has been validated for a wide range of industrial applications [19]. The flow variables used to write continuity, momentum and energy equations can be expressed by a generic variable ψ consisting of the sum of time averaged and fluctuating values, hence:

Table 3.1 Physical properties of materials and surfaces.

	k [$\mathrm{W\,m^{-1}\,K^{-1}}$]	ε [-]	Thickness [m]
Sidewalls	16	0.85	–
Vertical fins	16	0.85	0.01
Collector	177	0.12	0.02

$$\psi(t) = \Psi(\tau) + \psi'(t) \tag{2}$$

where the mean value is averaged over a period τ (with $\tau \gg t$). The conservation equations are rewritten based on Equation 2 and are time-averaged by assuming that fluctuations are completely random and the covariance of the product of fluctuating variables are not necessarily zero. Then, the continuity, the momentum and the energy equations for an incompressible flow become:

$$\frac{\partial U_i}{\partial x_i} = 0 \tag{3}$$

$$\frac{\partial U_i}{\partial t} + U_j \frac{\partial U_i}{\partial x_j} = -\frac{1}{\rho}\frac{\partial P}{\partial x_i} + \frac{\partial}{\partial x_j}\left[\nu\left(\frac{\partial U_i}{\partial x_j} + \frac{\partial U_j}{\partial x_i}\right) - \overline{u_i' u_j'}\right] + f g_i (T_s - T)\beta \tag{4}$$

$$\frac{\partial T}{\partial t} + U_j \frac{\partial T}{\partial x_j} = \frac{\partial}{\partial x_j}\left[\left(\frac{\nu}{\mathrm{Pr}} + \frac{\nu_t}{\mathrm{Pr}_t}\right)\frac{\partial T}{\partial x_j} - q_{r,j}\right] \tag{5}$$

In these equations, U_i, P and T are the mean values of velocity, pressure and temperature of the air; ρ, ν, β and Pr the density, the kinematic viscosity, the volumetric thermal expansion coefficient and Prandtl's number; g_i is the component of the gravity vector and f is a switch coefficient that can be equal to 0 or 1 (i.e. when $f = 0$ buoyancy is not included into the RANS momentum conservation equation). The averaged flow equations are mathematically equivalent to those of laminar flows, except for the term $\overline{u_i' u_j'}$, which corresponds to the Reynolds stress tensor. The components of this tensor are modelled based on the turbulent Boussinesq's approximation [18] and they are written as:

$$-\overline{u_i' u_j'} = \nu_t\left(\frac{\partial U_i}{\partial x_j} + \frac{\partial U_j}{\partial x_i}\right) - \frac{2}{3}k\delta_{ij} \tag{6}$$

where ν_t is the turbulent viscosity to be estimated according to the mixing length theory, k is the turbulence kinetic energy ($k = \frac{\overline{u_i' u_j'}}{2}$) and δ_{ij} is the Kronecker's delta. The system of Equations 3 to 5 are closed by a set of turbulence model equations. Several turbulence models are available in the open literature and they differ by the number of equations to be solved; thus, one-, one-and-half and two- equation models can be selected. The latter ones have been extensively used; they are considered as the most reliable amongst RANS turbulence models [19]. Within the present framework, the $k\varepsilon$ with buoyancy term (i.e. $f = 1$ in Equation 4) [80] and the standard $k\omega$ model without buoyancy ($f = 0$ in Equation 4) [18] are tested[1].

The "chtMultiRegionSimpleFoam" solver is used to solve the system of equations under steady state conditions. It is coupled with one of the previously selected turbulence mod-

[1]These turbulence models are given in Appendix C.

els, i.e. "buoyantkEpsilon" or "kOmega". A radiation heat transfer model (described by the Equation 7 given in the following section), is introduced by calling the "viewFactor" tool. The derivatives terms are discretized according to the Finite Volume Method[2] (FVM); second order discretization is applied to the divergence terms, while the central differentiating scheme is used for the other terms. The SIMPLE algorithm of Patankar is used for coupling pressure and velocity, with a single underrelaxation coefficient of 0.7[3]. The Geometric-Algebraic Multi-Grid (GAMG) solver is used to compute the discrete algebraic equation for the pressure, while all other equations are computed using the Preconditioned Bi-Conjugate Gradient Stabilized solver (PBiCGStab). The simulations are carried out in a workstation containing 8 processors.

3.4.3 Boundary conditions

According to the problem outlined in the previous sections, the boundary conditions for the solid and the fluid regions need to be specified. The solution of the heat transfer as well as the energy conservation equation, necessitates Dirichlet or Neumann boundary conditions.

Referring to Figure 3.1, a Neumann boundary condition is imposed on the backside of the sidewall of the cell, i.e. the surface 1 perpendicular to the plane of the figure; thus, an entering heat flux is imposed to this wall. Since this value may change according to pot operation conditions, its effects are parametrically studied in the Section 3.5.2. For the surfaces 2 and 3 (i.e. the external surfaces of the beams in Figure 3.1), zero-gradient boundary conditions are applied. Due to the symmetry that exists between similar pots mechanically in series, such adiabatic conditions are physically plausible, while surfaces 3a and 3b do not considerably contribute to heat transfer because the beams are assumed to be in perfect thermal contact with the heat collector (see Figure 3.1). The term $q_{r,j}$ in Equation 5 corresponds also to a Neumann condition, which is not known a priori. To simulate the heat transfer using a direct or forward CFD method, this condition is initially imposed on the backside wall of the heat collector (i.e. the surface 4 in thermal contact with the gas of a hypothetical Stirling engine). To this purpose, a radiation heat flux is initially estimated assuming that infrared light travels through a non-participating medium, i.e. the air, enclosed in a cavity containing N surfaces. Hence, the radiation flux from surrounding surfaces i to the surface j is initially estimated by using the following

[2]A description of the Finite Volume Method is given in Appendix D.
[3]The flow chart of the Simple algorithm of Patankar is given in Appendix E.

equation [40]:

$$\sum_{j=1}^{N}\left(\frac{\delta_{ij}}{\varepsilon_j}-F_{ij}\frac{1-\varepsilon_j}{\varepsilon_j}\right)\frac{\dot{Q}_j}{A_j}=\sum_{j=1}^{N}F_{ij}\sigma\left(T_i^4-T_j^4\right) \tag{7}$$

In this equation, ε_j are surface emissivity coefficients as given in the Table 3.1, F_{ij} is the view factor between the surfaces i and j, and σ is the Stefan-Boltzmann constant ($\sigma = 5.67 \times 10^{-8}\ \mathrm{W\,m^{-2}\,K^{-4}}$). The heat flux estimated using this method corresponds to 600 $\mathrm{W\,m^{-2}}$; thereafter, the temperature distribution on the collector will be analyzed to determine the possibility of recovering wasted heat only by radiation heat transfer. It is obvious that the value obtained from Equation 7 does not represent the rate of radiative heat flux on the collector; rather, it is simply the boundary condition required to close the system of equations. The actual radiative thermal power flux on the collector depends not only on radiation, but also on the amount of heat transported by convection. It is then expected that the radiative power flux calculated by the CFD tool will be different from the initial value estimated from Equation 7. In addition to the boundary conditions, to solve Equation 5 it is assumed that the air behaves as an ideal gas (i.e. it obeys to $P = \rho RT$). It is important to mention that the objective of this work consists on the evaluation of heat transfer from the sidewall to a heat collector of a Stirling engine; therefore, the magnetohydrodynamics processes within the cell itself are not included in the simulations[4].

As mentioned above, the gas region contains four air-inlet nozzles (see the Figure 3.1 and Figure 3.2). Inlet conditions of the air velocity, temperature, turbulent kinetic energy and dissipation rate as well as turbulence frequency are specified, while the inlet pressure gradient is set to 0 $\mathrm{kPa\,m^{-1}}$ [19]. The inlet turbulent kinetic energy is estimated by assuming a turbulence intensity I of 5%; thus, $k \approx \frac{3}{2}\left(IU_o\right)^2$, with U_o equal to the inlet average velocity. When the $k\varepsilon$ turbulence model is used, the inlet dissipation rate is estimated as $\varepsilon = \frac{C_\mu^{0.75}k^{1.5}}{l}$; the mixing length l is calculated as $l = 0.038d_o$, where d_o is the inlet nozzle diameter. For the $k\omega$ model, the turbulence frequency is computed as $\omega = \frac{\varepsilon}{\beta_o^* k}$ [18]. Depending on pot working conditions and on the period of the year, the velocity and the air temperature can change. Therefore, a parametric analysis of the effect of these variables is performed.

The upper cross-section of the pot (Figure 3.1) is opened to the atmosphere. Consequently, it is assumed that the outlet flow is completely developed and at this location the gradients of all variables are 0, except for the flow pressure field whose values are considered to be uniform and equal to the atmospheric pressure.

[4]The magnetic field outside the cell does not affect the cell cooling because (i) it decays with the square of the distance, (ii) the air is not a good conductor, and (iii) the air velocities is low.

In addition, at the fluid/solid interfaces, no-slip conditions are applied and it is also assumed that the gas layers in contact with solid walls are at isothermal conditions and at zero pressure gradients [19]. The boundary conditions for k, ω and ε are OpenFOAM functions that evaluate the dimensionless distance y^+ at the first cell next to the wall. When this value is higher than 30, the near-wall flow is treated according to the law of the wall; otherwise, the entire layer is solved according to the chosen turbulence model [81]. This means that the OpenFOAM wall functions can be used in both low- and high-Reynolds turbulence models. However, two aspects should be mentioned. The selected turbulence model imposes a constraint on the acceptable values of y^+; the $k\varepsilon$ model is valid for $y^+ > 30$ (i.e. in thick layers), while the $k\omega$ model can be used if $y^+ \approx 1$ (i.e. in the viscous sublayer). Furthermore, both models badly perform when $5 < y^+ < 30$; in this case, the two-layer approach and blending functions are implemented in the OpenFOAM wall function for the $k\omega$ model. The choice of the turbulence model may significantly affect the numerical simulations. According to the near-wall treatment mentioned above, the use of the $k\omega$ model seems to be more flexible than the $k\varepsilon$ one. In fact, on the one hand, it may happen that in some regions of the control volume shown in Figure 3.1, (e.g. far away from the jets), the air velocity can be slow enough that the air flow close to the walls becomes laminar. At these conditions, it is impossible to use the $k\varepsilon$ model and simultaneously respect the y^+ criterion. On the other hand, it should be mentioned that the $k\varepsilon$ model is well suited to predict turbulent free-shear flows, as is the case for air-jets [18, 19]. For these reasons, the appropriate choice of the turbulence model must be justified by a proper validation. Such a validation is presented in the following sections.

3.4.4 Validation of the numerical model

The only way to determine the most appropriate turbulence model required to solve the system of Equations 3 to 5 is to compare the simulations with experimental data. Nevertheless, data collected at the industrial plant under analysis are not available. Therefore, the proposed methodology is validated by comparing the numerical simulations with simplified analytical solutions available in the open literature. Within this framework, two interrelated physical processes can be distinguished within the control volume of Figure 3.1. Mixed convection-radiation heat transfer from constant cross-section fins and four air flow jets. In this section, we analyze these two cases in which these two phenomena are separately simulated by coupling Equations 1 and 3 to 5 by using either the $k\varepsilon$ or the standard $k\omega$ model. Afterward, the predictions are compared with the results obtained from well known analytical solutions.

The mixed convection-and-radiation heat transfer problem from constant cross-sectional fin

The first case to be discussed corresponds to the cooling of a uniform cross-sectional fin due to mixed convection-radiation heat transfer. The model presented in Section 3.4.2 is used to predict the air flow around the fin and its temperature distribution; the numerical results are compared with those obtained from the analytical solution of this kind of problem, as explained below.

The analytical model Without loss of generality, it can be assumed that the heat transfer in the fin is unidimensional; thus, the temperature T as a function of the spatial coordinate x can be evaluated by solving the following stationary non-linear differential equation:

$$\frac{\mathrm{d}^2T}{\mathrm{d}x^2} - \frac{hP}{kA} - \frac{\sigma\varepsilon P}{kA}\left(T^4 - T_\infty^4\right) = 0 \tag{8}$$

where h is the convective heat transfer coefficient, P is the perimeter of the fin, k is the thermal conductivity, A is the cross-section area, T_∞ is the air free-stream temperature and σ is the Stefan-Boltzmann constant. Shouman [82] has obtained the solution of Equation 8 by assuming a known temperature at the fin base and the heat flux on its tip, which yields:

$$\left(\frac{2\sigma\varepsilon PT_o^3}{5kA}\right)^{1/2} x = \pm\int_0^{\theta_x}\left[\theta^5 - 5\theta_s^4\theta + r\left(\theta^2 - 2\theta_s\theta + C\right)\right]^{-1/2}\mathrm{d}\theta \tag{9}$$

where T_o is the temperature at the fin tip, $\theta = \frac{T}{T_o}$, $C = g + 5\theta_s^4 - 1 + r\left(2\theta_s - 1\right)$, $r = \frac{5h}{2\sigma\varepsilon T_o^3}$ and $\left(\frac{\mathrm{d}\theta}{\mathrm{d}x}|_{x=0}\right)^2 = g\frac{2\sigma\varepsilon PT_o^3}{5kA}$. To use the Shouman's solution, a convective heat transfer coefficient is required, which certainly depends on the fin geometry. It can be estimated choosing an appropriate experimental correlation.

Validation results The cooling of a circular rod having a diameter and length of 0.05 m and 0.4 m, respectively is modelled. The base temperature is 500 °C and the fin tip is adiabatic. The fin is cooled by an air flow having a velocity is 10 $\mathrm{m\,s^{-1}}$ and a free-stream temperature of 20 °C. A value 80 $\mathrm{W\,m^{-1}\,K^{-1}}$ is used for the thermal conductivity of the fin and the convective heat transfer coefficient is estimated according to the following experimental correlation [83]:

$$\overline{\mathrm{Nu}_D} = 0.3 + \frac{0.6\mathrm{Re}_D^{1/2}\mathrm{Pr}^{1/3}}{\left[1 + (0.4/\mathrm{Pr})^{2/3}\right]^{1/4}}\left[1 + \left(\frac{\mathrm{Re}_D}{282000}\right)^{5/8}\right]^{4/5} \qquad \mathrm{Pr}\,\mathrm{Re}_D \geq 0.2 \tag{10}$$

where $\overline{\mathrm{Nu}_D}$, Re_D and Pr are the surface averaged Nusselt, Reynolds and Prandtl numbers, respectively. A Gaussian quadrature is used to approximate the integral in Equation 9; then, the numerical solution is compared with the temperature distributions obtained from two distinct cases. For the first one, the cooling flow is evaluated using the $k\varepsilon$ model, while for the second one, the $k\omega$ model is used. The comparison between the analytical and numerical simulations of the temperature distributions is shown in Figure 3.3. The error bounds shown in this figure are estimated from an error propagation analysis carried out on the correlation given by the Equation 10. This figure shows that the temperature distributions obtained by using both turbulence models agree quite well with the solution of Equation 9. Nevertheless, for a distance 0.05 m $< x <$ 0.25 m, the $k\varepsilon$ model performs better. Based on this comparison, we consider that the $k\varepsilon$ model is more suitable to handle this kind of problem.

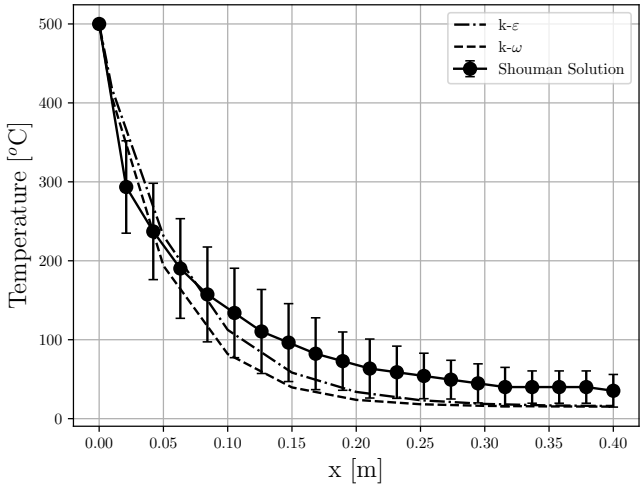

Figure 3.3 Comparison of cylindrical fin temperature distributions calculated using Equation 9 and the numerical simulations performed using both $k\varepsilon$ and $k\omega$ turbulence models.

Comparison of the simulations of velocity and temperature fields for air jet flows with analytical solutions

The second physical process that may affect the heat transfer between the sidewall and the thermal collector of the Stirling engine is due to four non-isothermal air-jet inlet flows (Figure 3.1). In this case, the principal concern consists on the determination of the most appropriate turbulence model for simulating the air-jets. To this aim, numerical simulations of a single air-jet, carried out by using the same models studied before, are compared with appropriate analytical solutions.

The analytical model Both radial and axial velocity and temperature profiles of a subsonic jet are a function of several parameters, amongst others: the orifice diameter, the type of fluid, the inlet fluid velocity u_o and the inlet fluid temperature T_o. To compare different jets, dimensionless analyses are often used. To this aim, consider a jet of a hot-fluid discharging inside a big chamber containing a stationary cold fluid. It is expected that maximum values of the velocity (u_m) and the temperature (T_m) occur at the centerline of the jet (i.e. at $y = 0$, with y the radial coordinate having its origin located at the center of nozzle's orifice), and the minimum values of the velocity (u_H) and the temperature (T_H) corresponds to those of the free flow stream (i.e. at $y \to \infty$). If $y_c\,(x)$ is the radial position at which the jet velocity is $0.5u_m$ at the axial location x, Schlichting proposed a radial dimensionless coordinate defined as [84]:

$$\xi\,(x, y) = \frac{y}{2.27 y_c\,(x)} \tag{11}$$

By introducing the dimensionless velocity $\Delta\overline{u}$ and temperature $\Delta\overline{T}$ as:

$$\Delta\overline{u} = \frac{u\,(y) - u_H}{u_m - u_H}, \quad \Delta\overline{T} = \frac{T\,(y) - T_H}{T_m - T_H} \tag{12}$$

Schlichting has demonstrated that the following equations correlate quite well $\Delta\overline{u}$ and $\Delta\overline{T}$ as function of the dimensionless radial coordinate $\xi\,(x, y)$:

$$\Delta\overline{u} = f\,(\xi) = \left(1 - \xi^{3/2}\right)^2 \tag{13}$$

$$\Delta\overline{T} = \sqrt{f\,(\xi)} = 1 - \xi^{3/2} \tag{14}$$

These relations are valid independently of the kind of fluid under analysis. In the literature, Equations 13 and 14 are usually referred to as the 3/2 law, or Schlichting formulas.

Validation results The experimental facility given in [85] is modeled to perform the numerical simulations. An air jet produced by a nozzle having a radius of 1 mm discharges in a chamber of $0.063 \times 0.063 \times 1.5$ m^3. The inlet jet velocity and temperature are 4.5 m s^{-1} and 43°C, respectively. The velocity and the temperature of the free-stream flow are 0.6 m s^{-1} and 20°C, respectively. This domain is used to simulate the air flow jet using the RANS equations coupled with either the $k\varepsilon$ or the $k\omega$ models. The predictions of these models are compared with the results of the Schlichting formulas. The dimensionless flow velocity and temperature profiles are shown in the Figure 3.4a and Figure 3.4b,

respectively.

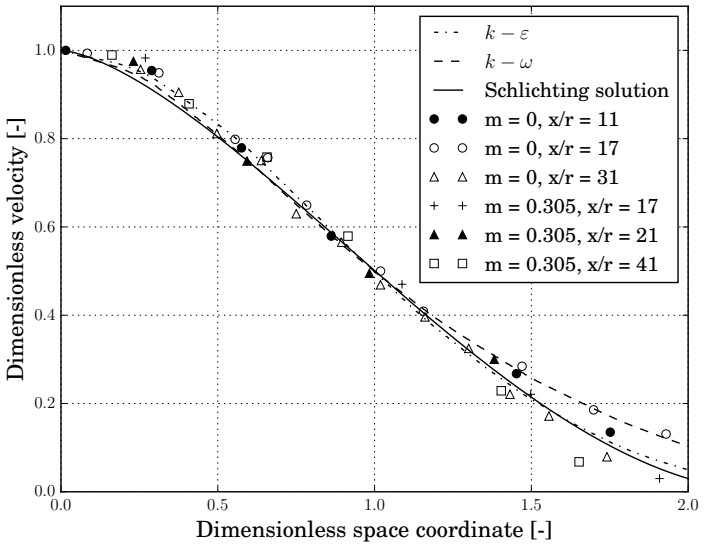

(a)

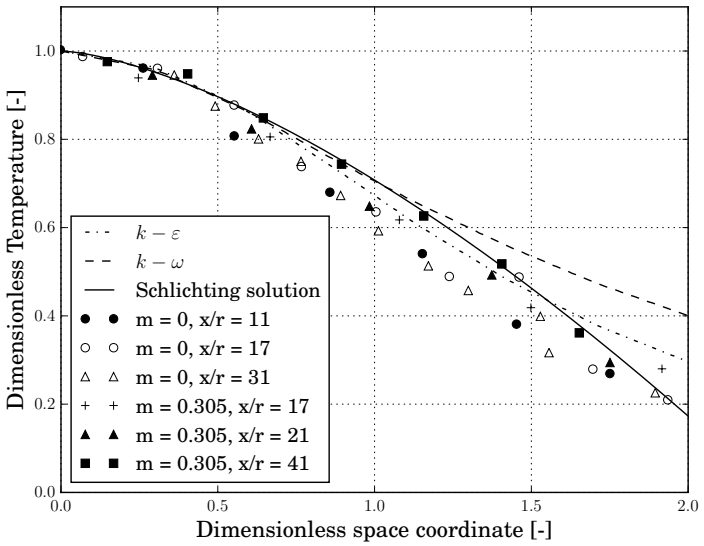

(b)

Figure 3.4 Comparison of CFD simulations with results obtained using Schlichting formulas [84]: (a) flow velocity distribution; (b) flow temperature profile.

These figures also show experimental data used to validate Schlichting formulas [84], where m is a parameter that takes into account the temperature difference between the fluid in the discharge chamber and the air-jet. It is observed that the $k\varepsilon$ turbulent model seems to better predict the free-shear air flow. In fact, the values of the Root Mean Square

(RMS) given in the Table 3.2, are lower when the $k\varepsilon$ model is used. In particular, for the temperature profiles the RMS value for the $k\omega$ model is almost twice the RMS of the $k\varepsilon$ one. Hence, based on these observations, for the rest of the work it is considered that the $k\varepsilon$ model is most suitable to perform CFD heat transfer simulations between the pot sidewall and the Stirling engine heat collector.

Table 3.2 RMS errors for the $k\varepsilon$ and $k\omega$ turbulence models.

Flow variable	RMS $(k\varepsilon)$	RMS $(k\omega)$
Velocity profiles	3.05×10^{-2}	3.42×10^{-2}
Temperature profiles	4.24×10^{-2}	7.32×10^{-2}

3.5 Modeling waste heat recovery from aluminum electrolysis cells

In agreement with the results given in Sections 3.4.4, the CFD simulations presented in this section are carried-out using the $k\varepsilon$ model. However, before discussing the numerical results, the convergence criterion applied to the simulations is briefly presented. It is important to recall that the thermophysical properties of solid materials are constant and a very low emission coefficient is arbitrarily selected for the surface of the thermal collector exposed to infrared radiation (see Table 3.1).

3.5.1 Assessment of convergence

To determine an appropriate criterion that can be applied to establish when the simulations reaches convenient converge, a preliminary air flow heat transfer test case is performed. To this purpose, both the control volume and the computational domain are same to those shown in Figure 3.1 and Figure 3.2, respectively. The boundary conditions for the test case are those presented in Section 3.4.3. Furthermore, it is assumed that the heat flux from the pot wall, the velocity of the cooling air and its temperature are fixed and equal to the values provided by the aluminum smelter under analysis. Under these conditions, several simulations are performed and the variation of the residuals as well as the radiative flux absorbed by the collector are monitored as a function of the number of iterations. Figure 3.5a shows the residuals for the turbulent dissipation rate ε, the enthalpies of the solid regions h, the turbulent kinetic energy k, the flow pressure P and the three components of the flow velocity U. Even though some of the residuals are higher than 10^{-4}, they do not increase after 5000 iterations; this means that the simulation does not diverge. Moreover, after 20,000 iterations, all the residuals become constant.

Figure 3.5b shows the variation the radiative power flux $\dot{q}_r$ absorbed by the heat collector as a function of the number of iterations; it is quite clear that this key variable becomes constant after 15,000 iterations. For these reasons, it is considered that a final solution is satisfactorily achieved at the 20,000th iteration.

3.5.2 Numerical results

As previously mentioned, the operation of the electrolysis cells is subjected to different working conditions; thus, the cooling of the pot sidewalls may change accordingly. For this reason, in this section, different sidewall thermal power flux as well as air cooling conditions will be applied and their effects on the recovered thermal power will be analyzed. Since we are interested in recovering the radiative thermal losses using a plate heat collector, the mean temperature and the heat flux upon this component are evaluated as a function of different working conditions. Figure 3.6 shows how the sidewall thermal power flux affects the heat recovered by the collector, while the effects of the cooling air inlet flow velocities and temperatures are presented in Figure 3.7a and Figure 3.7b, respectively. Also, these figures show the temperature of the sidewall T_{sw} for the different cooling scenarios.

As expected, Figure 3.6 shows that both the average temperature and the radiation flux upon the collector increase with increasing the thermal power flux from the sidewalls. From this figure, it can be stated that when the flux from the pot increases (that is, when it is necessary to cool further the electrolysis cell), the average temperature of the sidewall T_{sw} increases as well. Consequently, both the average temperature and the thermal radiation upon the collector increase almost linearly with increasing the sidewall thermal power flux (this agrees with the theory, because radiative heat flux is proportional to σT^4).

Similar considerations can be confirmed from Figure 3.7. It is well known that the efficient cooling of the pot sidewall by convective heat transfer is achieved by increasing the air-nozzle inlet velocity and by reducing the air temperature. Figure 3.7 clearly shows that when the air velocity increases (or when the air temperature decreases), the temperature of the pot sidewall decreases. Therefore, both the average temperature and the flux upon the heat collector decrease.

The parametric study presented in the Figure 3.6 and Figure 3.7 indicates the conditions under which the recovery of wasted heat by radiation may be useful (i.e. when the sidewall average temperature is high). However, Equation 7 shows that radiation flux is not only a function of the temperature difference between the sidewall and the collector, but also of the view factors F_{ij}, which strongly depend on the geometrical configuration of the surfaces. The heat flux between two surfaces increases with increasing the view factors, which

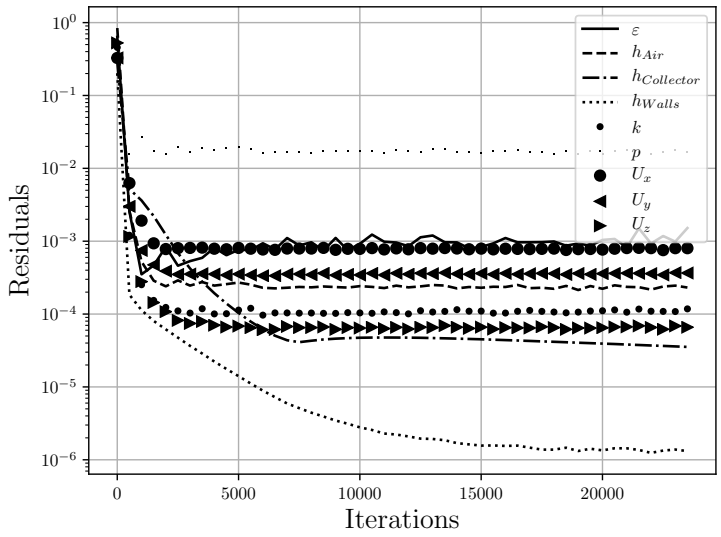

(a)

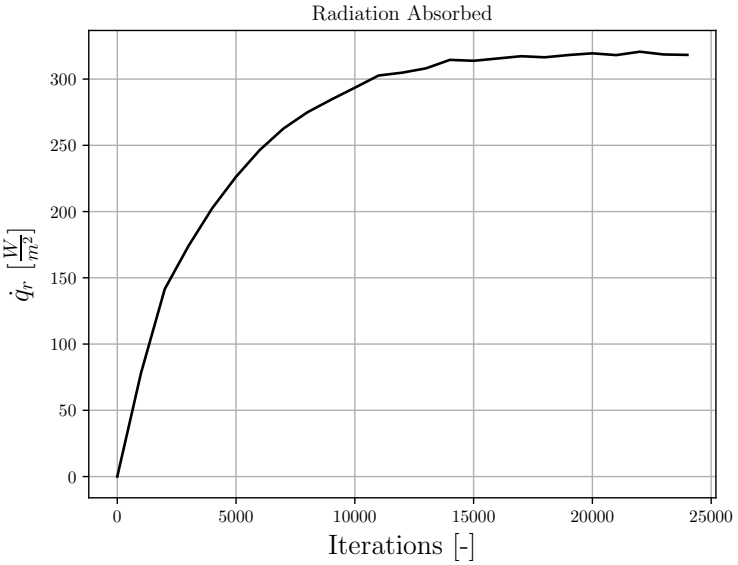

(b)

Figure 3.5 Convergence behavior as a function of the number of iterations. (a) variations of the residuals; (b) radiative thermal power at the Stirling engine heat collector.

in turn are inversely proportional to the square of the distance between the surfaces [40]. Therefore, a substantial increase of the heat flux and the average temperature on the collector should be expected by approaching the collector to the sidewall. For this reason, the same case studied in Section 3.5.1 is simulated by reducing by half the distance between the collector and the sidewall; the results are summarized in Table 3.3. As expected, it

can be observed that approaching the collector to the sidewall surface increases the surface averaged temperature on the heat collector T_c. However, at these conditions, it can be also expected an increase in the heat flux to occur. According to the implemented CFD code, the radiative flux $\dot{q}_r$ barely changes. This behavior is probably due to a decrease of the control volume. In fact, since the inlet air velocity is kept constant, for a smaller volume, the air flow velocities increase everywhere which in turn produce a more efficient forced convection cooling of the pot shell. This causes the average temperature on the sidewall surface T_{sw} to decrease and in agreement with the considerations discussed in the previous paragraph, the radiative flux upon the collector must also decrease.

Table 3.3 Effect of the distance between the pot sidewall and the surface of the thermal collector exposed to radiation heat transfer ($u_{jet} = 25\ \mathrm{m\,s^{-1}}$, $T_{jet} = 20°\mathrm{C}$).

Distance	T_c (°C)	$\dot{q}_r$ ($\mathrm{W\,m^{-2}}$)	T_{sw} (°C)
$\frac{\Delta x}{2}$	98.4	313.7	313.9
Δx	85.8	318.8	349.5

It is reasonable to conclude that the increase of the average temperature T_c, as given in this table, is mainly due to the reduction of the distance between the collector and the sidewall. Nonetheless, additional improvements of this temperature can be accomplished by reducing the inlet air flow velocity as well as its temperature (Figure 3.7). It should be mentioned that decreasing the collector distance even further should not enhance the

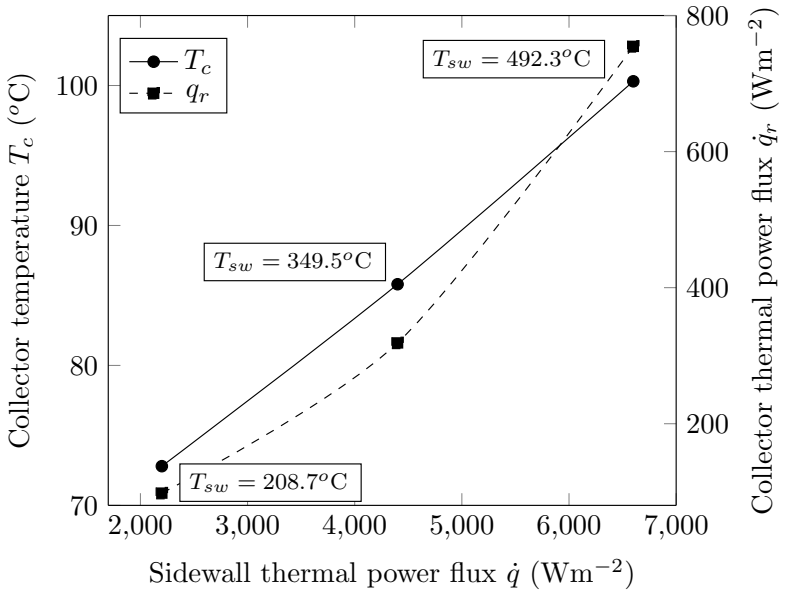

Figure 3.6 Effect of the sidewall thermal power flux on the collector average temperature and the thermal power flux recovered by radiation.

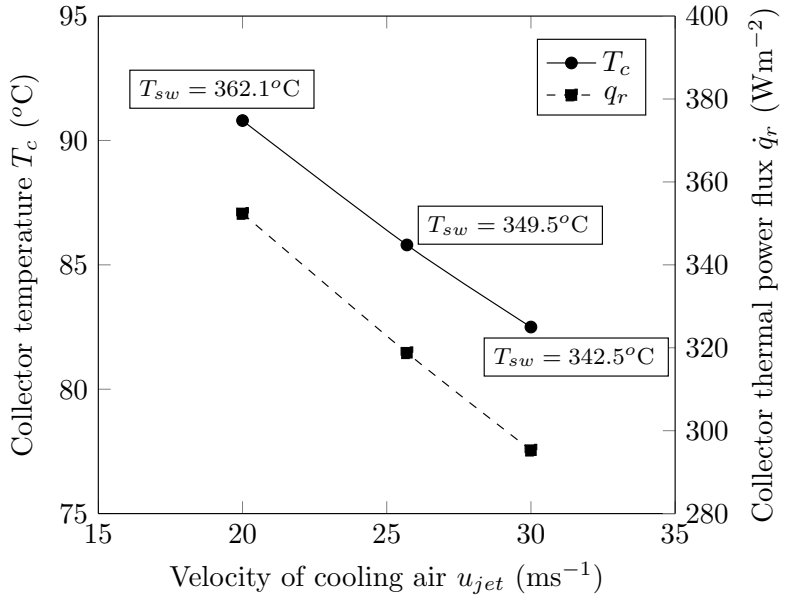

(a)

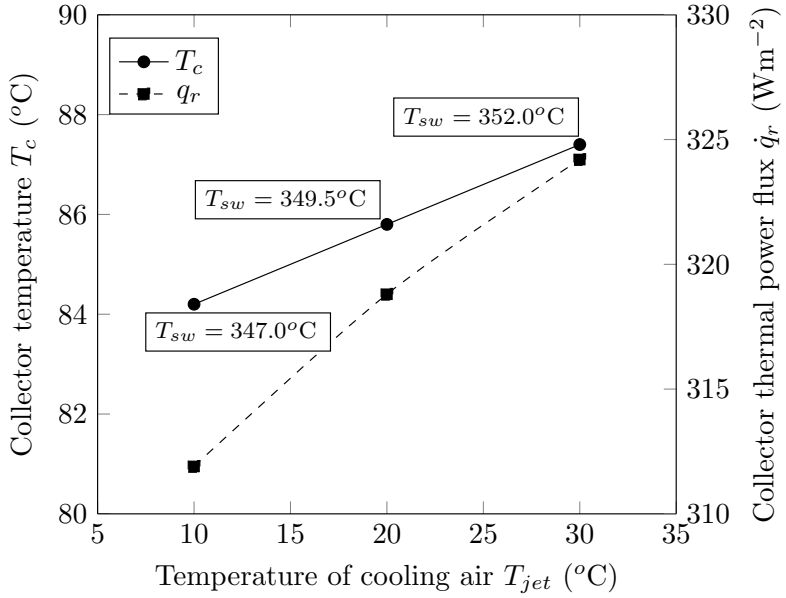

(b)

Figure 3.7 Effect of inlet air cooling conditions on the thermal collector: (a) average temperature and radiation flux upon the collector as a function of the air-nozzle inlet velocity; (b) collector average surface temperature.

efficiency of the heat recovery system without changing the air inlet conditions. In fact, the collector will increase its temperature (as shown in Table 3.3), but, at the same time, the effects of the cooling air become more important. To highlight the importance of forced convection, the average temperature on the surface of the collector is estimated by neglecting this heat transfer mode. For this case, it is not necessary to solve the RANS

equations; the energy balance is governed only by Equation 7. By applying this equation and if the distance is maintained equal to $\frac{\Delta x}{2}$, the average surface temperature of the collector is approximately equal to 113°C. This temperature is considerably higher than that obtained for the similar case shown in the Table 3.3. Therefore, it can be stated that the heat collector to be used by a Stirling engine will reach lower averaged temperatures when radiation heat transfer from the sidewall is combined with convection (i.e. when the effects of convection cannot be neglected). It is obvious, that the control of these conditions concerns operation and safety requirements of each specific aluminum production plants. Nevertheless, for a wide range of flow conditions, the results shown in Figure 3.7 provide quite interesting values of power flux that could be converted into useful mechanical and/or electrical power.

3.6 Conversion of sidewall thermal losses into useful power

In this section, the conversion of the thermal wastes into useful power by means of a Stirling engine is discussed. As previously mentioned, two engine scenarios are considered: i) the engine thermal collector recovers heat only by radiation and ii) the engine heater is in direct thermal contact to the pot sidewall.

Considering the first scenario, for an air inlet temperature of about 20°C and a velocity of 25 $\mathrm{m\,s^{-1}}$, in agreement to pot's operation conditions (see Section 3.5.2) and results shown in Figure 3.6 and Figure 3.7, the engine collector can recover about 318.8 $\mathrm{W\,m^{-2}}$, at an average surface temperature between 80 to 98°C. Note that since the thermal collector is in contact with the lateral beams of the pot (see Figure 3.1), a non-negligible fraction of thermal power can be transferred by conduction as well. Nevertheless, the purpose of this work consists of evaluating the amount of heat that could be gained by radiation alone. It is thus necessary to determine the appropriate Stirling system that can run at this condition. Within this view point, the engine proposed by Tavakolpour et al. [59] designed for working with solar radiation, or the one proposed by Kato [60] designed for working with maximum temperatures ranged between 65 and 95°C, could be used. For a regenerator efficiency of 90%, Tavakolpour et al. [59] have estimated that the overall efficiency of the proposed engine is about 4.5% (this value is not available for Kato's system). A simple calculation based on the available thermal power flux applied to the Tavakolpour et al.'s engine demonstrates that the latter can convert the thermal power to about 14.3 $\mathrm{W\,m^{-2}}$ of mechanical power.

For the second scenario, it is assumed that the hot source of the engine can be in direct

thermal contact with the sidewall; thus, the thermal losses are transferred to the engine by conduction. The temperature of the thermal source is assumed to be equal to that of the sidewall (i.e. the effects due to the thermal contact resistances are neglected). According to the CFD simulation presented in the previous section, when the pot heat flux is around 4.4 $\mathrm{kW\,m^{-2}}$, the temperature of the sidewall is about 350°C. At this temperature, it is possible to drive the Stirling proposed by Karabulut et al. [73], whose hot temperature is 300°C, or the engine described by Dochat [74], whose hot temperature is 350°C. The overall efficiency of Karabulut et al.'s engine is estimated at 15%, while that of the Dochat's is 25%. If one of these units are designed to convert the pot sidewall thermal losses, the useful mechanical power would vary between 0.66 and 1.1 $\mathrm{W\,m^{-2}}$. It must be pointed out that the recovery of the thermal losses by direct thermal conduction is also feasible by using thermoelectric modules. However, it is well known that that their efficiency is relatively low; assuming an optimistic value for the figure of merit ($Z = 1.2 \times 10^{-3}$ $\mathrm{K^{-1}}$, which is quite high), the thermoelectric converter ideal efficiency will be 7.3%.

The efficiency of the Tavakolpour et al.'s Stirling engine [59] is lower than that of the thermoelectric modules attached on the pot sidewall. In spite of that, an efficiency of 7.3% should be considered as an upper limit for the thermoelectric generator, while Stirling engines can easily attain much higher values. For instance, the LTD machine designed by Formosa et al. [13] has an efficiency equal to one half that of an ideal unit working under the same temperature differential. If such an engine could be manufactured to recover heat at 80°C, its efficiency could be as high as 11% that is, half the efficiency of a Carnot engine operating at the same temperature (i.e. about 22%).

The efficiency of thermoelectric modules in direct thermal contact to the sidewall are substantially lower than an equivalent Stirling engine working at the same hot temperature. Therefore, using Stirling engines to recover heat by conduction constitutes a quite interesting alternative. If a power flux of around one kilowatt per square meter is available, it can be converted and used to satisfy other energy needs required by aluminum smelters (e.g. lighting, air conditioning, etc.). Nonetheless, it should be reminded that the cooling required by electrolysis cells are not necessarily constant during their operation. Consequently, the energy recovery system must be controlled in such a way that it must collect only the wasted portion of the energy, without affecting neither the plant operation nor the safety requirements. It is evident that the control of the sidewall temperature could affect the dynamic response of the Stirling engine. In such a case, the simulation should integrate a dynamic model of this unit as well [23]. Within this context, according to Figure 3.1 it is obvious that the allocation of a Stirling engine in contact with the sidewall is impossible due to the presence of the vertical fins. In addition to this major drawback,

the location of these engines should not block the access of the cooling air, which can be required to guarantee the correct operation of each electrolysis cell (i.e. to avoid excessive pot wall temperatures).

Plant control and safety purposes make the recovery of heat wastes by radiation using Stirling engines a more convenient alternative. It has been demonstrated that the temperatures of the sidewall and the engine thermal collector change by varying the distance (see Table 3.3). Therefore, it should be possible to determine an optimum distance from the sidewall that assures the most appropriate temperature conditions. This task will necessitate many simulations as well as the use of an optimization technique. The resulting information, however, could certainly help to establish a relation between these variables and thus to propose a controlling system of the sidewall temperature based on the distance between the sidewall and the radiative heat collector. Hence, it can be assured that the operation of the Stirling engine will not cause any excessive cooling of the pot.

Even though the heat recovered by thermal radiation and its conversion using Stirling is relatively low, the overall efficiency could be increased by increasing the thermal collector temperature. On the one hand, this improvement can be moderately satisfied by approaching further the thermal collector to the sidewall and by reducing the available energy which is normally transported away by convection. On the other hand, there exists the possibility of designing a more appropriate kind of thermal collector. The objective of the present work is to present a proof of concept based on the worst possible operating conditions. For this reason, a plate thermal collector having a very low emissivity is selected. In turn, the use of a concentrator with higher emissivity should be a better option to be applied. In fact, the use of these types of configurations, coupled to Stirling engine have been widely studied [86].

3.7 Conclusion

This paper presents a proof of concept intended to recover thermal wastes, available in the pots of aluminum smelters, by using Stirling engines. The analysis is focused on studying the thermal behavior of the sidewalls, which are currently cooled by mixed convection-radiation heat transfer. Within this framework, only the portion of radiative wastes recovered by means of the simplest possible thermal collector (i.e. a metallic plate having very low emissivity) is used. OpenFOAM 5.0 is selected as a CFD tool to simulate heat recovery by radiation under different conditions.

Before performing pot numerical simulations, the effects of different turbulence models are numerically tested and the results are compared with appropriate analytical solutions.

It is thus determined that the $k\varepsilon$ model is the most appropriate one for treating the proposed problem. Therefore, this model is coupled with the RANS equations to simulate the heat transfer in a typical pot of an aluminum smelter. A parametric study is performed to investigate the working conditions under which the thermodynamic potential of the recovered wastes could be useful to convert them into useful power. The conversion of the thermal wastes by using Stirling engines is studied for two scenarios: a Stirling engine driven by thermal radiation, and a Stirling engine driven by direct heat conduction.
It was demonstrated that the temperature of the radiative collector may be high enough to be coupled to some existing LTD Stirling engines described in the open literature. However, to increase their efficiencies, it is mandatory to increase the thermal collector temperature. Such a task could be achieved, amongst others by: using other types of collectors (e.g. concentrators), approaching the heat recovery system to the pot sidewall or reducing the heat transported by forced convection. It is also demonstrated that the use of some Stirling units placed in direct thermal contact to the pot sidewall could permit energy conversion rates as high as 1.1 $\mathrm{kW\,m^{-2}}$. Nevertheless, their applications are almost impossible without introducing major modifications in the pot itself (i.e. eliminate the lateral vertical fins). In addition, this solution can strongly affect the safe operation of the plant, because it interferes with the entrance of the cooling air.
So far, this paper has demonstrated that it is possible to recover heat wastes from aluminum electrolysis cells by using Stirling engines. Nevertheless, to guarantee appropriate operation and safety conditions, these units must be placed at a convenient distance from the sidewall; consequently, heat must be recovered by radiation heat transfer. Improving further the overall efficiency of this process requires the use of better heat collectors and the optimization of both the distance between the engine and the side wall, as well as the air inlet cooling conditions.

CHAPTER 4

MODELING THE OPERATION OF STIRLING ENGINES BY MEANS OF AN EQUIVALENT ELECTRICAL CIRCUIT

Avant-propos

Auteurs et affiliation :

- Franco Cascella, étudiant au doctorat, Département de génie mécanique, Université de Sherbrooke ;
- Mikhail Sorin, professeur, Département de génie mécanique, Université de Sherbrooke ;
- Fabien Formosa, professeur, Université Savoie Mont Blanc ;
- Alberto Teyssedou, professeur, Institut de génie nucléaire, Département de génie physique, Polytechnique Montréal.

Date d'acceptation : 9 August 2017.
État de l'acceptation : version finale publiée.
Revue : Energy Conversion and Management.
Référence : Cascella, F., Sorin, M., Formosa, F. and Teyssedou, A., 2017. Modeling the dynamic and thermodynamic operation of Stirling engines by means of an equivalent electrical circuit. *Energy Conversion and Management*, 150, pp.295-303.
Titre français : Modélisation du fonctionnement dynamique et thermodynamique des moteurs Stirling à l'aide d'un circuit électrique équivalent.
Titre anglais : Modeling the dynamic and thermodynamic operation of Stirling engines by means of an equivalent electrical circuit.
Contribution au document : Dans ce chapitre, la seconde contribution scientifique de cette recherche doctorale est présentée. Il s'agit du premier article rédigé dans le cadre de cette recherche et qui est présente à la suite de la deuxième publication pour conserver la cohérence de la thèse.
Dans cet article, la description et la validation d'un modèle d'analogie électrique utilisé

pour prédire le comportement des machines Stirling sont traitées. La nouveauté de ce modèle est l'introduction de l'équation de conservation l'énergie dans le modèle d'analogie électrique. De cette façon, les effets thermiques de la machine sont introduits explicitement dans le modèle.

Résumé français : Les moteurs Stirling sont intrinsèquement efficaces ; leurs cycles thermodynamiques sont les seuls à atteindre l'efficacité de Carnot. Ainsi, cette technologie est intéressante car elle fonctionne sous n'importe quelle différence de température entre les sources chaudes et froides. Pour ces raisons, ces moteurs peuvent être considérés comme des systèmes de conversion de fiable énergie pour promouvoir la conversion de la chaleur résiduelle générée par les installations industrielles. Le besoin d'un modèle pour prédire le comportement de ces moteurs est primordial. Néanmoins, une grande difficulté est rencontrée dans le développement d'un tel modèle car il n'est pas simple de prendre en compte les effets thermodynamiques et dynamiques, qui sont couplés dans ces moteurs. C'est la raison principale pour laquelle plusieurs modèles utilisent des analogies électriques pour décrire les moteurs Stirling (en particulier les machines à piston libre) ; en supposant que la pression est équivalente à une tension et le débit à un courant électrique, une analyse du moteur peut être effectuée en tenant compte des effets dynamiques et thermodynamiques. Dans cet article, un circuit électrique dont le comportement est équivalent à celui du moteur est dérivé à partir de la théorie de l'analogie électrique. Pour ce faire, un modèle d'analogie électrique basé sur les trois lois de conservation (masse, quantité de mouvement et énergie) est proposée. Les résultats obtenus avec le modèle proposé sont en accord avec données expérimentales collectées au centre de recherche Lewis de la NASA pour un moteur Stirling à piston libre, c'est-à-dire le moteur RE-1000.

4.1 Abstract

The Stirling engines are inherently efficient; their thermodynamic cycles reach the Carnot efficiency. These technologies are suitable to operate under any low temperature difference between the hot and the cold sources. For these reasons, these engines can be considered as reliable power conversion systems to promote the conversion of low-grade waste heat generated by industrial plants. The need of a model to predict the behavior of these engines is of primary importance. Nevertheless, a great difficulty is encountered in developing such a model since it is not simple to take into account coupled thermodynamic and dynamic effects. This is the main reason why several models make use of electrical analogies to describe Stirling engines (in particular, free-piston machines): by assuming the pressure equivalent to a electrical potential and the flow rate to an electrical current, a coupled dynamic-thermodynamic analysis of the engine can be performed. In this paper, an electrical circuit whose behaviour is equivalent to that of the engine is derived from the electrical analogy theory. To this aim, we propose an electrical analogy model based on the three conservation laws (mass, momentum and energy). Since limited experimental information is available in the open literature, the results obtained with the proposed model are compared with the experimental data collected at the NASA Lewis Research centre for a FPSE i.e. the RE-1000 engine.

Keywords: Electrical analogy, FPSE, RE-1000, conservation equations, equivalent circuit, Laplace transform.

4.2 Introduction

Many industrial plants are energy intensive. This aspect has brought many engineers to investigate solutions to enhance the energy efficiency; such an improvement cannot be reached by simply reducing the energy consumption, as the latter is usually proportional to the production of output goods (e.g. the aluminum production in a smelter is linearly proportional to its energy consumption). Therefore, recovering thermal wastes, which are usually rejected to the environment, is of primary importance. They can be used for heating purposes (e.g. district heating) or converted into useful work, by means of an appropriate conversion technology (for instance, by using Organic Rankine Cycle engines, thermoelectric modules or Stirling engines) [11].

Amongst all these technologies, Stirling engines have gained the interest of the scientific community [14, 48]. Several reasons justify this concern. An analysis of the ideal Stirling cycle shows that it reaches the Carnot-efficiency limit, since it undergoes two isothermal

and two isochoric processes [31, 87]. Another important aspect of Stirling engines is their ability of converting any heat source into useful work. Several patents of Stirling engines powered by solar energy [55], as well as by fossil fuels [14, 15, 48], are available in the open literature. Moreover, some of them are able to work under low temperature differential [47, 51, 56] . For instance, Formosa et al. [13] assembled a Stirling engine for which the hot source is at 150°C and the cold one is at 40°C. This characteristic makes these systems attractive for low-potential energy recovery purposes [56]. Furthermore, the Stirling engine technology is reliable at relatively low cost [13, 14, 48, 56] and satisfies several industrial safety requirements, as the working fluid is not hazardous for metallurgic plants (i.e. the working fluid may be a gas, such as air, helium or nitrogen).

The need of trustworthy models able to predict the behaviour of these engines is mandatory. According to the most recent reviews [56], two modelling approaches are available in the open literature: those based on the heat transfer analysis and those based on the electrical analogy theory. The well known Schmidt's analysis [88] falls into the heat-transfer category model; it describes the thermodynamics of the engine (expansion and compression chambers, heat exchangers), but it does not take into account the mechanical dynamics (i.e. the power piston and the displacer are not modelled). Thus, it is important to couple the aforementioned analysis with the Newton's laws of the moving parts. This approach has been firstly proposed by Urieli and Berchowitz [47], who studied several units; however, they observed noticeable errors between the predictions and the experimental data [47]. For instance, their model over predicts the power output of a GPU-3 (General Motors Ground Power Unit) system with an error of at least 69%.

The second kind of model involves the use of the electrical analogy theory. The aim of this approach is to establish an analogy between the current with the volumetric flow rate and the voltage differentials with pressure variations. Such theory has been proposed by Swift [68] in order to predict the behaviour of thermoacoustic systems. Moreover, the electrical analogy theory can be used to obtain an equivalent electrical network for free-piston systems. The electrical analogy theory [68] has been extensively validated in the literature. In particular, it is suitable to predict the behaviour of thermoacoustic Stirling refrigerators. Huang and Chuang have used it to develop a linear model for an orifice pulse tube refrigerator [89]. Nika and Bailly have evaluated the equivalent electrical circuit of a double inlet miniature pulse tube refrigerator [90, 91]. Similar works have been conducted, amongst others, by Iwase et al. [92] and by Tan and Dang [93].

Despite its application that is limited to thermoacoustic devices, the electrical analogy theory is interesting for Stirling engines too. Effectively, the transformations that the working gas undergoes in a thermoacoustic engine (both heat engines and refrigerators)

are equivalent to those of a conventional Stirling system. However, it cannot be used to describe a conventional Stirling one because in thermoacoustic machines, there are no moving pistons. Thus, in order to describe a Stirling engine, the thermoacoustic approach can be used only if it is coupled to an appropriate dynamical analysis. Formosa et al. [13] proposed such a model; according to their theoretical approach, which has been extended by Féniès et al. [94], the dynamical effects are analyzed by means of the Newton's equation applied to the moving parts (following the approach given by Urieli and Berchowitz) [47]. They have applied the continuity and the momentum conservation equations to evaluate the gas pressure and velocity in the expansion and compression chambers, in the heater, in the cooler and in the regenerator [13, 94].

In this paper, we present a theoretical approach that can be used to predict the behaviour of FPSEs. We propose to extend the Formosa et al.'s modelling approach by introducing the energy equations for the heat exchangers and the regenerator. In order to do that, the thermoacoustic approach of Huang and Chuang [89] is considered. It is noteworthy to highlight that the analysis of the energy equation has the only effect of introducing a source term, while the resistors, the capacitor and the inductor associated to the mass and the momentum conservation equations remain unchanged [68, 95]. A detailed description of the model is presented in Section 4.3; thereafter, a comparison of the predictions with the data collected for a FPSE [49] is outlined in Section 4.4. A parametric study is performed to investigate the influence of main design parameters, such as the mean gas pressure, the hot and cold gas temperatures in the heat exchangers. Finally, the predicted behavior of the engine is used to compute the output power.

4.3 Description of the model

The electrical analogy between the flow rate/electrical current and the pressure variations/voltage differentials is outlined. To model the thermodynamics effects occurring in any component of a Stirling engine, a simplified sketch is shown in Figure 4.1. It is essentially formed by a compression piston, two heat exchangers separated by a regenerator chamber and an expansion device (i.e. a displacer). The following conservation equations [96] are applied to each mechanical component; the continuity:

$$\frac{\partial \rho}{\partial \tau} + \nabla \cdot \rho \vec{u} = 0 \tag{1}$$

the momentum:

$$\frac{\partial \rho \vec{u}}{\partial \tau} + \nabla \cdot \rho \vec{u} \otimes \vec{u} = -\nabla p + \mu \nabla^2 \vec{u} \tag{2}$$

the energy conservation:

$$\rho c_p \left(\frac{\partial t}{\partial \tau} + \nabla \cdot t\vec{u} \right) - \left(\frac{\partial p}{\partial \tau} + \nabla \cdot p\vec{u} \right) = \nabla \cdot \vec{q} \tag{3}$$

In the momentum equation, it is assumed that $\frac{\partial \rho \vec{u}}{\partial \tau} \gg \nabla \rho \vec{u} \otimes \vec{u}$, according to the modelling approach proposed by Swift [68]. Moreover, the hypothesis that the variables under analysis (flow rate, gas pressure and temperature) can be written as the summation of a mean and an oscillatory term, where only the latter depends on the temporal coordinate, is used [97]. Therefore, the generic form of a variable ψ is written as $\psi(x,\tau) = \overline{\psi}(x) + \psi'(x,\tau)$. Nonetheless, by assuming a harmonic velocity, the velocity mean value is null; also, the mean value of the pressure cannot be a function of of any spatial coordinate (otherwise, the acceleration of the gas would take place) [68].
In order to solve the simplified system of Equations 1, 2 and 3, a state equation is necessary; since the working gas of a Stirling engine may be helium, argon or air, the ideal gas law is introduced ($p = \rho \overline{R} t$). Thus, the thermodynamic properties of the working gas (i.e. density, thermal conductivity and heat capacity) will be evaluated for each component as a function of the local value of the temperature and mean pressure. With these hypotheses, an electrical analogy model for the time-dependent equations is obtained. The equations listed above can be used to model the expansion and the compression chambers, the heater, the cooler and the regenerator of a Stirling engine. In addition, from the momentum equation, the Newton's second law is obtained. Therefore, this equation is used to describe the dynamics of the system, that is, the effects of the motions of both the power piston and the displacer (Figure 4.1). In turn, the conservation of mechanical into electrical energy requires a generator unit (i.e. an alternator). This kind of component has been extensively analyzed in the open literature [62, 63, 98]. For this reason, and despite its relevance, it is not taken into account in the following modeling approach.

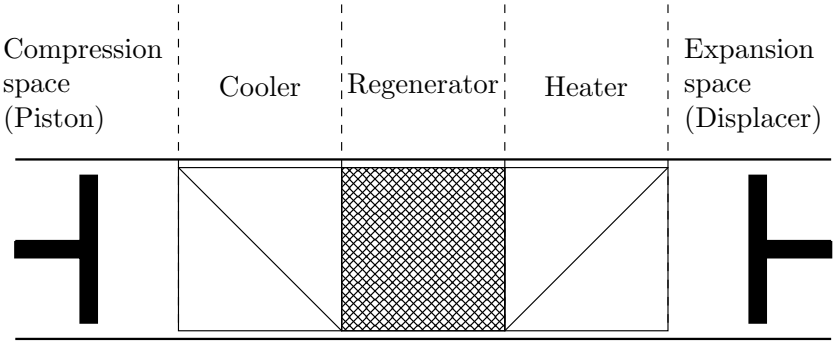

Figure 4.1 Simplified sketch of a Stirling engine.

As previously mentioned, the model described below can be used to obtain an equivalent electrical circuit for the engine. In this paper, the equivalent electrical network for the RE-1000 free piston Stirling unit [49], for which several experimental data are available, is presented. A simplified schematic of this system is presented in Figure 4.2; it uses helium as working fluid. The thermophysical properties for this gas can be estimated by using a proper thermodynamic library [99]. The gas flows back and forth along the expansion chamber throughout the heater, the regenerator, the cooler and the compression chamber. As shown in this figure, the pressure variations of the working gas in the compression chamber move a power piston. The total power produced by this piston is dissipated by friction in the damper shown in the figure. The displacer assures the gas flow from the expansion to the compression chamber (and *vice versa*) to occur. Its oscillatory motion is maintained by the spring effects of the working gas [47, 49, 64].

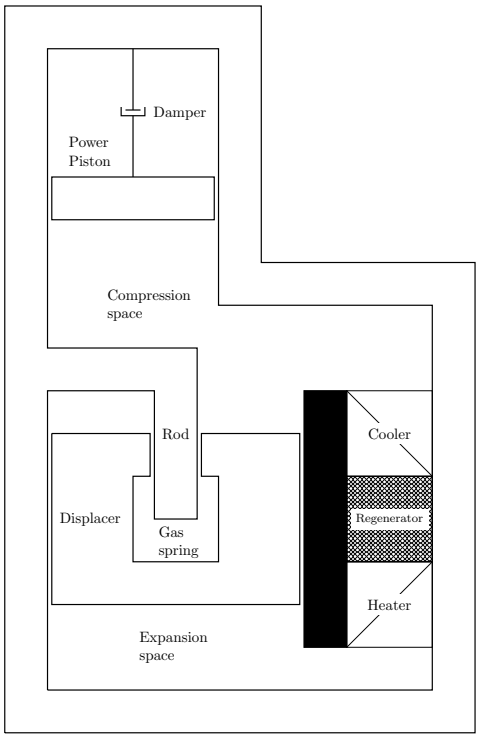

Figure 4.2 Sketch of the engine under analysis [49].

4.3.1 Expansion and compression chambers

To obtain the electrical-analogy equations for both the expansion and the compression chambers, it is assumed that within these components, the pressure is spatially uniform and that the gas temperature is constant [13, 89]. Therefore, only the continuity equation

is considered. Taking into account $p = \rho \overline{R} t$ and $\dot{v} = Au$, Equation 1 is rewritten as:

$$\frac{1}{\overline{R}\overline{t}} \frac{\partial p\left(x,\tau\right)}{\partial \tau} + \frac{\partial}{\partial x}\left[\rho \frac{\dot{v}\left(x,\tau\right)}{A}\right] = 0 \tag{4}$$

Since the mean value of the pressure is not a function of time, we get:

$$\frac{A}{\overline{R}\overline{t}} \frac{\partial p'\left(x,\tau\right)}{\partial \tau} + \frac{\partial \rho \dot{v}'\left(x,\tau\right)}{\partial x} = 0 \tag{5}$$

By introducing a capacitance C_{ec}, defined as:

$$C_{ec} = \frac{A\Delta x}{\overline{p}} \tag{6}$$

and recalling that the density is estimated by means of the ideal gas law, Equation 5 can be integrated over the spatial coordinate, hence:

$$C_{ec} \frac{\partial p'\left(x,\tau\right)}{\partial \tau} + \Delta \dot{v}'\left(x,\tau\right) = 0 \tag{7}$$

with $\Delta \dot{v}'\left(x,\tau\right) = \dot{v}'\left(x_{out},\tau\right) - \dot{v}'\left(x_{in},\tau\right)$. This equation has the same form of the differential equation describing the relationship between the current and the voltage drop in an electrical circuit. Thus, an equivalent electrical circuit shown in Figure 4.3 is derived from Equation 7.

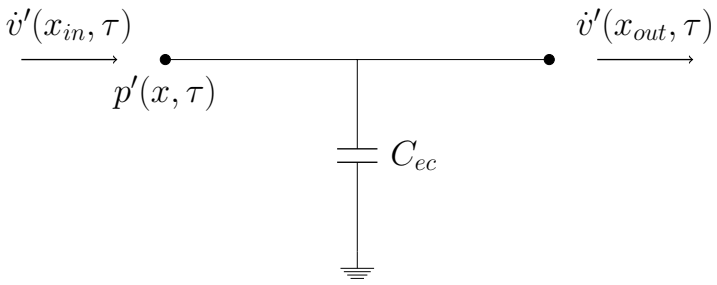

Figure 4.3 Equivalent circuit for the compression/expansion chamber.

4.3.2 Heater and cooler

In the heat exchangers, the pressure and the temperature variations over the spatial coordinate cannot be neglected; therefore, all conservation equations must be considered. Since $\dot{v} = Au$, $\nabla p = \frac{\partial p'(x,\tau)}{\partial x}$ and that $\mu \frac{\partial^2 u}{\partial x^2} = \frac{\mu}{A} \frac{\partial^2 \dot{v}'(x,\tau)}{\partial x^2} = \frac{\kappa \rho}{A} \dot{v}'\left(x,\tau\right)$ [89, 100], then, Equation 2 becomes:

$$\frac{\rho}{A} \frac{\partial \dot{v}'\left(x,\tau\right)}{\partial \tau} + \frac{\partial p'\left(x,\tau\right)}{\partial x} + \frac{\kappa \rho}{A} \dot{v}'\left(x,\tau\right) = 0 \tag{8}$$

where κ (s^{-1}) is an experimental coefficient given by Roach and Bell [101] for oscillatory flows:

$$\kappa = 0.1556 \mathrm{Re}_{max}^{-0.201} \frac{u_{max}}{d_h} \tag{9}$$

Re_{max} is the Reynolds number evaluated at the maximum velocity of the oscillating flow (u_{max}) and d_h is the hydraulic diameter. To determine u_{max}, we assume that the velocity is governed by a periodic function (i.e. a sine wave); therefore, from the known value of its root mean square u_{rms}, the amplitude of such a wave is found according to the following relationship [95]:

$$u_{max} = \sqrt{2} u_{rms} \tag{10}$$

The momentum equation can be integrated over the spatial coordinate, by introducing a resistance R_{hk} and an inductance L_{hk} defined as:

$$R_{hk} = \frac{\kappa \rho \Delta x}{A}, \quad L_{hk} = \frac{\rho \Delta x}{A} \tag{11}$$

thus,

$$-\Delta p'(x,\tau) = L_{hk} \frac{\partial \dot{v}'(x,\tau)}{\partial \tau} + R_{hk} \dot{v}'(x,\tau) \tag{12}$$

which is equivalent to the differential equation describing an electrical circuit having a resistance and an inductance connected in series. Let us now consider the continuity equation; introducing the ideal gas law into Equation 1 and neglecting second order terms, we obtain [100]:

$$\frac{1}{\overline{R}\overline{t}^2} \left[\overline{t} \frac{\partial p'(x,\tau)}{\partial \tau} - \overline{p} \frac{\partial t'(x,\tau)}{\partial \tau} \right] + \frac{\rho}{A} \frac{\partial \dot{v}'(x,\tau)}{\partial x} = 0 \tag{13}$$

In order to simplify the analysis, this equation is represented in the Laplace domain; the validity of this approach is justified by the fact that Equation 13 is linear. Therefore, this equation is transformed as:

$$\frac{1}{\overline{R}\overline{t}^2} \{ \overline{t} [sP'(x,s) - p'(x,0)] - \overline{p} [sT'(x,s) - t'(x,0)] \} + \frac{\rho}{A} \frac{\mathrm{d}\dot{V}'(x,s)}{\mathrm{d}x} = 0 \tag{14}$$

It is obvious that this expression requires $T'(x,s)$. Introducing the boundary condition $\vec{q} = -k_s \frac{\partial t(x,\tau)}{\partial x} = h [t_w(\tau) - t(x,\tau)]$ into Equation 3 written for the heater and assuming

that the wall temperature may change over time, results in,

$$\frac{\partial}{\partial \tau}\left[\rho c_p t\left(x,\tau\right)\right]+\frac{\partial}{\partial x}\left[\rho c_p t\left(x,\tau\right)u\left(x,\tau\right)\right]-\frac{\partial p\left(x,\tau\right)}{\partial \tau} - \frac{\partial}{\partial x}\left[p\left(x,\tau\right)u\left(x,\tau\right)\right]=\frac{4}{D}h\left[t_w\left(\tau\right)-t\left(x,\tau\right)\right] \quad (15)$$

similarly, for the cooler, it yields:

$$\frac{\partial}{\partial \tau}\left[\rho c_p t\left(x,\tau\right)\right]+\frac{\partial}{\partial x}\left[\rho c_p t\left(x,\tau\right)u\left(x,\tau\right)\right]-\frac{\partial p\left(x,\tau\right)}{\partial \tau} - \frac{\partial}{\partial x}\left[p\left(x,\tau\right)u\left(x,\tau\right)\right]=-\frac{4}{D}h\left[t_w\left(\tau\right)-t\left(x,\tau\right)\right] \quad (16)$$

In these equations, h stands for the convective heat transfer coefficient. For an oscillating gas flow, it can be evaluated according to the following experimental correlation for turbulent flows [89, 102]:

$$\mathrm{Nu}=\frac{h\,d_h}{k}=0.036\mathrm{Re}^{\frac{4}{5}}\mathrm{Pr}^{\frac{1}{3}}\left(\frac{d_h}{\Delta x}\right)^{0.055} \quad (17)$$

Introducing the state equation into the energy balance of the heater (where $t_w\left(\tau\right)>t$) and recalling that for an oscillating flow, $\dot{\bar{v}}\triangleq 0$ [68], we obtain:

$$\frac{\partial p'\left(x,\tau\right)}{\partial \tau}+\frac{\overline{p}}{A}\frac{\partial \dot{v}'\left(x,\tau\right)}{\partial x}=\zeta\left[t_w\left(\tau\right)-t_{gx}\right] \quad (18)$$

with $\zeta=\frac{4h\overline{R}}{\left[D\left(c_p-\overline{R}\right)\right]}$ and $t_{gx}=\bar{t}+t'\left(x,\tau\right)$; in the Laplace domain we get:

$$sP'\left(x,s\right)-p'\left(x,0\right)+\frac{\overline{p}}{A}\frac{\mathrm{d}\dot{V}'\left(x,s\right)}{\mathrm{d}x}=\zeta\left[T_w\left(s\right)-\frac{\bar{t}}{s}-T'\left(x,s\right)\right] \quad (19)$$

which provides an expression for the temperature $T'\left(x,s\right)$. Thus, coupling this equation with Equation 14, results:

$$\frac{A}{\overline{p}}\left[sP'\left(x,s\right)-p'\left(x,0\right)\right]+\frac{\mathrm{d}\dot{V}'\left(x,s\right)}{\mathrm{d}x}=\frac{\overline{A}}{\bar{t}}\frac{sT_w\left(s\right)-\bar{t}-t'\left(x,0\right)}{1+\frac{\overline{p}s}{\bar{t}\zeta}} \quad (20)$$

If the volumetric flow rate is assumed to be the analogue of an electrical current in the heater, Equation 20 can be inversely-transformed and thereafter integrated over the spatial

coordinate in order to obtain the equivalent electrical equation, written as:

$$C_h \frac{\partial p'(x,\tau)}{\partial \tau} + \Delta v'(x,\tau) = g_h(\tau) \tag{21}$$

with $g_h(\tau) = \mathscr{L}^{-1}\left\{\frac{\overline{V}}{\overline{t}} \frac{sT_w(s) - \bar{t} - t'(x,0)}{1 + \frac{\overline{p}s}{\overline{t}\zeta}}\right\}$, $C_h = \frac{\overline{V}}{\overline{p}}$ and $\overline{V} = A\Delta x$. Thus, Equation 21 describes a circuit in which a capacitor is in parallel with a source term (i.e. the right-side of Equation 21). Coupling Equations 21 and 12, we obtain the electrical circuit shown in Figure 4.4. It can be assumed for the cooler that its cold temperature is time-dependent (i.e. $t_w = t_w(\tau) < t(x,\tau)$). Thus, an equation similar to Equation 21 is obtained:

$$C_k \frac{\partial p'(x,\tau)}{\partial \tau} + \Delta v'(x,\tau) = g_k(\tau) \tag{22}$$

with $g_k(\tau) = \mathscr{L}^{-1}\left\{\frac{\overline{V}}{\overline{t}} \frac{sT_w(s) - \bar{t} - t'(x,0)}{1 - \frac{\overline{p}s}{\overline{t}\zeta}}\right\}$, $C_k = \frac{\overline{V}}{\overline{p}}$ and $\overline{V} = A\Delta x$. Since Equation 21 is equivalent to Equation 22, both electrical circuits are similar. Therefore, Figure 4.4 represents the cooler equivalent network as well. It is noteworthy to remind that in this figure, R_{hk} has been represented as a variable resistor; in this way, it has been highlighted the dependency of R_{hk} with the velocity and, thus, with the mass flow rate.

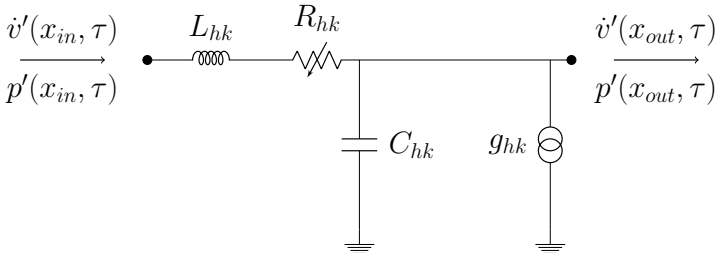

Figure 4.4 Equivalent circuit for both heater and cooler.

4.3.3 Regenerator

The approach outlined for the heat exchangers is now applied to the regenerator. Equation 2 is written as [103]:

$$\frac{\rho}{A}\frac{\partial \dot{v}'(x,\tau)}{\partial \tau} + \frac{\partial p'(x,\tau)}{\partial x} - \frac{\mu}{A}\frac{\partial^2 \dot{v}'(x,\tau)}{\partial x^2} = 0 \tag{23}$$

The third term on the left-hand side of this equation represents the pressure gradient due to viscous forces; it can be evaluated as [103]:

$$\Delta p = c_f \frac{\Delta x \rho u^2}{4d}, \quad c_f = C_{fd} + \frac{C_{sf}}{\mathrm{Re}} \tag{24}$$

C_{fd} and C_{sf} are experimentally evaluated coefficients and Re is the Reynolds number, calculated as $\mathrm{Re} = \frac{\rho u d_h}{\mu}$. Several correlations are available in the open literature; in this work, the expression for c_f provided by Tong and London [104] is used. Introducing Equation 24 into Equation 23, we obtain

$$\frac{\rho}{A}\frac{\partial \dot{v}'(x,\tau)}{\partial \tau} + \frac{\partial p'(x,\tau)}{\partial x} + \frac{c_f \rho}{4d}\left[\dot{v}'(x,\tau)\right]^2 = 0 \tag{25}$$

Integrating over the spatial coordinate and introducing the equivalent inductance $L_r = \frac{\rho \Delta x}{A}$ and the equivalent non-linear resistance $R_r = \frac{c_f \rho \Delta x \dot{v}'(x,\tau)}{4d}$ yields:

$$-\Delta p'(x,\tau) = L_r \frac{\partial \dot{v}'(x,\tau)}{\partial \tau} + R_r \dot{v}'(x,\tau) \tag{26}$$

This equation is coupled with Equation 13 in order to find the equivalent electrical circuit; in the mass conservation equation, an expression for the gas temperature as well for the metallic matrix must be introduced. Since $t = \frac{p}{\rho R}$ and $u = \frac{\dot{v}}{A}$, the energy conservation equation of the working fluid in the regenerator is given by:

$$\varepsilon V\left(\frac{c_p}{\overline{R}} - 1\right)\left\{\frac{\partial p(x,\tau)}{\partial \tau} + \frac{\overline{p}}{A}\frac{\partial\left[p(x,\tau)\,\dot{v}(x,\tau)\right]}{\partial x}\right\} = hA_{HT}\left[t_s(x,\tau) - t(x,\tau)\right] \tag{27}$$

where ε is the porosity of the regenerator, defined as the ratio of the empty volume to the total volume of the porous medium ($0 < \varepsilon < 1$). Assuming an oscillating flow, (i.e. $\dot{\overline{v}} = 0$) and introducing $\beta = \frac{hA_{HT}\overline{R}A}{\left[\overline{p}V\varepsilon\left(c_p - \overline{R}\right)\right]}$, Equation 27 becomes:

$$\frac{A}{\overline{p}}\frac{\partial p'(x,\tau)}{\partial \tau} + \frac{\partial \dot{v}'(x,\tau)}{\partial x} = \beta\left[t_s(x,\tau) - t(x,\tau)\right] \tag{28}$$

In the Laplace domain, it is transformed as:

$$\frac{A}{\overline{p}}\left[sP'(x,s) - p'(x,0)\right] + \frac{\partial \dot{V}'(x,s)}{\partial x} = \beta\left[T_s'(x,\tau) - T'(x,\tau)\right] \tag{29}$$

An expression for $T_s'(x,\tau)$ is required. Thus, the energy conservation equation for the metallic matrix is written as:

$$\rho_s C V_r(1-\varepsilon)\frac{\partial t_s(x,\tau)}{\partial \tau} = -hA_{HT}\left[t_s(x,\tau) - t(x,\tau)\right] \tag{30}$$

According to Tong and London [104], the convective heat transfer coefficient, h, can be estimated by the following experimental correlation:

$$\mathrm{Nu} = \left(0.384 + 1.075\mathrm{Re}^{0.578}\right)\left[1 - 1.356\left(1-\varepsilon\right)\right] \tag{31}$$

where Nu represents the Nusselt number. In the Laplace domain, Equation 30 becomes,

$$\tau_{sr}\left[sT'_s\left(x,s\right) - t_s\left(x,0\right)\right] = T'\left(x,s\right) - T'_s\left(x,s\right) \tag{32}$$

with $\tau_{sr} = \frac{\rho_s C V_r (1-\varepsilon)}{h A_{HT}}$; therefore,

$$T'_s\left(x,s\right) = \frac{T'\left(x,s\right) - \tau_{sr} t'_s\left(x,0\right)}{1 + s\tau_{sr}} \tag{33}$$

Introducing Equation 33 into Equation 29, the following expression for $T'\left(x,s\right)$ is obtained:

$$T'\left(x,s\right) = \frac{t'_s\left(x,0\right)}{s} - \frac{1+s\tau_{sr}}{\beta\tau_{sr}s}\left\{\frac{A}{\overline{p}}\left[sP'\left(x,s\right) - p'\left(x,0\right)\right] + \frac{\mathrm{d}\dot{V}'\left(x,s\right)}{\mathrm{d}x}\right\} \tag{34}$$

Combining this equation with Equation 14 yields:

$$\frac{A}{\overline{p}}\left[sP'\left(x,s\right) - p'\left(x,0\right)\right] + \frac{\mathrm{d}\dot{V}'\left(x,s\right)}{\mathrm{d}x} = \frac{\overline{V}}{\overline{t}}\frac{t'_s\left(x,0\right) - t'\left(x,0\right)}{1 + \frac{(1+s\tau_{sr})A}{\tau_{sr}\beta\overline{t}}} \tag{35}$$

The inverse Laplace transform and its integration over the spatial coordinate, gives:

$$C_r\frac{\partial p'\left(x,\tau\right)}{\partial\tau} + \Delta\dot{V}'\left(x,\tau\right) = g_r\left(\tau\right) \tag{36}$$

with $g_r\left(\tau\right) = \mathscr{L}^{-1}\left\{\frac{\overline{V}}{\overline{t}}\frac{t'_s(x,0)-t'(x,0)}{1+(1+s\tau_{sr})A\left(\tau_{sr}\beta\overline{t}\right)^{-1}}\right\}$, $C_r = \frac{\overline{V}}{\overline{p}}$ and $\overline{V} = A\Delta x$. Similarly to the heat exchangers, the continuity equation of the regenerator (Equation 36) correspond to an equivalent electrical circuit in which a capacitance C_r is connected in parallel with

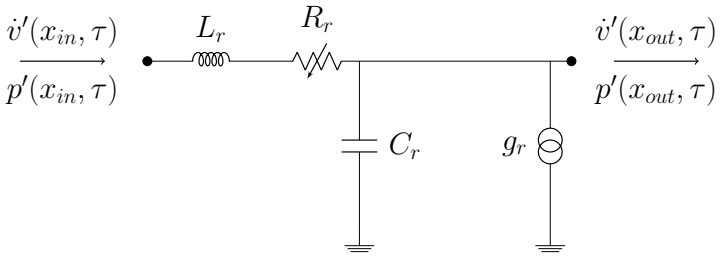

Figure 4.5 Equivalent circuit for the regenerator.

a source term. Thus, coupling this differential equation with Equation 12 yields the equivalent electrical circuit shown in Figure 4.5.

4.3.4 Displacer and power piston

In order to find an equivalent electrical circuit for the displacer, a balance of forces is applied to this component (see Figure 4.6). It should be highlighted that the displacer is not properly a piston; in most applications, it looks like a rod with a cylindrical cavity on one side. This cavity is filled with gas that behaves as a spring. For this reason, the side of the displacer facing the compression pressure has a smaller surface than the one facing the expansion pressure. Then, the balance of forces is written as [47]:

$$m_d\ddot{x}_d = (p_e - p_c)\,A_d + (p_c - p_d)\,A_r - C_{hdc}\dot{x}_d - m_d\|\vec{g}\| \tag{37}$$

Urieli and Berchowitz [47] proposed a linearisation for the action of the gas spring with its pressure, given by:

$$p_d = \overline{p}\left[1 + \gamma\frac{A_r}{V_d}x_d\right] \tag{38}$$

were V_d is the mean volume of the gas spring. The coefficient C_{hdc} takes into account the hysteresis effects. According to Urieli and Berchowitz [47], C_{hdc} can be estimated as:

$$C_{hdc} = \frac{\lambda}{2}\sqrt{\frac{\omega}{2\alpha_0}}\gamma\,(\gamma - 1)\,T_w A_r\left(\frac{A}{\omega V_{gs}}\right) \tag{39}$$

Thus, the balance of forces becomes:

$$m_d\ddot{x}_d = A_d\,(p_e - p_c) + p_c A_r - \overline{p}A_r - \overline{p}\frac{A_r^2\gamma}{V_d}x_d - m_d\|\vec{g}\| - C_{hdc}\dot{x}_d \tag{40}$$

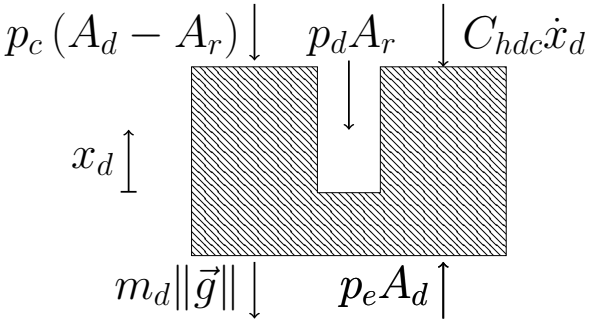

Figure 4.6 Forces acting on the displacer.

Let assume $\dot{x}_d = u_d = \frac{\dot{v}_d}{A_d}$; then,

$$\frac{m_d}{A_d^2}\frac{\mathrm{d}\dot{v}_d}{\mathrm{d}\tau} + \frac{C_{hdc}}{A_d^2}\dot{v}_d + \frac{\overline{p}\gamma}{V_d}\left(\frac{A_r}{A_d}\right)^2 \int_0^\theta \dot{v}_d(\tau)\,\mathrm{d}\tau = p_e - p_c\left(1 - \frac{A_r}{A_d}\right) - \left(\overline{p}\frac{A_r}{A_d} + \frac{m_d\|\vec{g}\|}{A_d}\right) \quad (41)$$

Introducing $L_d = \frac{m_d}{A_d^2}$, $R_d = \frac{C_{hdc}}{A_d^2}$, $\frac{1}{C_d} = \frac{\gamma\overline{p}}{V_d}\left(\frac{A_r}{A_d}\right)^2$ and $U_d = \frac{m_d\|\vec{g}\|}{A_d} + \overline{p}\frac{A_r}{A_d}$, it results:

$$L_d\frac{\mathrm{d}\dot{v}_d}{\mathrm{d}\tau} + \frac{1}{C_d}\int_0^\theta \dot{v}_d(\tau)\,d\tau + R_d\dot{v}_d = p_e - p_c\left(1 - \frac{A_r}{A_d}\right) - U_d \quad (42)$$

This equation corresponds to the electrical circuit shown in Figure 4.7. It should be mentioned that the source in Figure 4.7 has been introduced to take into account the effects of the gravity and of the mean pressure in the engine.

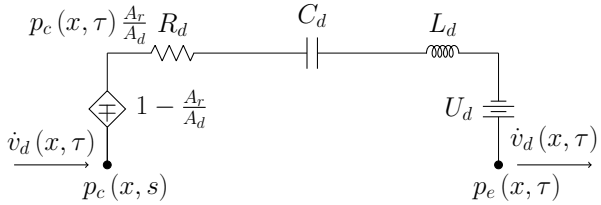

Figure 4.7 Equivalent electrical circuit of the displacer.

In order to obtain the equivalent electrical circuit of the power piston, the Newton's second law is applied to this component (see Figure 4.8); thus:

$$m_p\ddot{x}_p = (p_c - p_w)\,A_p - m_p\|\vec{g}\| - F_d \quad (43)$$

F_d is the load force, which cannot be modelled with a linear function; therefore, it will be assumed that [49]:

$$F_d = \alpha\dot{x}_p^n \quad (44)$$

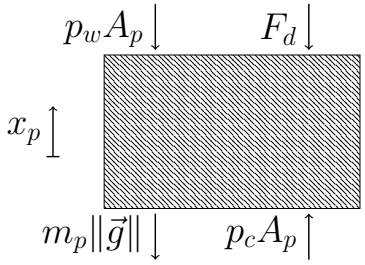

Figure 4.8 Power piston force balance.

More details about the coefficients α and n are provided in Section 4.4. Similarly to the former case, the buffer-space pressure is given by the following equation [47]:

$$p_w = \overline{p}\left[1 + \gamma\frac{A_p}{V_b}x_p\right] \tag{45}$$

Hence:

$$m_p\ddot{x}_p = A_p p_c - A_p\overline{p}\left[1 + \gamma\frac{A_p}{V_b}x_p\right] - c\dot{x}_p - m_p\|\vec{g}\| \tag{46}$$

with $c = \alpha\dot{x}_p^{n-1}$. Assuming $\dot{x}_p = u_p = \frac{\dot{v}_p}{A_p}$, we obtain

$$\frac{m_p}{A_p^2}\frac{\mathrm{d}\dot{v}_p}{\mathrm{d}\tau} + \frac{c}{A_p^2}\dot{v}_p + \frac{\overline{p}\gamma}{V_b}\int_0^\theta \dot{v}_p(\tau)\,\mathrm{d}\tau = p_c - \overline{p} - \frac{m_p\|\vec{g}\|}{A_p} \tag{47}$$

Assuming $L_p = \frac{m_p}{A_p^2}$, $R_p = \dfrac{c}{A_p^2}$, $\dfrac{1}{C_p} = \dfrac{\overline{p}\gamma}{V_b}$ and $U_p = \overline{p} + \dfrac{m_p\|\vec{g}\|}{A_p}$, we get

$$L_p\frac{\mathrm{d}\dot{v}_p}{\mathrm{d}\tau} + R_p\dot{v}_p + \frac{1}{C_p}\int_0^\theta \dot{v}_p(\tau)\,\mathrm{d}\tau = p_c - U_p \tag{48}$$

This equation has the same form of the differential equation describing the electrical circuit shown in Figure 4.9. It should be mentioned that in this figure, the non-linear effects of the load are implicitly included in the non-linear resistance R_p and that the source takes into account the effect due to gravity and to the mean gas pressure.

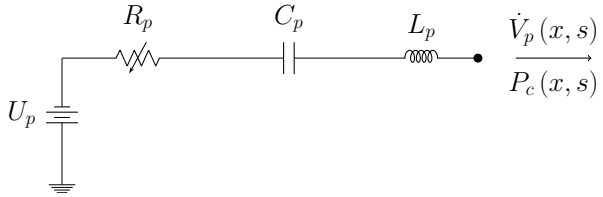

Figure 4.9 Equivalent electrical circuit of the power piston.

4.4 Results and discussion

In the previous section, the expansion and the compression chambers, the heat exchangers, the regenerator, the displacer and the power piston have been modelled. For most Stirling engine configurations, these elements constitute the main components. Therefore, the circuits presented in the previous section can be used to establish the equivalent electrical network for any Stirling-engine configuration.

Following the aforementioned methodology, the electrical circuits obtained in Section 4.3

are arranged in such a way to follow the configuration of the RE-1000 unit, which yields the equivalent electrical network shown in Figure 4.10. It must be pointed out that in this figure, only one of the four non-linear resistance is considered (i.e. the one associated to the power piston). Effectively, this resistance represents the damper, whose non-linear behaviour is essential to assure the stable operation of any engine. However, as it will be discussed later, the coefficients α and n used to calculate the force F_d are not known. Therefore, these coefficients will be chosen in such a way to match the model piston stroke with that measured for the engine optimal working conditions (listed in Table 4.1).

Table 4.1 Working conditions of the RE-1000 engine.

Design parameters	
Mean pressure, $\overline{p}$	7 MPa
Hot temperature, t_h	600°C
Cold temperature, t_c	25°C
Piston weight m_p	6.2kg
Displacer weight m_d	0.426kg
Regenerator porosity, ε	79.2%

Moreover, for the other resistances representing the viscous pressure drop in the heat exchangers, their mean values are estimated from the available pressure drop data [49]. Finally, in order to use the equivalent network, the thermal sources should be defined. The regenerator one can be neglected by assuming thermal equilibrium between the working gas and the metallic matrix. Also, for the heat exchangers, a proper wall-temperature function must be introduced in order to use Equations 21 and 22. For instance, in Equation 20, the Heaviside step function can be used to model the sudden change of the heater temperature, hence:

$$T_{w,h}(s) = \frac{T_h}{s} \tag{49}$$

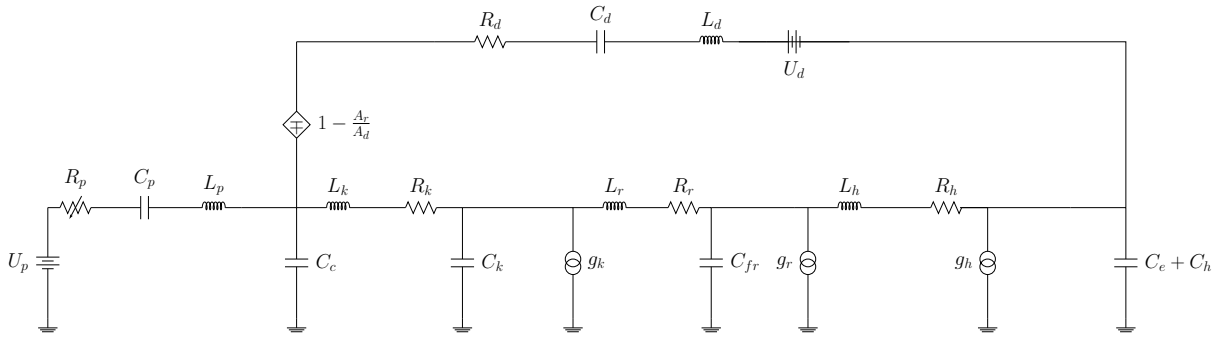

Figure 4.10 Equivalent electrical network for the RE-1000 Stirling engine.

In order to solve the circuit shown in Figure 4.10, a Matlab® (version 2015a) script has been developed.

4.4.1 Validation of the model

In this section, the predictions obtained using the proposed modelling approach are compared with experimental data collected at the NASA Lewis research center for the RE-1000 FPSE [49]. The operation conditions of this system are listed in Table 4.1. Our modeling approach can be used to predict the engine start-up. Thus, we can evaluate the behavior of the system when it is initially off and the heat exchangers are turned-on at a given time (see Equation 49). Figure 4.11 shows the power piston motion, the compression pressure as a function of time and the pressure-volume diagram of the compression chamber. As it has been previously discussed, the coefficients α and n are chosen in such a way to minimize the difference between the measured and the predicted stroke for the operation conditions given in Table 4.1. For this simulation, $\alpha = 128.4$ and $n = 1.5$. Results concerning the start-up of the unit are shown in Figures 4.11a and 4.11b. These figures show that the steady-state condition is reached after 15 s. From this simulation, the operation frequency is determined; the computed value is 26.0 Hz and the measured one is 30.1 Hz (relative error of 14.6%). Moreover, Figure 4.11c shows that the simulated compression pressure amplitude is 0.833 MPa. This value is lower than the measured one, which is 1.147 MPa (relative error of 27.3 %). The data presented in Figures 4.11a and 4.11b are used to draw the working gas cycle in the pressure-volume diagram (see Figure 4.11c).

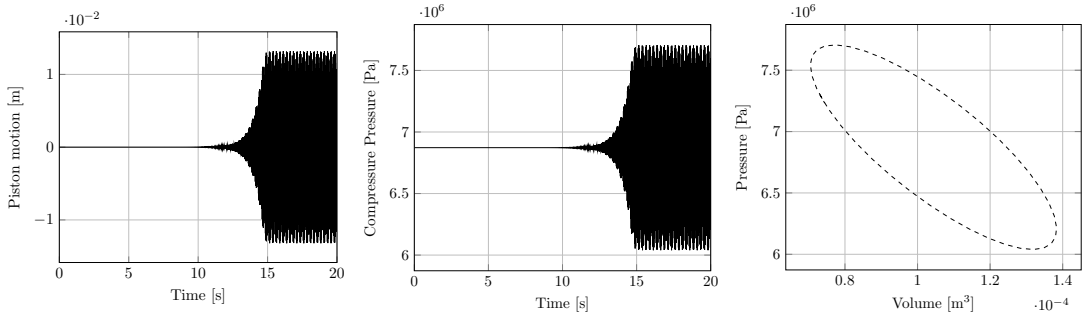

(a) (b) (c)

Figure 4.11 Electrical analogy model predictions (design working conditions): (a) power piston motion; (b) compression pressure; (c) pressure-volume diagram of the compression space.

® Matlab is a registered trademark of the Mathworks Inc.

4.4.2 Analyses of the proposed model

The validity of the proposed modeling approach has been further tested by analyzing the predictions for working conditions different from those listed in Table 4.1. For instance, Figure 4.12 shows how the experimental pressure affects the engine operation, as well as the predictions of the model. As this figure shows, the proposed model can be used to estimate the frequency f (Figure 4.12a), the amplitude of the compression pressure $|p_c|$ (Figure 4.12b) and the piston stroke $|x_p|$ (Figure 4.12c). These are key variables, because they directly affect the output power. The difference between the prediction and the data can be highlighted; in particular, the mean relative errors for f, $|p_c|$ and $|x_p|$ are 14.3%, 22.0% and 7.4%, respectively. The simulation shown in Figure 4.12c indicates that the predicted stroke decreases with increasing the pressure, while the measured values are constant. These differences can be explained by a possible external control of the energy dissipation in the damper force (consequently, on the coefficients α and n) imposed during the collection of the experimental data. Nevertheless, this kind of information is not available in reference [49]; therefore, it makes the comparison between the measured and the predicted data to be cumbersome. For this reason, the values of the coefficients α and n have been kept constant in order to obtain the results shown in Figure 4.12.

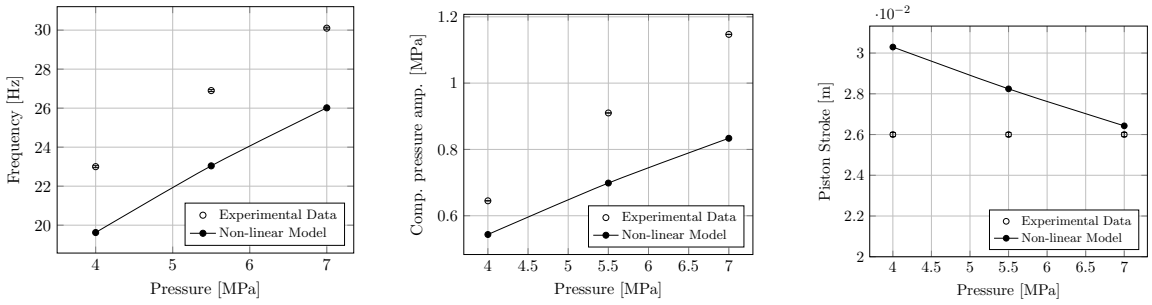

(a) (b) (c)

Figure 4.12 Predictions of the model in off-design operating conditions: (a) frequency; (b) compression pressure amplitude; (c) piston stroke.

4.4.3 Discussion

The difficulties encountered in estimating load force coefficients make it cumbersome to predict the power of the engine too. It can be evaluated from Figure 4.11, according to the following expression:

$$\dot{W} = \frac{\omega}{2\pi} \oint p \mathrm{d}V \tag{50}$$

where $\omega = 2\pi f$. By using this expression, the validation of the proposed approach is carried out by estimating the power for a wide range of working conditions. In particular, we analyzed how the pressure, the heater and the cooler temperatures affect the predictions. In our view, assuming α and n constant is too strong, even though other simplifying hypotheses may influence the results of the model (for instance, the constant value of the viscous pressure drop in the heat exchangers and in the regenerator); for this reason, a further evaluation of the power has been performed by introducing the Beale number Be, defined as [105]:

$$\dot{W} = \overline{p} A_p |x_p| f \mathrm{Be} \tag{51}$$

This parameter characterizes the performance of a Stirling system [14, 47, 48]. For each experience, the Beale number has been measured and these data are available in reference [49]. Therefore, the predicted frequency, stroke and pressure can be used with the measured Beale number not only to evaluate the power, but also to take into account any unknown control NASA has applied on the damper. Figure 4.13 shows the results obtained with this approach. This figure clearly shows that the predictions and the data follow almost the same trends. We notice a maximal relative error of 37.5% for a pressure of 4 MPa, while, for the other data-points, the relative errors do not exceed 12.7%.

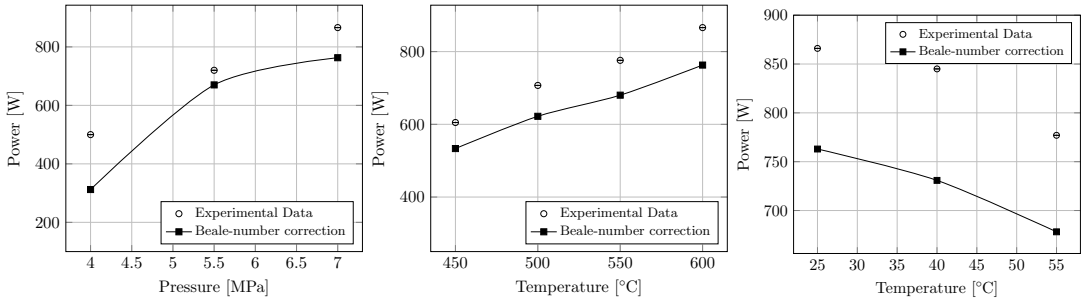

(a) (b) (c)

Figure 4.13 Power evaluation from the electrical analogy model as a function of the mean pressure (a), the heater temperature (b) and the cooler temperature (c).

4.5 Conclusion

In this paper, a model used to estimate the behavior of FPSEs has been proposed. It is based on the works found in the thermoacoustic literature [68, 89, 100] and those regarding the modelling of the Stirling engines [13, 47, 94]. The proposed model takes into account not only the mass and the momentum equations, but also the energy conservation equations. It is thus possible to couple both thermodynamic and dynamic effects. Moreover,

we have been able to establish an electrical analogy where the pressure is analogous to a electrical potential and the volumetric flow rate to an electrical current. As a consequence, it is possible to develop an equivalent electrical network and to predict the dynamic behaviour of the system.

The proposed modeling approach has been validated by comparing its predictions with the experimental data collected for the RE-1000 FPSE. Despite the lack of information about the conditions under which the data have been collected, the model is able to predict both design and off-design engine operation. In fact, in general a quite good agreement has been achieved. However, a complete and satisfactory validation cannot be obtained without having better information for evaluating the parameters α and n, which should depend on the working operation conditions (i.e. pressure, temperatures of the heat exchangers). To highlight this aspect, we compared two strategies to calculate the engine power: firstly, the aforementioned parameters have been kept constant; secondly, we introduced the Beale number, which indirectly takes into account the variation of α and n. Even though the model has been validated by comparing its predictions with the data collected from a single unit, additional work should be carried out to treat other engine configurations (e.g. α, β, γ, double action, etc.).

CHAPTER 5

DISCUSSION

In this chapter, an overall discussion of the research outlined in Chapter 3 and Chapter 4 is presented. This discussion is divided into three sections where the following topics are treated. Section 5.1 judges the thermodynamic feasibility of a Stirling engine using the pot sidewall wastes collected by radiation; the thermal power converted according to this proposed solution is estimated. Even though the calculated conversion rates are very attractive, the introduction of this solution in aluminum smelters may not be justified if the financial feasibility is not proven. For this reason, an economic analysis is provided (Section 5.2). Finally, the study presented in this thesis has opened further research avenue; some of these that should be examined in the near future, are listed in Section 5.3.

5.1 The operation of a Stirling engine converting the radiative thermal wastes from the pot sidewalls

The subjects treated in Chapter 3 and 4 would be useless if their main results are not coupled together to estimate the mechanical power output of an engine converting the radiation thermal wastes of the pot sidewall; such a procedure is proposed in this section. Before outlining the methodology followed to estimate the conversion rates, it should be recalled that the operation of a Stirling mover can be predicted by means of the CFD-simulation results [106]. In fact, a model for the whole engine can be implemented by using a proper software (e.g. COMSOL® Multiphysics); then, several CFD simulations could be carried out to study the influence of the working conditions on the Stirling unit. Nonetheless, implementing these simulations may be difficult[1] and time consuming. For this reason, in this thesis it is proposed to use the data obtained from the CFD simulations (e.g. the collector temperatures, see Figure 3.6 and 3.7) and coupling them with the electrical analogy model given in Section 4.3. This methodology permits the parametric study mentioned above to be implemented in a straightforward way. To carry this part of the work, it will be assumed that the Stirling engine used to convert the thermal wastes of the pot sidewall has the same design of the RE-1000 unit manufactured by Sunpower Inc. for the NASA Lewis Research Center [49]. This assumption permits to study a Stirling

® COMSOL is a registered trademark.

[1] Among the other, the principal complexity is due to the introduction of a dynamic mesh [20].

mover having the same components of the RE-1000 system (that is, a power piston, a displacer, a heater, a cooler and a regenerator) but not necessarily the same dimensions. More appropriate dimensions are calculated by introducing a scale factor ε [70, 71]; the size of the engine is estimated by multiplying the lengths, the surfaces and the volumes of the RE-1000 components by a factor equal to ε, ε^2 and ε^3, respectively. Similarly, the piston masses of the new unit are estimated by multiplying those of the RE-1000 unit by a factor ε^3. Moreover, as a consequence of the assumption mentioned above, the new Stirling unit must belong to the FPSE family. Limiting our study to FPSEs and then excluding kinematic engines makes it possible to apply the electrical analogy theory described in Section 4.3. Consequently, the operation of the new Stirling mover is predicted by the equivalent electrical circuit shown on Figure 4.10.

The main goal of this parametric analysis is to study the effects of three variables on the engine operation by following the pot thermal conditions. The first variable is the aforementioned scale factor ε, whose value is chosen to be smaller than 1; for this reason, the analysis is limited to engines smaller than the actual RE-1000 unit. The physical dimensions of the Stirling units under analysis are listed in Table 5.1 (further data regarding this unit are available in Appendix F). The second variable is the degree of pressurization of the system; therefore, the influence of the working fluid mean pressure $\overline{p}$, which is supposed to vary from 2 to up to 10 MPa, is analyzed. Finally, the last variable introduced in this study is the collector temperature T_h. The possible values for this parameter must be in agreement with the collector temperature predicted by the CFD analysis in Chapter 3 (see Figure 3.6 and 3.7); then, 70°C$\leq T_h \leq$100°C. Furthermore, it should be mentioned that temperatures higher than 100°C will not be considered in this study; even though the Stirling engine would benefit from an increase of this variable, the latter may affect the sidewall temperature and the pot operation, as it can be seen from Equation 7 given in Chapter 3 and from Figure 3.6.

Following the methodology presented in Section 4.4.2, the electrical elements of the FPSE equivalent circuit are calculated according to the value of ε, $\overline{p}$ and T_h; thus, the circuit is simulated to obtain the power-piston stroke $|x_p|$ (m) and the engine operating frequency f (Hz). Then, the variations of these two key variables as a function of ε, $\overline{p}$ and T_h are studied. The results obtained from this modeling approach are presented in Figure 5.1. It is clearly shown that, as long as the scale factor ε increases (that is, as long as the dimension of the engine approaches that of the RE-1000 unit), the piston stroke increases and the engine frequency decreases[2]. These considerations are valid either for a given value

[2]In particular, this value approaches the design frequency for the RE-1000 unit, that is, $f = 30$ Hz, for $\varepsilon \to 1$ and $p = 7$MPa.

of mean pressure $\overline{p}$ or for a given value of the heater temperature T_h. Furthermore, for a given scale factor, Figure 5.1a and 5.1b seem to indicate that the heater temperature T_h has a small influence on the variables under analysis, while, in agreement with Schreiber et al. [49], a more important effect of the mean pressure $\overline{p}$ on the engine operation is observed (see Figure 5.1c and 5.1d).

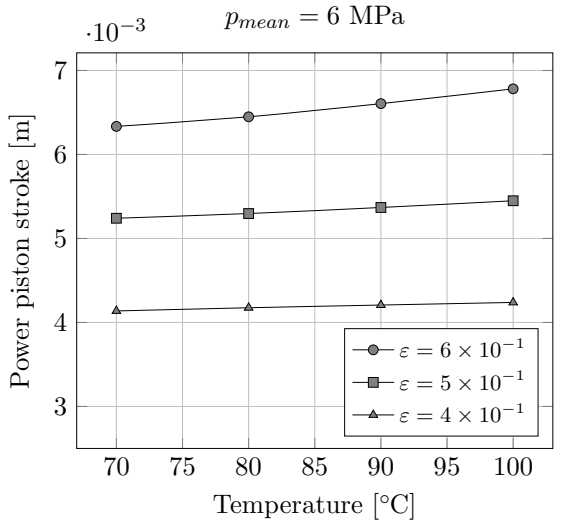

(a)

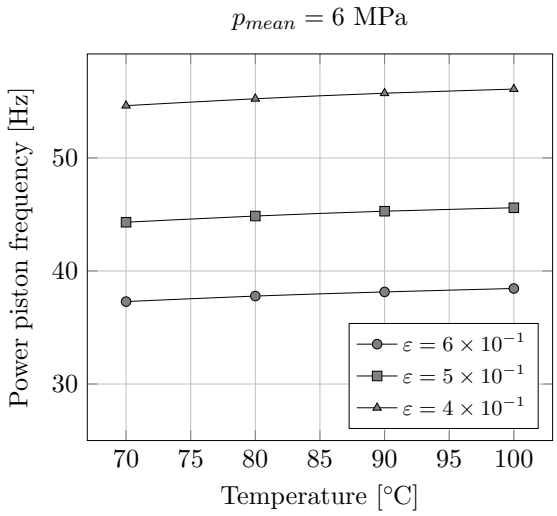

(b)

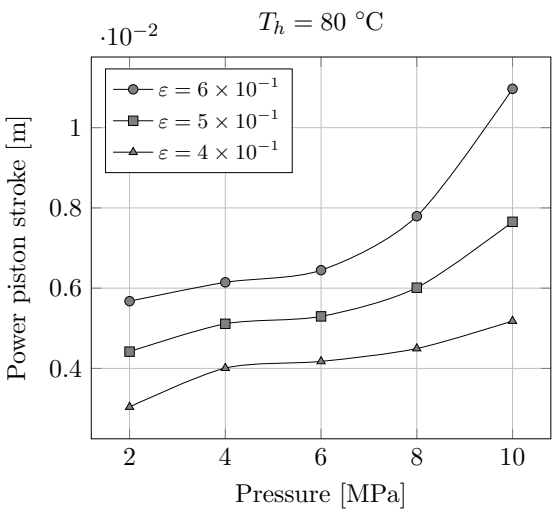

(c)

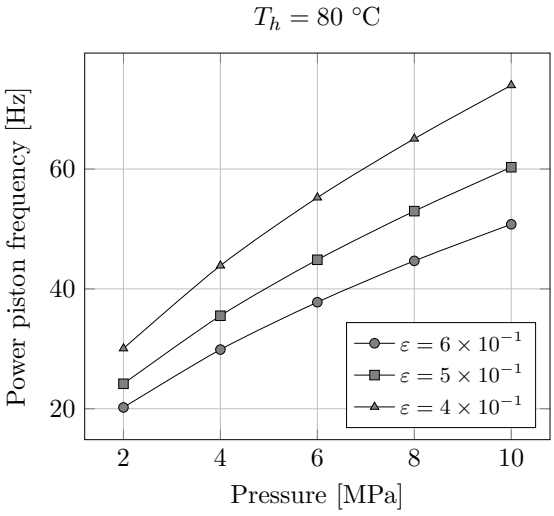

(d)

Figure 5.1 Operation of the Stirling engine as a function of various values of the scale factor ε: (a) piston stroke $|x_p|$ and (b) frequency f as a function of the heater temperature T_h; (c) piston stroke $|x_p|$ and (d) frequency f as a function of the engine mean pressure $\overline{p}$.

Table 5.1 Characteristic variables of the Stirling unit under analysis.

	Piston		Displacer		Heater		Cooler		Regenerator	
	m_p [kg]	d [m]	m_d [kg]	d [m]	d_h [m]	L [m]	d_h [m]	L [m]	d_h [m]	L [m]
RE-1000	5.97	5.72×10^{-2}	0.43	5.67×10^{-2}	2.36×10^{-3}	18.3×10^{-2}	8.95×10^{-4}	7.92×10^{-2}	2.8×10^{-3}	6.44×10^{-2}
Min	0.38	2.3×10^{-2}	0.03	2.3×10^{-2}	9.4×10^{-4}	7.3×10^{-2}	3.6×10^{-4}	3.2×10^{-2}	1.1×10^{-3}	2.6×10^{-2}
Max	1.29	3.4×10^{-2}	0.09	3.4×10^{-2}	1.4×10^{-3}	1.1×10^{-2}	5.4×10^{-4}	4.7×10^{-2}	1.7×10^{-3}	3.9×10^{-2}

Instead of evaluating the piston stroke and frequency, it would be more interesting to investigate the influence of the parameters ε, $\overline{p}$ and T_h on the useful power of the engine $\dot{W}$. This variable can be estimated by using the following expression [47]:

$$\dot{W} = \frac{\omega}{2\pi} \oint p \mathrm{d}V \tag{1}$$

where $\omega = 2\pi f$ and the periodic variations of the gas pressure p and volume V are calculated from the electrical circuit analogy. Despite its thermodynamic validity, this approach may lead to misleading results. Actually, Equation 1 is used to evaluate only the mechanical power; however, as mentioned in Section 4.4.3, the load is not properly modelled in the electrical analogy theory; the energy dissipation system is assumed to be a damper whose force is a non-linear function of the piston velocity (see Equation 44 of Chapter 4). It is thus expected that the mechanical power will be different if the load operation is introduced in the model. On the one hand, Ulusoy [67] has demonstrated that this approach may not be suitable, since the force of the load should be estimated from the solution of a proper differential equation. On the other hand, the sensitivity results of Schreiber et al. [49] have been collected by varying the engine working conditions and, in particular, the behaviour of the load. To overcame these problems, in Section 4.4.3 the effects of the load have been indirectly considered by introducing the dimensionless Beale number Be, defined as [47]:

$$\mathrm{Be} = \frac{\dot{W}}{\overline{p} A_p |x_p| f} \tag{2}$$

where A_p is the power piston cross section. In this document, it was demonstrated that the power outputs estimated from Equation 2 are in agreement with the experimental data (see Section 4.4.3) [23]. For this reason, it is proposed to calculate the useful power of the Stirling engine from Equation 2 rather than from Equation 1. In order to do that, the values for the piston strokes $|x_p|$ and the operating frequency f in Figure 5.1 are used; moreover, since Equation 2 requires a value for the Beale number, it is supposed that this dimensionless group is constant and equal to the one measured by Schreiber et al. [49] for the design condition of the RE-1000 unit (i.e. Be = 0.0776).

The conversion rates obtained using this methodology are shown in Figure 5.2. It can be stated that the dimension of the engine has a deep influence on the power output. As the engine size increases, the power output increases too. Furthermore, for a given mean pressure, the effect of the collector temperature are significant only for $\varepsilon = 0.6$ (see Figure 5.2a). In particular, it is estimated that the power is a linear function of the collector temperature. Differently, for a given heater temperature, the degree of pressurization affects the conversion rates for any dimension of the engine. In this case, the power varies

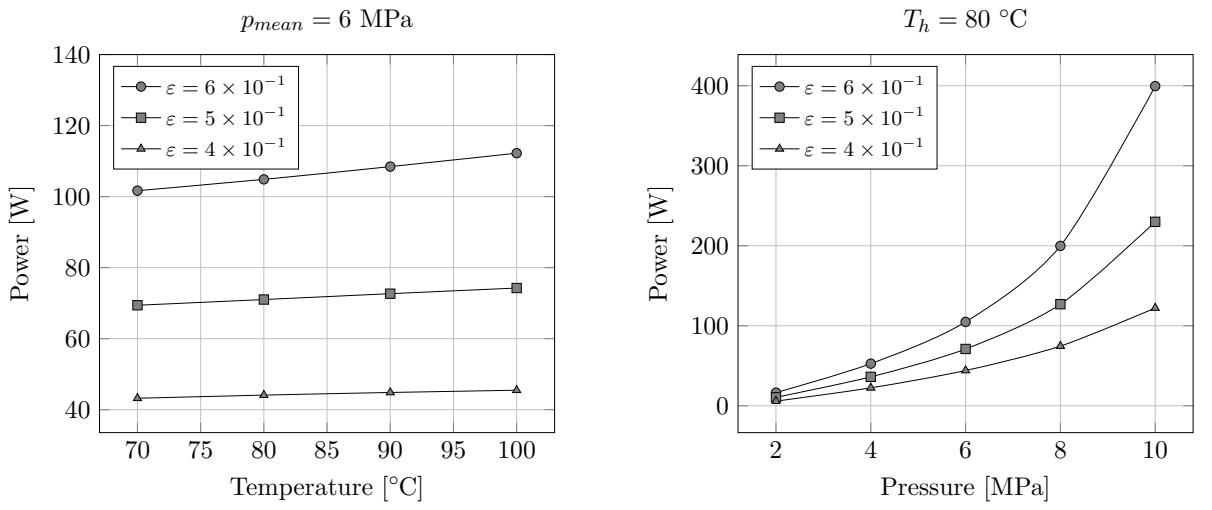

(a) (b)

Figure 5.2 Operation of the Stirling engine as a function of various values of the scale factor ε: power output as a function of (a) the heater temperature T_h and (b) the engine mean pressure $\overline{p}$.

non linearly with the mean pressure of the working fluid.

5.1.1 Validity of the proposed coupling approach

The results presented in the previous section may be questionable; Figure 5.2a indicates that the power output of the designed engine remains constant when the temperature of the collector varies from 70 to up to 100°C. Clearly, this is in contradiction with the second principle of Thermodynamics. This unusual behavior of the electrical-analogy model is probably due to the limited knowledge of the reduced-size engines. In fact, when the equivalent circuit is simulated, two main sources of uncertainty arise.

1. The effects of the damper, and
2. The effects of the heat exchanger operation (i.e. pressure losses and convective heat transfer coefficients).

These phenomena vary with the scale factor ε, the mean pressure $\overline{p}$ and the heater temperature T_h. The influence of the damper has been taken into account by introducing the Beale number; however, the data collected by Schreiber et al. [49] seem to indicate that this dimensionless group varies with the engine working conditions (i.e. ε, $\overline{p}$ and T_h). Since the variation of the Beale number as a functions of the engine operation is unknown for the engine to be designed, it is assumed that this value is constant; however, this hypothesis

should be revised. Moreover, in Section 4.4, the resistances due to the viscous pressure drops in the heat exchangers R_k, R_r and R_h and the convective heat transfer coefficients h_k, h_r and h_h, have been estimated from the Schreiber et al. experimental data [49]. In the present study, such an information is not available. The velocity field is not known *a priori*; this information is required to estimate the coefficients κ and c_F in Equation 11 and 24 of Chapter 4 and the Nusselt number in Equation 17 and 31 of the same chapter. These coefficients could be calculated by implementing an iterative procedure; however, the use of this methodology will increase the complexity of solving the equivalent circuit. For these reasons, the resistances for the Stirling configurations presented in Figure 5.2 have been calculated from the values of κ and c_F experimentally measured for the RE-1000 unit. The same methodology is used for the convective heat transfer coefficients, which are estimated from the Reynolds number measured by Schreiber et al. [49]. It should be mentioned that these assumptions will surely lead to an overestimation of the pressure losses and heat transfer rates.

Because of the aspects highlighted above, the use of other models for the Stirling engine, already available in the open literature [47, 67, 106], could be preferred over the electrical-analogy model presented in this document. However, it should be recalled that these models are usually complex, as they involve the solution of a non-linear system of differential equations. Furthermore, the use of these models does not always ensure satisfactory results [47, 65]. Instead, the parametric study in Figure 5.1 and Figure 5.2 was carried out in a straightforward way, that is, by solving the equivalent electrical circuit shown in Figure 4.10. The system of differential equations is relatively simple to solve, as it presents only one non-linearity, i.e. the load (which is mandatory to obtain a stable solution). Within this framework, the use of the electrical analogy theory becomes interesting; the equivalent circuit can be useful to perform analyses such as the one presented in this section. In this way, it is possible to obtain approximate data about the operation of an engine that needs be designed. These results are required when a preliminary design should be provided, for instance, for justifying the use of the Stirling technology as an energy conversion system in a given environment, such as in aluminum smelters.

A theoretical aspect regarding the approach used to couple the studies presented in Chapters 3 and 4 should be mentioned. In fact, it is recalled that a Neumann boundary condition was applied for the collector operation (see Section 3.4.3), while the heater temperature was imposed in the equivalent electrical circuit (see Section 4.4). An alternative coupling approaches could be considered; for instance, further simulations can be carried out by imposing a Dirichlet boundary condition for the temperature of the collector. In this way, the same heater temperature could be used in the electrical analogy theory in order to

achieve a more rigorous coupling of the two models. In spite of that, it should be recalled that the operation of the collector (i.e. the temperature and the heat flux) is the main unknown to be calculated. It is obvious that using either the coupling approach presented in this section or the one proposed in this paragraph do not allow the complete estimation of the collector behavior; this is mainly due to the introduction of this system itself, that is, a heat exchanger for which the temperature and the heat flux are unknown *a priori*.

5.2 Economic analysis

In the previous sections, the conversion rates of a Stirling engine powered by the thermal wastes of the pot sidewall have been estimated. Even though we have emphasized the limits of the methodology used to obtain the data presented in Figure 5.2, they are quite useful. In fact, they demonstrate that an improvement of the aluminum smelter energy efficiency is feasible. Still, these data do not completely justify the use of Stirling engines because aluminum producer would implement such an energy-efficiency solution only if it respects some given financial criteria. These criteria can be verified by applying the Net Present Value (NPV) analysis to the aforementioned solution [107, 108].
The NPV measures the monetary value of the cash flows for a given period of time (usually some number of years) by taking into account different factors (e.g. the inflation). It is calculated according to the following expression [108]:

$$\mathrm{NPV}\,(r, N) = \sum_{t=0}^{N} \frac{C_t}{(1+r)^t} \tag{3}$$

where N represents the period under analysis (usually expressed in years), C_t is the cash flow for the year t and r is the discount rate (that is, the rate at which money is lent for an investment with similar risk). In order to determine the cash flows, the variables in Equation 3 are calculated in the following way.

1. C_0 represents the cash flow for the first year; it is the capital cost of the Stirling units. Since it represents a cost, it is negative defined. Such an engine has not been designed yet, therefore, it is difficult to estimate its cost. In order to obtain this information, several companies involved in the Stirling engine technology have been contacted; however, few of them have provided the requested information in a satisfactory way. Therefore, these data have been taken from a technical report written in 2002 for the Electric Power Research Institute (EPRI) [109]. The author

of that report documented several Stirling engines and their prices. Therefore, it is suggested that these units should cost around 1,000 $\$kW^{-1}$.

2. C_t represents the cash flow for the year t; it may be either positive or negative, since it is calculated as the difference of the monetary value of their output (i.e. useful power) and the operating costs of the machine. The value of the power converted by the engine is estimated from the HydroQuébec "L" rate, which defines the price of energy billed to industrial costumers demanding more than 5 MW of power level; then, this price is 3.27 $¢kWh^{-1}$ [110]. Also, according to the EPRI technical report, the operating costs for FPSEs are almost null with respect to those of kinematic engines (estimated at 0.5 $¢kWh^{-1}$).

3. Finally, three values for the discount rates are investigated, that is, 1.76%, 2.29% and 4.5%; it should be recalled that these values are chosen according to the interest rate of 10-year Canadian bonds, that is, $r = 2.29\%$ [111]. However, it is well known that big companies (such as aluminum producers) can loan money at discount rates different from the government interest rate.

The data listed above can be used to perform an economical analysis based on Equation 3. It is supposed that a Stirling engine is installed at each location represented by Figure 3.1. Since the geometry in this figure is repeated 24 times for each cell and that an aluminum smelter may have as much as 300 cells, 7,200 Stirling units are considered in this study. Also, the engine power output is assumed to be 30 W, which is an estimate from Figure 5.2. This power level should be provided uninterruptedly over the year since the aluminum smelter works 24 hours per day and 365 days per year; however, a utilization factor of 95% is considered in this study. Since the capital cost of the Stirling engine is unknown, three values for this variable are considered in this study[3] ($C_{0,1} = 500$ $\$kW^{-1}$, $C_{0,2} = 750$ $\$kW^{-1}$ and $C_{0,3} = 1{,}000$ $\$kW^{-1}$) [109, 112]. Finally, as suggested in the EPRI's technical report, the operating costs for the FPSE units under analysis are neglected.
The results of this analysis are shown in the bar plots of Figure 5.3. Such a representation allows the reader to note the conditions for which the investment should be undertaken. In fact, by using Equation 3, it is possible to calculate the NPV for each investment scenario. These values are highlighted on each bar plot in Figure 5.3; thus, the NPV values are interesting only if both the capital costs and the interest rates are low (e.g. $C_0 < 750$ $\$kW^{-1}$ and $r = 1.76\%$). Furthermore, in this figure, the pay-back period is highlighted; this variable represents the year when the cash flows become positive (usually called break-even point); in other words, it represents the span required for an investment

[3] Economies of scale are neglected in this study.

to be profitable. It is fundamental to compare the pay-back period with the useful life time of Stirling engines. It is for this reason that in all the bar plots of Figure 5.3, a red and a green line have been introduced to highlight the minimum and maximum useful life time documented in the EPRI technical report. On the top of each bar plot, the discount rate r and the capital cost C_0 used to perform the analysis are recalled. Also, for each investment simulation, the Internal Rate of Return (IRR) and the Return On Investment (ROI) are calculated. The IRR is the minimal discount rate for which Equation 3 is null;

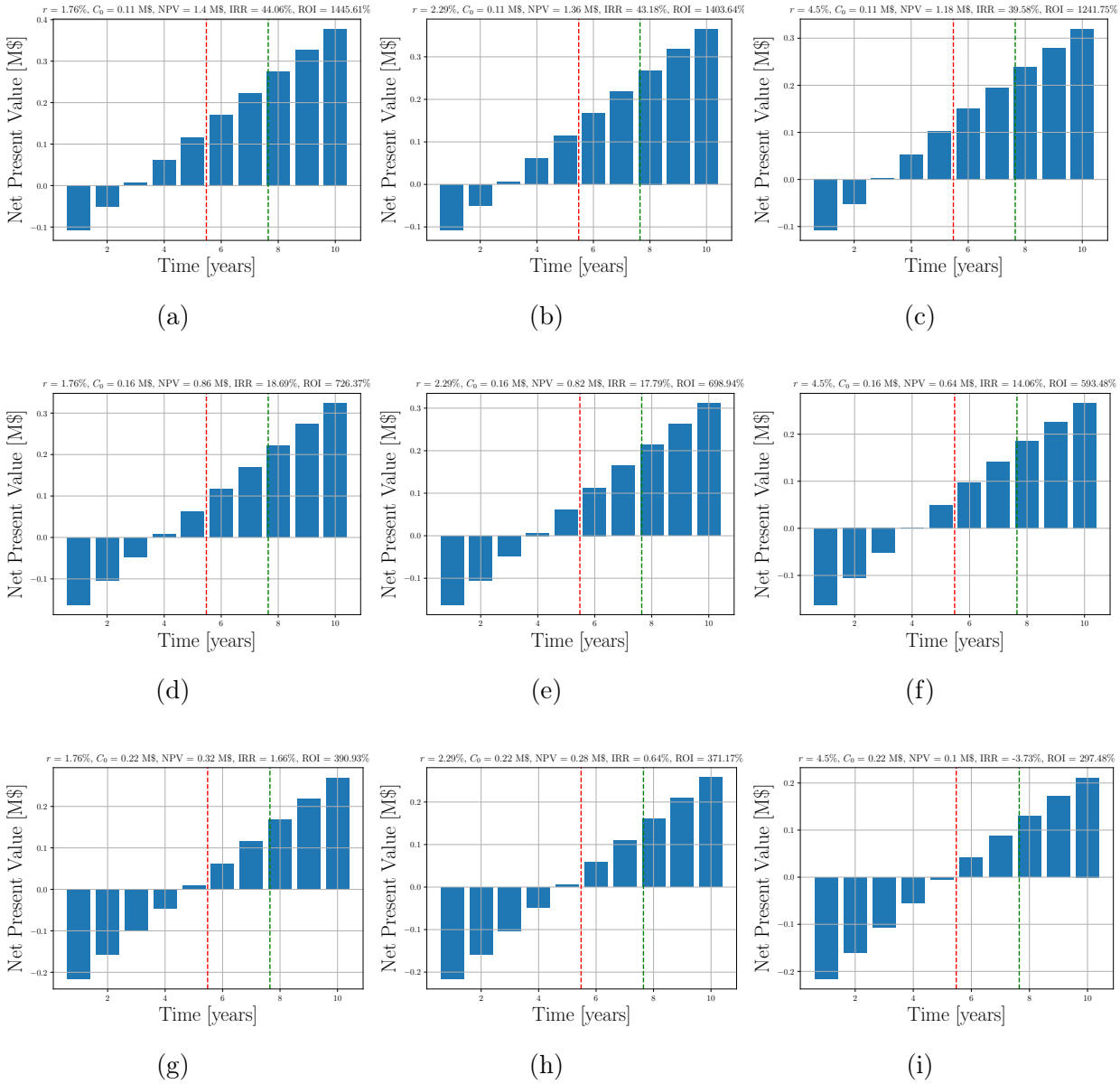

Figure 5.3 Economic analysis: bar plots showing the Stirling engine investment cash flows under different scenarios.

thus, it is estimated from the following expression [108]:

$$C_0 = \sum_{t=1}^{N} \frac{C_t}{(1 + \mathrm{IRR})^t} \tag{4}$$

A high value of IRR means that the cash flows are mostly positive over the investment life span. The ROI is the ratio of the net profits of an investment and the capital cost [108]:

$$\mathrm{ROI} = \frac{\sum_t \{C_t | C_t > 0\}}{C_0} \tag{5}$$

thus, it can be considered as a measure of the economical efficiency of the investment. These two metrics are useful to judge the profitability of an investment.

From Figure 5.3, a deep influence of the initial capital cost can be highlighted. If it is assumed that $C_{0,1} = 500$ \$kW^{-1} (Figure 5.3a, 5.3b and 5.3c), the investment is interesting because onder these conditions, the highest value of NPS (see Equation 3) is achieved. Moreover: the break-even point occurs between the second and the third year; the pay-back period is lower than the minimal useful life documented for Stirling engines [109]; the IRRs are considerably higher than the discount rates used to perform these analyses; and the ROIs are interesting (each dollar invested in the Stirling engine technology turns into about 13 \$ of profits). As the capital cost of the Stirling engine increases ($C_{0,2} = 750$ \$kW^{-1}), the NPV decreases while the pay-back period increases; however, the investment is still interesting due to the values of both the IRR and ROI (see Figure 5.3d, 5.3e and 5.3f). Finally, for $C_{0,3}$ =1,000 \$kW^{-1}, the Stirling engine technology is not profitable; the lowest value of NPV are calculated for those conditions; moreover, the break-even point is too close to the minimal useful life documented in the EPRI report; even though the ROI indexes are higher than 100%, the IRRs are too low. In detail, the IRR values are smaller than the respective discount rates; also, the sum of the cash flows is almost null (Figure 5.3g and 5.3h) or even negative (Figure 5.3i) over the investment life span; for the latter scenario, the investment turns into a loss of capital.

The data shown in Figure 5.3 can be applied to justify the use of Stirling engine to recover the pot sidewall thermal losses by radiation only if both the capital costs and the interest rates are low (e.g. $C_0 < 750$ \$kW^{-1} and $r = 1.76\%$). However, another aspect should be considered. The introduction of such a solution will affect the operation of the electrolysis cell; in particular, as it has been noted in Section 3.6 and by Namboothiri et al. [37], a proper recovery of the sidewall thermal losses can guarantee the safe service temperature of the pot. Under these conditions, the pot efficiency (see the footnote at page 17) can increase; consequently, the amount of produced aluminum will increase as well. In this

section, the limited knowledge of the electrolysis process did not allow us to estimate such an increment in production. However, the aluminum surplus will surely lead to an increase of the profits that should be considered in the economic analysis [37]. These economic benefits have not been considered in this section; however, we can assume that introducing these profits in Equation 3 will surely improve the results shown in Figure 5.3. In detail, the investment NPV will become more interesting, the pay-back period would decrease and both the IRR and ROI metrics would increase, making the investment of the proposed solution even more attractive for aluminum producers.

5.3 Future perspectives

The main objectives of this research were: (i) to estimate the pot sidewall thermal losses, and (ii) to evaluate the possibility of using the Stirling engine technology for energy conversion purposes. Even though these objectives have been achieved, it is without doubts that this work is far from being concluded. As in any research project, we encountered several issues that have opened new ideas for the future research. Some of them are listed in this section.

In Chapter 3, the recovery of the pot thermal losses was treated. In order to perform the recovery, a collector is considered; then, the operation of this system is simulated by means of a validated CFD tool. According to the author's knowledge, the future research regarding the operation of the radiative collector should focus on the following three topics.

- An experimental validation of the predictions shown in Figure 3.6 and 3.7 should be performed. This can be done by collecting data directly at the aluminum plant under analysis. Nonetheless, if this procedure is not feasible, another validation strategy must be implemented. We remind that the operation conditions of the thermal collector were predicted by using the $k\varepsilon$ turbulence model [23], which belongs to the RANS family. However, other numerical methods, such as the LES and the DNS, are available [18, 19]. Usually, these models, if properly used, are more reliable than the RANS equations; thus, it would be useful to compare the predictions obtained using different CFD numerical methods.

- The characteristics of the collector should be analyzed in order to investigate the possibility of improving its performance. It should be recalled that a flat collector with a low value of emissivity has been proposed to perform the actual study. This case is not the most suitable for such a heat exchanger. For instance, if it is desired to achieve temperatures higher than those presented in Figure 3.6 and 3.7, a parabolic concentrator, such as the one considered by Siva Reddy et al. [86], should

be used. Afterwards, as predicted by Equation 7 of Chapter 3, increasing the value of the emissivity turns into an increment of the heat flux captured by the collector. Therefore, this system will benefit from a change in both geometry and emissivity; these modifications should be properly estimated; however, it should be recalled that high collector temperature will reduce the heat flux. This aspect must be considered in the aforementioned estimation to propose a safe thermal recovery system.

- As previously mentioned, it is mandatory to carry out further simulations to properly understand the influence of the collector on the pot operation. In particular, it has been demonstrated that there is a relationship between the distance of the collector from the sidewall and the temperature of the latter (see Table 3.3). Thus, it is fundamental to study this relationship; if this is known, it can prevents an excessive cooling of the pot by means of the radiative collector to occur. Hence, such a relationship could be used to make the collector not only a simple heat exchanger recovering the thermal losses, but also a more appropriate system aiming to assure the safe working temperature of the pot.

Chapter 4 describes a model for FPSEs based on the electrical analogy theory. Even though the model has been validated with experimental data [49], some hypothesis have been introduced to simplify its development; in fact, most of the non-linear phenomena are estimated from the experimental data collected by Schreiber et al. [49]. Therefore, this methodology makes the validity of the developed model limited to the RE-1000 unit. According to the author's knowledge, in order to extend the validity of the electrical analogy model, some non-linearities must be considered. They are mainly due to the pressure drop and the convective heat transfer coefficient in the heat exchangers. These parameters can be estimated from the experimental correlations proposed in the open literature. Since a large number of correlations are available, the choice of the most suitable ones is cumbersome. In particular, in some works, these effects are estimated from the correlations obtained for unidirectional flow [13, 65, 67], while the use of those for oscillating flows is preferred by other researchers [89, 113]. Whether or not one theoretical approach is preferred to the other, both the pressure drop and the convective heat transfer coefficient are expressed as a function of the Reynolds number and, consequently, of the velocity field in the Stirling engine. Therefore, if these expressions are introduced in the electrical analogy theory, it would be possible to derive non-linear functions for the resistances and the sources; in other words, an equivalent electrical circuit representation for the Stirling engine is still possible. For this reason, it is proposed to test these expressions by comparing the predictions of a new non-linear circuit with the experimental data of the RE-1000

unit [49, 95]. It should be mentioned that introducing the non-linearities requires an iterative procedure; it is obvious that this will increase the complexity of the solving process of the model.

The main novelty of the model proposed in Chapter 4 is the introduction of the energy equation in the electrical-analogy theory of Formosa et al. [13]. The methodology followed in this research has been inspired from the work of Huang and Chuang [89], who assumed that the heat flux can be expressed by $q'' = -k_s \frac{\partial t(x,\tau)}{\partial x} = h\left[t_w(\tau) - t(x,\tau)\right]$ in Equation 3 of the previous chapter. Within this framework, the author of this thesis is currently investigating if it is possible to introduce the energy equation under a different form. Indeed, the 1st principle of thermodynamics applied to any of the components of the Stirling engine (i.e. expansion chamber, cooler, regenerator, heater and expansion chamber) can be written as [114]:

$$\delta Q_{flow} + \delta Q_{wall} = \mathrm{d}U + p\mathrm{d}V \tag{6}$$

where Q_{flow} is the flow-transport energy, Q_{wall} is the heat exchanged through the walls, $\mathrm{d}U$ is the change in internal energy and $p\mathrm{d}V$ represents the mechanical work. Then, Equation 6 can be developed depending on the engine component under analysis; for instance, for both expansion and compression chambers, and recalling that the working fluid is a gas, the time derivative of the energy balance is written as follows [67, 114]:

$$c_p T_f \frac{\mathrm{d}m}{\mathrm{d}t} + hA_s\left(T_w - T\right) = \frac{\mathrm{d}}{\mathrm{d}t}\left(mc_v T\right) + p\frac{\mathrm{d}V}{\mathrm{d}t} \tag{7}$$

where c_p and c_v are the specific heat at constant pressure and constant volume, respectively, T_f is the inlet temperature of the fluid, h is the convective heat transfer coefficient, A_s is the heat transfer area, T_w is the average temperature of the walls and T, m and p are the gas temperature, mass and pressure, respectively. Equation 7 is worthy of studying because it can be applied to any component of the Stirling engine; furthermore, by doing that, it is possible to take into account the heat transferred to each component of the Stirling machine. Currently, we are investigating a model where Equation 7 is applied to both the expansion and the compression chambers. Even though this model has not been numerically implemented yet, it can be demonstrated that an equivalent-circuit representation for the engine is still possible.

Another fundamental aspect that needs to be analyzed is the engine load. In some works available in the open literature, the force applied by the energy-conversion system on the engine power piston is either linearized [47, 65] or supposed to be a non-linear function of the power-piston velocity (see Equation 44 of Chapter 4) [13, 23, 64]. The validity of these hypotheses has been discussed in the literature; for instance, Ulusoy [67] has demon-

strated that these approximations can lead to unphysical results. As a consequence, several models for the electromechanical conversion system have been proposed in the literature. Ulusoy [67] considered the theoretical approach proposed by Boldea and Nasar [115]; their model was used to predict the stator current of a linear alternator coupled to the power piston of the RE-1000 unit. With the aim of analyzing piston-less engines, Arroyo et al. and Huet et al. [116, 117] have proposed a theoretical approach for the operation of piezoelectric generators, which seems to be suitable for micro-scale Stirling engines.

The introduction of a model for the electromechanical conversion in the theory obtained in Chapter 4 may be challenging at first sight. On the one hand, the physical meanings of the current and potential in the electrical analogy theory are those of a volumetric flow rate and pressure drop, respectively; on the other hand, "real" currents and voltages occur in an electromechanical converter. Despite this difference between electrical and analog variables, it is possible to modify the equivalent electrical circuit in order to introduce a theoretical approach for the conversion of mechanical work into electrical one. According to Beranek and Mellow [118] and Senturia [119], such a coupling is possible by considering a transformer (or a transducer); effectively, this system makes it possible to analyze different physical phenomena by means of a single analog circuit. This approach was successfully applied by Formosa and Fréchette [120], who proposed an equivalent electrical circuit for a piston-less micro-scale Stirling engine; since this machine uses piezoelectric generators for the electromechanical conversion, Formosa and Fréchette considered the transformer to estimate the electrical power produced by their Stirling engine [120].

An alternative to piezoelectric generator for the electromechanical conversion is the linear alternator. According to Boldea and Nasar, the electromotive force (expressed in V) for an alternator can be estimated as [67, 115]:

$$\xi = -MI_f \frac{\pi}{\tau} \dot{x}_p \sin\left(\frac{\pi}{\tau} x_p + \frac{\pi}{\tau} x_{so}\right) \tag{8}$$

where M is the magnetizing inductance, I_f is the permanent-magnet equivalent current, τ is the pole pitch, $\dot{x}_p$ is the piston velocity, x_p is the piston position and x_{so} is the distance between the stator and the plunger magnetic axis when $x_p = 0$. Furthermore, if i_s is the stator current, W is the piston work and q is the electrical charge, a relationship between the force applied by the piston and the electromotive force is established as follow:

$$\xi = \frac{\mathrm{d}W}{\mathrm{d}q} = \frac{F_d}{i_s} \frac{\mathrm{d}x_p}{\mathrm{d}t} = \frac{F_d}{i_s} \dot{x}_p - \frac{F_d}{i_s A_p} \dot{v}_p = \frac{p_d \dot{v}_p}{i_s} \tag{9}$$

where F_d is the piston load (see Equation 44 of Chapter 4), $\dot{v}_p$ is the volumetric flow rate at the compression chamber and A_p is the power piston cross section. It should be highlighted that this variable was the main unknown in the power-piston force balance in Equation 43 of Chapter 4. According to Equation 9, the alternator load force can be estimated as:

$$F_d = -MI_f \frac{\pi}{\tau} i_s \sin\left(\frac{\pi}{\tau} x_p + \frac{\pi}{\tau} x_{so}\right) \tag{10}$$

which is the same result obtained by Ulusoy [67]. Following the approach proposed by Beranek and Mellow [118] and Senturia [119], an equivalent transducer can be introduced; this system has four nodes and two sides, that is, an "electrical" and a "mechanical" side. On the electrical side, the voltage is imposed by the electromotive force defined by Equation 8; on the mechanical side, the equivalent pressure (i.e. the analog of the electrical potential) is imposed by the value of p_d introduced in Equation 9 [118, 119]. Under the electrical analogy, this energy transfer can be introduced in the model as an analogue transformer.

The previous paragraphs have highlighted the validity of using the electrical-analogy theoretical approach to estimate the behavior of Stirling engines. It should be mentioned that the electrical circuit obtained from this theory should not only be considered as a tool to predict the operation of an existing engine; instead, it must be employed to simplify the complex task of designing such a conversion machine. It is for this reason that three methodologies to perform this task are proposed. The first one consists on the development of a model which takes into account the non-linearities such as the convective heat transfer and the friction coefficients, as well as the operation of the load. Thus, an iterative procedure should be implemented in order to take into account the coupled effects of the load and those of the engine (i.e. both dynamic and thermodynamic). An anletrnative way to perform the aforementioned task is to couple the models for the load and for the machine to obtain a non-linear system of second order differential equations; this approach has been proposed by Ulusoy [67], who applied the center manifold theory and the normal analysis to study the stability of the dynamical system. Finally, the simplest way to study the stability of the engine is to rewrite the conservation equations given in Chapter 4 in dimensionless form [71]. Then, a new equivalent circuit for the engine can be derived; since the elements of this circuit (such as the resistances, the capacitances, the inductances and the sources) will be dimensionless, their values could be considered as reference to design a new FPSE.

5.4 Research assessment

We conclude this chapter by providing an assessment of the results obtained throughout this thesis. In Chapter 2, it was estimated that the thermal losses due to mixed convection and radiation from the pot sidewall are 4.4 kW m^{-2}. By carrying out the numerical simulations, it was proven that thermal radiation account for about 22% of these losses, while forced convection is responsible for the remaining 78%. Since a thermal flux of 0.96 kW m^{-2} is currently lost by radiation, a recovery system was proposed in Chapter 3; thus, this system can be used to recover up to 318 W m^{-2} (i.e. the efficiency of the thermal collector is around 33%). Then, the electrical analogy theory was used to predict the operation of the Stirling engine under the collector working conditions. Since the temperature of the collector is lower than 150°C, it can be assumed that the engine thermodynamic efficiency cannot be higher than 20%. Therefore, the power output is 64 W m^{-2}.

The results outlined in the previous paragraph state that only a small amount of the thermal losses can be converted into useful work by means of a collector coupled to a Stirling engine. According to the author, this result may be misleading, since it can lead to a negative judgment of the proposed solution. It is for this reason that these results are represented in Figure 5.4 by means of a Sankey diagram. In this way, it is possible to highlight reliable ways to improve the efficiency of the proposed system. On the one hand, this variable strongly depends on the collector temperature; thus, as previously mentioned in this document, it is mandatory to study the working conditions that allow this variable and the safe operation of the pot to be increased. On the other hand, even though Fig-

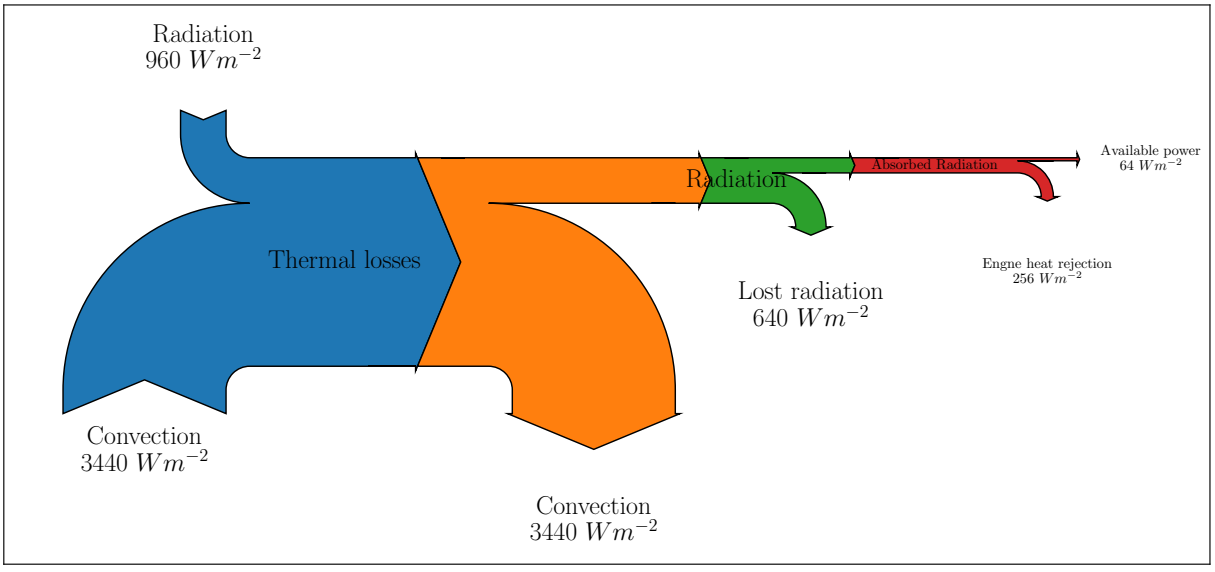

Figure 5.4 Sankey diagram for the proposed recovery-and-conversion system.

ure 5.4 shows that convection is responsible for an important thermal loss, it should be recalled that the proper value of the collector temperature (e.g. the heater of the Stirling engine) should be estimated from an optimization study. Effectively, as demonstrated in this chapter, a coupling analysis is required to assure the stable behavior of the engine and the safe operation of the electrolysis cell. In order to explain this aspect, let us assume that pot sidewall behave as a gray surface; furthermore, it is supposed that the radiative heat transfer between the cell wall and the collector surface is estimated as follows:

$$q''_r = \sigma \varepsilon A (T_s^4 - T_c^4) \tag{11}$$

where T_s is the sidewall temperature and T_c is that of the captor. By assuming that the efficiency of the Stirling engine is equal to the Carnot factor, the power per unit of surface w_s is given by:

$$w_s = \eta q''_r = \left(1 - \frac{T_o}{T_c}\right) \sigma \varepsilon A (T_s^4 - T_c^4) \tag{12}$$

Thus, the temperature value for which the Stirling engine produces the maximal work is obtained by solving the following equation:

$$\frac{\mathrm{d}w_s}{\mathrm{d}T_c} = 0 \Rightarrow 4T_c^5 - 3T_o T_c^4 - T_s^4 T_o = 0 \tag{13}$$

The polynomial in this equation has one real root for T_c =89°C (it is assumed that T_s =350°C and T_c =20°C) and four imaginary ones (whose meaning is unphysical). It is obvious that the previous equation is a simplification obtained to apply the optimization analysis. Therefore, any improvement of the recovering thermal energy and conversion based on Stirling engines can be taken into account by applying a more exhaustive optimization study. This aspect should be considered within the framework of the future research.

CHAPTER 6

CONCLUSION FRANÇAISE

Un bref résumé de la thèse est donné à la Section 6.1 ; ensuite, les contributions de ce projet de doctorat sont listées (Section 6.2). Enfin, les sujets de recherche qui doivent être étudiés dans un futur proche sont décrites à la Section 6.3.

6.1 Résumé de la recherche

La grande quantité de pertes thermiques dus à la production de l'aluminium a conduit à la recherche présentée dans cette thèse. Notre objectif principal était d'étudier la possibilité d'améliorer l'efficacité énergétique des fonderies d'aluminium. Ceci est fait en atteignant les sous-objectifs énumérés ci-dessous.
En nous référant aux questions de recherche présentées à la Section 1.2, nous nous sommes demandé si la réduction des pertes thermiques des usines produisant aluminium est possible. Nous avons donc étudie le procédé industriel de Hall-Héroult ; cette étude amène à conclure que les opérations correctives agissant sur la chimie des cuves d'électrolyses sont la principale cause des pertes thermiques.

- Afin de maintenir la concentration de certains composants chimiques dans le bain électrolytique sous des valeurs acceptables, la cuve d'électrolyse doit être fréquemment ouverte. Ceci est également requis pour certains modèles de cuves pour lesquels l'aluminium liquide est renversé. Pendant ces opérations, l'air ambiant pénètre dans la cuve et se mélange avec les gaz produits par le processus d'électrolyse. Ce mélange est ensuite chauffé à la température de fonctionnement de la cuve et finalement libéré dans l'environnement.

- L'électrolyte liquide peut attaquer les matériaux réfractaires dont sont faites les parois internes de la cuve. Afin d'éviter cette situation, à cet endroit, une couche solide de cryolite (c'est-à-dire l'électrolyte) est conservée en refroidissant les parois externes de la cuve. La chaleur est transférée par convection forcée ; puis, l'air de refroidissement est rejeté dans l'environnement.

Au Chapitre 2, nous avons mentionné que les pertes de chaleur dues au gaz chaud produit dans la cuve peuvent éventuellement être récupérées grâce à la technologie ORC ; cependant, l'analyse exergétique préliminaire et l'étude économique réalisée au Laboratoire des

technologies de l'énergie (LTE) de Shawinigan [5] semblent indiquer que ce n'est pas la solution la plus appropriée pour améliorer l'efficacité énergétique de ce type d'industrie. Ensuite, les pertes thermiques se produisant sur la paroi latérale de la cuve sont été étudiés.

L'étude d'une technologie appropriée pour récupérer et éventuellement convertir les pertes thermiques des parois s'est révélée difficile. En effet, le fonctionnement d'un tel système doit respecter les critères de sécurité stricts de la fonderie d'aluminium. Cet aspect rend le choix d'une solution d'efficacité énergétique limitée à quelques systèmes disponibles. Afin de proposer un système efficace et sûr, nous étudions la possibilité de récupérer les pertes par rayonnement thermique, puis de les convertir grâce à la technologie du moteur Stirling.

Vue l'impossibilité de collecter des données sur site, il a été décidé de calculer les pertes thermiques par rayonnement de la paroi latérale de la cuve par la méthode CFD. Dans ce contexte, les résultats préliminaires obtenus en utilisant un logiciel "open source" (OpenFOAM 5.0) ont d'abord été validés puis utilisés pour modéliser les phénomènes de transfert de chaleur sur les parois latérales de la cuve. En suite, le fonctionnement d'un collecteur plat est analysé en estimant à la fois les flux de chaleur par rayonnement et les températures moyennes de ce système.

Estimer le fonctionnement d'un moteur Stirling est plus difficile que la tâche précédente. Un moteur Stirling capable de convertir les pertes gaspillés par rayonnement n'a pas encore été fabriqué. C'est pour cette raison qu'il est difficile de mettre en œuvre un modèle capable de prédire le fonctionnement d'une telle machine. Ces problèmes ont été surmontés en développant un modèle basé sur la théorie de l'analogie électrique. À la suite de cette approche théorique, les équations de conservation de la masse, de la quantité de mouvement et de l'énergie ont été analysées pour obtenir une représentation du moteur par un circuit électrique éqivalante. Chaque élément du circuit équivalent (par exemple, résistances, inducteurs, condensateurs...) a une signification physique précise ; par exemple, les résistances électriques représentent des phénomènes dans lesquels l'énergie est perdue. En outre, il convient de mentionner que les équations de conservation sont étudiées de manière à rendre l'applicabilité du modèle aussi large que possible. La théorie développée dans le cadre de cette recherche a été utilisée pour modéliser le moteur RE-1000 [49] ; ensuite, une validation adéquate est implémentée en comparant les prédictions de la théorie de l'analogie électrique et les données expérimentales collectées par Schreiber et al. [49].

Les résultats des deux études susmentionnées ont été utilisés pour étudier le fonctionnement du moteur Stirling en fonction des conditions de travail du collecteur. Ensuite, une stratégie de couplage est proposée dans la Section 5.1. De cette manière, le comportement

du modèle a été analysé en fonction de trois paramètres : la taille du moteur, la pression moyenne du fluide de travail et la température du réchauffeur. Donc, la dimension du moteur et la pression moyenne du fluide de travail ont une influence profonde sur la puissance de sortie de l'unité Stirling, alors qu'une faible dépendance de la température du capteur a été notée. Un tel comportement inattendu amène à réviser quelques hypothèses sur lesquelles la théorie de l'analogie électrique a été développée ; ainsi, l'estimation correcte des pertes de pression et des coefficients de convection dans les échangeurs de chaleur peut aider à prendre en compte l'effet de la température du réchauffeur. En outre, il convient de rappeler qu'une amélioration du modèle est obtenue en introduisant une description plus rigoureuse de la charge du moteur.
Enfin, comme ce projet de recherche vise à proposer un système d'efficacité énergétique à mettre en œuvre dans un proche avenir, une analyse économique préliminaire a été entreprise ; en effet, les partenaires industriels qui nous ont aidés lors de cette recherche ont explicitement noté que les résultats positifs de l'étude économique seront considérés comme une condition suffisante pour investir dans la solution proposée dans leur usine. Ensuite, les coûts liés à l'utilisation du système d'efficacité énergétique ont été analysé dans ce document ; la théorie de la valeur actualisée nette (VAN) est appliquée pour calculer certains paramètres d'investissement, tels que le seuil de rentabilité, le TRI (IRR en anglais) et le ROI, pour divers scénarios.

6.2 Contributions scientifiques

Les sujets les plus importants décrits dans cette thèse, qui sont la récupération des pertes thermiques des parois latérales de cuve d'électrolyse et leur conversion, font l'objet de deux articles scientifiques présentés dans les Chapitres 3 et 4, respectivement.
Dans l'article "Proof of concept to recover thermal wastes from aluminum electrolysis cells using Stirling engines", publié à la revue internationale Energy Conversion and Management, il est proposé d'estimer les rejets thermiques par rayonnement de la paroi latérale de la cuve par la théorie CFD. Un code "open source" (OpenFOAM 5.0) est utilisé pour simuler deux phénomènes physiques se produisant sur la paroi latérale de la cuve, c'est-à-dire :

- Le transfert de chaleur mixte, c'est-à-dire, par conduction couplé à la convection et au rayonnement, et
- L'écoulement de jets non isotherme.

Un accord satisfaisant est trouvé entre les équations RANS couplées au modèle de turbulence $k\varepsilon$ implémenté dans OpenFOAM 5.0 et les lois analytiques trouvées dans la littérature [82, 84]. Ainsi, cette approche de modélisation est supposée être la plus appropriée pour simuler les phénomènes de transfert de chaleur de la paroi latérale de la cuve et pour calculer la puissance thermique récupérée par une plaque métallique placée parallèlement à la paroi. On estime qu'un flux de chaleur d'environ 320 Wm^{-2} à une température comprise entre 80 et 95°C peut être récupéré par cette plaque par rayonnement thermique seul. Ces températures sont suffisamment élevées pour faire fonctionner certains types de moteurs Stirling proposés dans la littérature ; cependant, il est obligatoire d'étudier les conditions de travail du collecteur pour lesquelles les flux de chaleur et les températures susmentionnés peuvent augmenter. De cette manière, des moteurs Stirling plus efficaces peuvent être utilisés.

L'absence d'un modèle satisfaisant pour prévoir le fonctionnement du moteur Stirling a conduit à en proposer un nouveau ; ce modèle est basé sur les équations de conservation (c'est-à-dire continuité, mouvement et énergie) appliquées aux composants du moteur (c'est-à-dire la chambre d'expansion, le réchauffeur, le régénérateur, le refroidisseur et la chambre de compression) et aux pièces mobiles (c'est-à-dire, le piston de puissance et celui de déplacement). Ensuite, une analogie électrique est établie pour dériver une représentation par circuit équivalent pour le moteur de Stirling. Cette approche théorique n'est pas complètement nouvelle, car elle a déjà été utilisée dans la littérature ; cependant, dans la plupart des modèles proposés, les équations de continuité et de conservation du mouvement sont étudiées, tandis que l'équation d'énergie est généralement négligée [13, 94]. La nouveauté de l'approche théorique décrite dans ce document est l'introduction de l'équation d'énergie. En faisant cela, il était possible de prédire le comportement thermodynamique et dynamique du moteur, qui sont généralement couplés. De plus, nous avons démontré que l'introduction de l'équation d'énergie n'empêche pas la possibilité d'établir un circuit électrique équivalent pour le moteur. Une validation est effectuée en comparant les données expérimentales disponibles pour le moteur RE-1000 et les prédictions du modèle proposé. Un accord satisfaisant a été trouvé malgré le manque d'informations sur la charge du moteur, pour laquelle les données n'étaient pas disponibles [49]. Une description détaillée du modèle est disponible dans un article scientifique "Modeling the dynamic and thermodynamic operation of Stirling engines by means of an equivalent electrical circuit" actuellement publié dans la revue internationale Energy Conversion and Management [23] ; de plus, quelques considérations théoriques préliminaires sur ce modèle ont été présentés lors d'un poster at de deux conférences internationales [95, 121]. En conclusion, une description détaillé de l'utilisation du logiciel OpenFOAM a été donnée dans le cadre du Thermal and

Fluids Analysis Workshop, organisé par la NASA en 2016 au U.S. Space & Rocket Center en Huntsville, Alabama.

6.3 Travaux futurs

Dans cette section, des pistes de recherche sont donnés pour poursuivre cette étude. Les sujets les plus importants à analyser dans le futur proche sont listés.

- Du point de vue de la théorie CFD, il existe sans doute que des modélisations théoriques plus performantes que celle utilisée pour analyser la récupération des pertes thermiques ; par exemple, l'utilisation des l'approches DNS ou LES peut être préférée à celle de RANS. Cependant, ce n'est pas le sujet le plus important à traiter à l'avenir. La stratégie CFD proposée au Chapitre 3 est significative, car elle démontrait que la récupération des pertes thermiques par rayonnement est possible. C'est pour cette raison qu'il est plus intéressant d'étudier si les flux de chaleur récupérés par la plaque planaire et leur température peuvent être augmentés. En suite, d'autres configurations de collecteurs thermiques doivent être étudiées ; par exemple, le fonctionnement d'un concentrateur parabolique doit être estimé. En outre, l'analyse de la distance entre le collecteur (ou le concentrateur) et la paroi latérale de la cuve peut s'avérer être un autre sujet crucial. En effet, il a été démontré que faire varier cette distance peut non seulement affecter l'opération du collecteur, mais aussi celle de la cuve. Ainsi, d'une part, le système proposé se comportera comme un échangeur thermique de récupération de pertes thermiques ; de l'autre, il peut être utilisé pour assurer la température de sécurité de la cuve, ce qui est fondamental pour préserver le processus d'électrolyse. Il est alors fondamental de prendre en compte cet aspect afin de bien concevoir un tel système. Cela signifie effectuer d'autres simulations pour comprendre la relation entre la température moyenne de la paroi et la distance du collecteur. Enfin, il convient de rappeler que dans les calculs effectués dans le cadre de cette recherche, le système de refroidissement existant (c'est-à-dire l'ensemble des buses d'air) a été considéré. Il est évident que le fonctionnement du collecteur bénéficiera de la modification de ce système. Ainsi, une nouvelle stratégie de refroidissement de la cuve doit être étudiée dans un futur proche, c'est-à-dire un scénario dans lequel le seul moyen de transférer de la chaleur est seulement par rayonnement thermique. En faisant cela, l'opération la plus appropriée pour le collecteur (c'est-à-dire, les flux de chaleur collectés à haute température) est atteinte.

- La plus grande limite du modèle proposé dans le Chapitre 4 est qu'il a été validé pour un seul moteur, c'est-à-dire le RE-1000 ; effectivement, plusieurs données sur cette unité étaient disponibles. Puisque la perte de pression et les échangeurs de chaleur étaient connus, ils ont été introduits dans le modèle ; cependant, ces paramètres devraient être prédits par le modèle. L'introduction de cette information étendra sûrement la validité du modèle, mais augmentera aussi sa complexité ; puisque les paramètres mentionnés ci-dessus sont des fonctions non linéaires du débit de gaz de travail, une procédure itérative doit être ajoutée dans le modèle. Malgré cela, l'amélioration de l'approche de modélisation n'empêchera pas d'obtenir une représentation du moteur Stirling par le circuit électrique équivalente, car ces effets seraient prédits par des résistances et des source non linéaires à introduire dans ce circuit. La procédure suivie dans l'article publié [23], c'est-à-dire l'introduction des pertes de pression et des coefficients de transfert de chaleur par convection dans le modèle, a permis d'étudier les effets de la charge du moteur, pour lequel le rapport de Schreiber et al. ne donne pas d'information. Ce composant s'est révélé fondamental pour garantir le bon fonctionnement du moteur. C'est pour cette raison qu'une description correcte de la charge (telle que l'alternateur linéaire considéré dans la thèse de Ulusoy) doit être envisagée à l'avenir. Cependant, il convient de rappeler que la prise en compte des effets de charge ajoute une nouvelle variable dans le modèle, c'est-à-dire l'intensité du courant électrique dans l'alternateur ; en faisant cela, un transformateur équivalente doit être introduit pour obtenir une représentation par circuit électrique pour le moteur Stirling.

Enfin, il convient de souligner que la sujet de cette thèse est principalement théorique ; il est certain que tout progrès ultérieur dans cette recherche exige l'étude de la fabrication du collecteur et du moteur Stirling devrait être entreprise dans un futur proche.

CHAPTER 7

ENGLISH CONCLUSION

A brief summary of the thesis is given in Section 7.1; then, the contributions of this doctoral project are listed (Section 7.2). Finally, the research topics that need to be better investigated in the future are discussed in Section 7.3.

7.1 Summary of the research

The large amounts of thermal losses due to the industrial production of aluminum have led us to undertake the research presented in this thesis. Thus, our primary objective was to study the possibility of improving the energy efficiency of aluminum smelters. This is done by achieving the sub-objectives listed below.
Referring to the research questions presented in Section 1.2, we asked ourselves whether or not the reduction of the thermal wastes of aluminum smelters is possible. Therefore, we studied the industrial Hall-Héroult process; we came to the conclusion that a proper sustainability of the chemical reactions occurring in the pot requires correcting operations, which seem to be the main cause of heat loss; therefore:

- In order to keep the concentration of some chemical species in the electrolytic bath under acceptable values, the cell needs to be frequently opened. This operation is also required for some pot design for which the liquid aluminum is spilled. During these operations, the ambient air that enters in the pot is mixed with the gases produced by the electrolysis process. This mixture is then heated to the operating temperature of the cell and finally released to the environment.
- Without an adequate protection, the electrolyte may attack the refractory materials of which the inner walls of the pot are made. In order to avoid this circumstance, at this location, a solid layer of cryolite is maintained by cooling the external walls of the pot. Consequently, heat is transferred by means of forced convection and the cooling air is released to the environment.

In Chapter 2, we mentioned that the heat losses due to hot gases from the pot can be eventually recovered by means of the ORC technology. The preliminary exergetic analysis in Section 2.3 and the economic study undertaken at the HydroQuebéc Energy Technology Laboratory [5] seem to indicate that this is not the most suitable solution to improve the

plant energy efficiency. For this reason, the recovery of the thermal wastes occurring at the sidewall of the pot have been studied.

The study of a proper technology to recover and eventually convert the sidewall thermal wastes revealed to be difficult. In fact, the operation of such a system must respect strict safety requirements of the aluminum smelter. This aspect makes the choice of an energy efficiency solution limited to few available systems. In order to propose an efficient an safe system, we have investigated the possibility of recovering the wastes by thermal radiation and then to convert them into mechanical power by using the Stirling engine technology. Due to the impossibility of collecting data at the industrial plant, we decided to calculate the radiative thermal losses from the sidewall by performing CFD simulations; to this aim, preliminary solutions obtained by using an open source software (OpenFOAM 5.0) were validated and then used to model the heat transfer from the lateral walls of the pot. Within the framework of this study, the operation of a flat collector was analyzed by estimating both the radiative heat flux and its mean surface temperatures.

The estimation of the operation of a Stirling engine was even more challenging than the previous task. In fact, a Stirling mover able to convert the pot radiative wastes has not been manufactured yet. For this reason, it was difficult to implement a model capable of predicting the operation of such a machine. We overcame this issue by developing a model based on the electrical analogy theory. Following this approach, the conservation equations for the mass, momentum and energy were analyzed to obtain an equivaent electrical circuit for the engine. Each element of this circuit (e.g. resistances, inductors, capacitors...) has a precise physical meaning; for instance, the electrical resistances represent phenomena in which energy is dissipated. Also, it is worthy mentioning that the conservation equations are studied in such a way to make the applicability of the model as wide as possible. The theory developed in the framework of this research was used to model the RE-1000 unit [49]. Therefore, a validation was carried out by comparing the predictions of the electrical analogy theory with the experimental data collected by Schreiber et al. [49].

The results of the two aforementioned studies have been analyzed to investigate the operation of the Stirling engine as a function of the working conditions of the collector. A coupling strategy was proposed in Section 5.1. Hence, we were able to analyze the model behavior as a function of three parameters: the engine size, the working-fluid mean pressure and the heater temperature. It was thus estimated that the engine dimension and the mean pressure of the working fluid have a strong effect on the power output of the Stirling unit, while a weak dependency of the collector temperature was noted. Such an unexpected behavior led us to revise some hypotheses under which the electrical analogy theory was developed. We noted that the correct estimation of both the pressure drops

and the convective coefficients in the heat exchangers could help to take into account the effect of the heater temperature. Furthermore, it should be recalled that an improvement of the model can be achieved by introducing a more rigorous description of the engine load.
Finally, since this research project aims to propose an energy-efficiency system to be implemented in the next future, a preliminary economic analysis was also undertaken. The industrial partners who helped us during this research have explicitly noted that the positive results of the economical study will be considered as sufficient condition to implement the proposed solution in the real plant. We studied the costs due to the use of the energy-efficiency system; the NPV theory is applied to calculate some financial metrics, such as the break-even point, the IRR and the ROI, for various scenarios. This analysis has demonstrated that a low capital cost of the Stirling engine is required to make the investment in the proposed solution profitable.

7.2 Scientific contributions

The most important topics treated in this thesis are: the recovery of the sidewall thermal wastes and their conversion into mechanical work. These subjects corresponds to the material we have included in two peer-reviewed journal papers presented in Chapter 3 and 4, respectively.
In the article "Proof of concept to recover thermal wastes from aluminum electrolysis cells using Stirling engines", published at the international journal of Energy Conversion and Management, it is proposed to estimate the radiative thermal wastes of the sidewall by using CFD simulations. An open source code (OpenFOAM 5.0) is used to simulate the following heat transfer mechanisms which occur at the pot sidewall. These mechanisms are:

- the conduction heat transfer coupled with mixed convection and radiation;
- the non-isothermal jet cooling flow.

A satisfactory agreement was found between the RANS equations coupled with the $k\varepsilon$ turbulence model implemented in OpenFOAM 5.0 and the analytical laws found in the open literature [82, 84]. Thus, this modeling approach was assumed to be the most appropriate to simulate the heat transfer phenomena from the pot sidewall and to calculate the thermal power collected by a metallic plate placed parallel to the sidewall. It was estimated that a heat flux of about 320 Wm^{-2} at a temperature ranging between 80 and 95°C can be collected by such a plate by thermal radiation alone. These temperatures are

high enough to drive some LTD Stirling engines found in the literature. However, it is mandatory to investigate collector working conditions which can help to increase the heat flux and the surface temperatures. In this way, more efficient Stirling engines can be used. The lack of a satisfactory model to predict the operation of Stirling engine led us to propose a new one; our model is based on the conservation equations (i.e, continuity, momentum and energy) applied to the components of the engine (i.e. the expansion chamber, the heater, the regenerator, the cooler and the compression chamber) and on the Newton laws for the moving parts (i.e. the power piston and the displacer). Then, an electrical analogy is established to write down an equivalent electrical-circuit for the Stirling mover. This theoretical approach is not completely new, as it has already been used in the literature. However, in most of the proposed models, the continuity and the momentum conservation equations are applied without considering the energy conservation equation [13, 94]. Hence, the novelty of the theoretical approach described in this document consists in introducing the energy equation into the electrical analogy. By doing this, it was possible to predict the coupled thermodynamic and dynamic behaviour of the engine. Furthermore, we were able to demonstrate that the introduction of the conservation equation for the energy does not prevent the possibility of establishing an equivalent electrical circuit analogy. A validation of the new model was carried out by comparing the predictions with the experimental data available for the RE-1000 unit. A satisfactory agreement was found despite the lack of information about the engine load, for which data were not available [49]. A detailed description of the new model is presently available in the scientific article "Modeling the dynamic and thermodynamic operation of Stirling engines by means of an equivalent electrical circuit", currently published at the international journal of Energy Conversion and Management [23]. Moreover, other preliminar theoretical considerations about the model are also available in a poster and two conference papers [95, 121]. Finally, a deep description of the OpenFOAM usage were provided in the framework of the Thermal and Fluids Analysis Workshop, held by NASA in 2016 at the U.S. Space & Rocket Center in Huntsville, Alabama.

7.3 Future works

The conclusion of a research project could be considered as the starting point of a new one. It is the case of the research reported in this thesis. Therefore, the most important topics that should be analyzed in the near future are listed below.

It is doubtless that there exists more performing theoretical modeling approaches than the one presented in this document for recovering the wastes. For instance, the use of the DNS

or LES approach may be preferred over the RANS one. However, we do not think that this is the most important topic to be treated in the future. Effectively, the CFD strategy proposed in Chapter 3 was meaningful, as it demonstrated that the recovery of the thermal wastes by radiation heat transfer is possible. It is for this reason that it would be more interesting to investigate if the heat flux collected by the flat plate and their temperature could be increased. From this viewpoint, other collector configurations should be studied; for instance, the operation of a parabolic concentrator should be estimated. Moreover, according to the author's knowledge, analyzing the effects of the distance between the collector (or the concentrator) and the sidewall may reveal to be another crucial topic. In fact, it was demonstrated that varying this distance may not only affect the collector operation, but also that of the pot. Thus, on the one hand, the proposed system will recover the thermal wastes and on the other, it can be used to assure the safe temperature of the pot, which is fundamental to preserve the electrolysis process. It is then fundamental to take into account this aspect in order to properly design the final system. This action requires to carry out further simulations to better understand the relationship between the sidewall mean temperature and the distance to the collector. Finally, it should be recalled that in the calculations performed in the framework of this research, the existing cooling system (i.e. the set of air nozzles) was considered. It is obvious that the operation of the collector will benefit from the removal of this system. Consequently, a new cooling strategy for the pot should be investigated in the next future, that is, a scenario in which the only way of transferring heat is by means of thermal radiation alone. By doing that, the most suitable operation for the collector (that is, high collected heat flux at high temperatures) is achieved.

The major limit of the model proposed in Chapter 4 is that it was validated for only one engine, namely, the RE-1000 unit, because several data are available in the literature. Since the pressure loss and the heat transfer were known, they were introduced into the model; however, these parameters should be predicted by the model. Introducing this information will surely extend the validity of the model, but it will also increase its complexity. Since these parameters are non-linear functions of the working gas mass-flow rate, a further iterative procedure should be added in the model. In spite of that, improving the modeling approach will not prevent the electrical-circuit analogy for the Stirling engine, as these effects would be predicted by non-linear resistances and source to be introduced in the analog circuit. The procedure given in [23], that is, introducing the pressure losses and the convective heat transfer coefficients in the model, allowed us to study the effects of the engine load, for which data were not available in the Schreiber et al.'s work [49]. The load is fundamental to ensure the good operation of the engine. It is for this reason

that a proper description of the load (such as the linear alternator outlined in Ulusoy's thesis [67]) should be considered in the future. However, it should be recalled that taking into account load effects would add a new variable in the model, i.e. the intensity of the electrical current in the alternator; nevertheless, in this way, an equivalent transducer should be introduced to obtain an equivalent circuit analogy for the Stirling engine.
Finally, it should be highlighted that the research discussed in this document was mainly theoretical. It is doubtless that any further progress requires the investigation of some practical aspects. Therefore, the fabrication of both the collector and the Stirling engine should be considered in the next future.

APPENDIX A

THE HALL-HÉROULT PROCESS: THEORETICAL ENERGY AND ACTUAL REACTIONS

A.1 Theoretical energy for the Hall-Héroult process

The minimal energy to perform Reaction R 1 can be estimated from the Gibbs function [31]:

$$\Delta G = \Delta H - T\Delta S \tag{1}$$

where ΔG is the Gibbs function, ΔH is the enthalpy variation ($\mathrm{kJ\,mol^{-1}}$), T is the temperature required to carry the reaction (K) and ΔS is the entropy variation ($\mathrm{kJ\,mol^{-1}\,K^{-1}}$); because of the physical meaning of the Gibbs function, ΔG is also called free energy of reaction. In order to use Equation 1, it is necessary to perform the enthalpy and the entropy balances. Thus, it is assumed that the reaction occurs at T_{Al} =1233 K and that the temperature of both reactants and products is T =298 K. Then, enthalpy and entropy variations of each chemical compound are evaluated by means of the following interpolation functions:

$$H^o - H^o_{298K} = AT + B\frac{T^2}{2} + C\frac{T^3}{3} + D\frac{T^4}{4} - \frac{E}{T} + F - H \tag{2}$$

$$S^o = A\log T + BT + C\frac{T^2}{2} + D\frac{T^3}{3} - \frac{E}{2T^2} + G \tag{3}$$

The values of the constants A, B, C, D, E, F G and H are listed in Table A.1 [27].
The constants for the graphite are not available; from thermodynamic tables found in [31], $(H^o - H^o_{298K})_C = 17.0\ \mathrm{kJ\,mol^{-1}}$ and $(S^o - S^o_{298K})_C = 29.1\ \mathrm{kJ\,mol^{-1}\,K^{-1}}$. With these data,

Table A.1 Constants to evaluate enthalpy and entropy of species

	Al	Al_2O_3	C	CO_2
A	6.71348	108,683	N/A	58.16639
B	-1.29418	37,2263	N/A	2.720074
C	2.04599	-14,2065	N/A	-0.492289
D	0.819161	2,193601	N/A	0.038844
E	-0.066294	-3,20988	N/A	-6.447293
F	-2.18623	-1701,6	N/A	-425.9186
G	14.7968	155,136	N/A	263.6125
H	0	-1656,86	N/A	-393.5224

it is possible to evaluate the enthalpy and the entropy of reaction:

$$\Delta H_{reac} = \sum \dot{m}_{in} \left[\bar{h}_f^o + \bar{h}\left(T_p\right) - \bar{h}^o\right]_{in} - \sum \dot{m}_{out} \left[\bar{h}_f^o + \bar{h}\left(T_p\right) - \bar{h}^o\right]_{out} \tag{4}$$

$$\Delta S_{reac} = \sum \dot{m}_{in} \left[\bar{s}\left(T_p\right) - \bar{s}^o\right]_{in} - \sum \dot{m}_{out} \left[\bar{s}\left(T_p\right) - \bar{s}^o\right]_{out} \tag{5}$$

Table A.2 lists the values of enthalpy and entropy variations for each chemical specie in Reaction R 1. With these data, Equation 1 can be used; thus, the minimal energy requirement is estimated to be 5.04 $\mathrm{MWh/t_{Al}}$.

A.2 Actual reactions in the Hall-Héroult process

Equation R 1, and consequently equation R 3 and R 4 are a strong simplification of the Hall-Héroult process. According to these reactions, the ionic components of the bath are Al^{3+} and O^{2-} (which is highly unstable, and therefore, absent in the bath); however, Na^+, F^-, AlF_3, AlF_4^- and $Al_xO_yF_z^{3x-2y-z}$ are also present. All these ions can react on the surface of the electrodes. Hence, the primary reaction occurring at the anode is given by:

$$4\,F^- + Al_2O_2F_4^{--} + C \longrightarrow 4\,e^- + 2\,AlF_4^- + CO_2 \tag{R 18}$$

At the cathode, the primary reaction is given by:

$$AlF_4^- + 3\,e^- \longrightarrow Al + 4\,F^- \tag{R 19}$$

while, the secondary ones are:

$$Na^+ + e^- \longrightarrow Na \tag{R 20}$$

$$4\,Al + 3\,C \longrightarrow Al_4C_3 \tag{R 21}$$

Therefore, at the bottom of the electrolytic cell, there is melted aluminum mixed with sodium and aluminum carbide (Al_4C_3); it should be noted that these elements cause the progressive erosion of the cathode. For this reason, once every five years, the graphite cathode must be replaced.

Table A.2 Thermodynamic data

Specie	N [mol]	$\bar{h}_f^o$ [kJ mol^{-1}]	M_m[kg mol^{-1}]	$\bar{h}\,(T_p) - \bar{h}^o$ [kJ mol^{-1}]	$\bar{s}\,(T_p) - \bar{s}^o$ [kJ mol^{-1} K^{-1}]
Al	1	0	26.98	27.65	76.3
Al_2O_3	0.5	-1675.7	101.96	113.0	202.5
C	0.75	0	12.01	17.0	274.0
CO_2	0.75	-393.5	44.01	274.03	29.1

APPENDIX B

RADIATION HEAT EXCHANGERS: A GENERAL OVERVIEW

According to Johansson and Söderström [41], a radiation heat exchanger, namely a collector, can be used to recover waste energy. However, this technology has not yet been widely employed because it is recent and not yet commercially available. This does not mean that radiation heat exchangers are not used in other industrial applications. In fact, they find applications in solar-energy heaters and coolers in space stations [122].
The solar energy collectors are mainly divided into two categories: non-concentrating (or stationary), that is, collectors that are fixed in space, and concentrating, that is, collectors that track the movement of the sun to increase the absorbed and intercepted radiation [122, 123]. For both stationary and concentrating collectors, several sub-configurations are available.
Flat-plate collectors (Figure B.1a) make use of a flat surface that absorbs the solar radiation to heat a working fluid flowing in a serpentine. These collectors can absorb both direct and diffuse radiation; their low manufacturing costs have made them widely employed by both the industrial and civil sectors. Compound parabolic collectors (Figure B.1b) are parabolic-shaped collector that do not absorb the solar radiation; rather, they reflect it to the focus of the parabola where a tubular absorber is placed. In this way, the working fluid flowing in the absorber can reach temperatures ranging from 60 up to 240°C. Evacuated tube collectors (Figure B.1c) make use of a principle well known from the theory; that is, scattering and absorbing effects do not affect a radiation travelling in a vacuum space [39]. Therefore, several vacuum-sealed heat pipes are connected to a manifold; evacuating the pipes makes sure that the heat losses are minimized. In each of these heat pipes, there is a heat-transfer fluid undergoing an evaporating-condensing cycle. So, the solar radiation heats the liquid fluid which changes it phase to vapour; because of the buoyancy forces, the vapour meets the working-fluid flow in the upside of the pipe and releases heat by condensing. In this way, the working fluid reaches temperatures ranging between 50 to

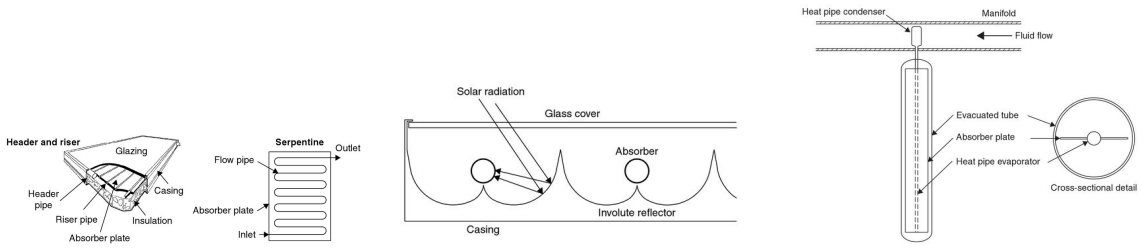

(a) (b) (c)

Figure B.1 Stationary collector configurations: flat–plate (a), compound parabolic (b) and evacuated tube collectors (c) [117, 118].

200°C [122].
An increase of collector efficiency can be achieved by introducing a sun-tracking system in such a way that the solar radiation absorbed or reflected by the collector is maximized, not only at noon, but even at early and late hours of the day. This is not the only advantage that these collectors present; in fact, the sun-tracking system could be used as a control system which assures a match between the requested and input energy. Moreover, these collectors have a cost per unit area lower than non-concentrating systems. Four configurations for concentrating collectors are available. Parabolic-trough collectors (Figure B.2a) are similar to compound parabolic ones; however, a sun-tracking system is added. In this manner, the heat-transfer fluid in the receiver tube (placed in the focal line of the parabola) can reach temperatures of up to 400°C. Fresnel collectors (Figure B.2b) are divided into Fresnel lens collectors, meaning, lens which direct the solar radiation in a point (in which there is a heat pipe) and linear Fresnel reflectors, which reflect the solar radiation and direct it in a point; for this category, several reflectors can be placed in a field in order to direct the radiation towards a target. In parabolic dish reflectors (Figure B.2c), a parabolic surface reflects the solar radiation to its optical focus. Both effects due to sun tracking and radiation concentration make this technology the most efficient and innovating of all collector systems. The heat transfer fluid could reach temperatures of up to 1500°C [124]; for this reason, parabolic dish engines are introduced. Generally,

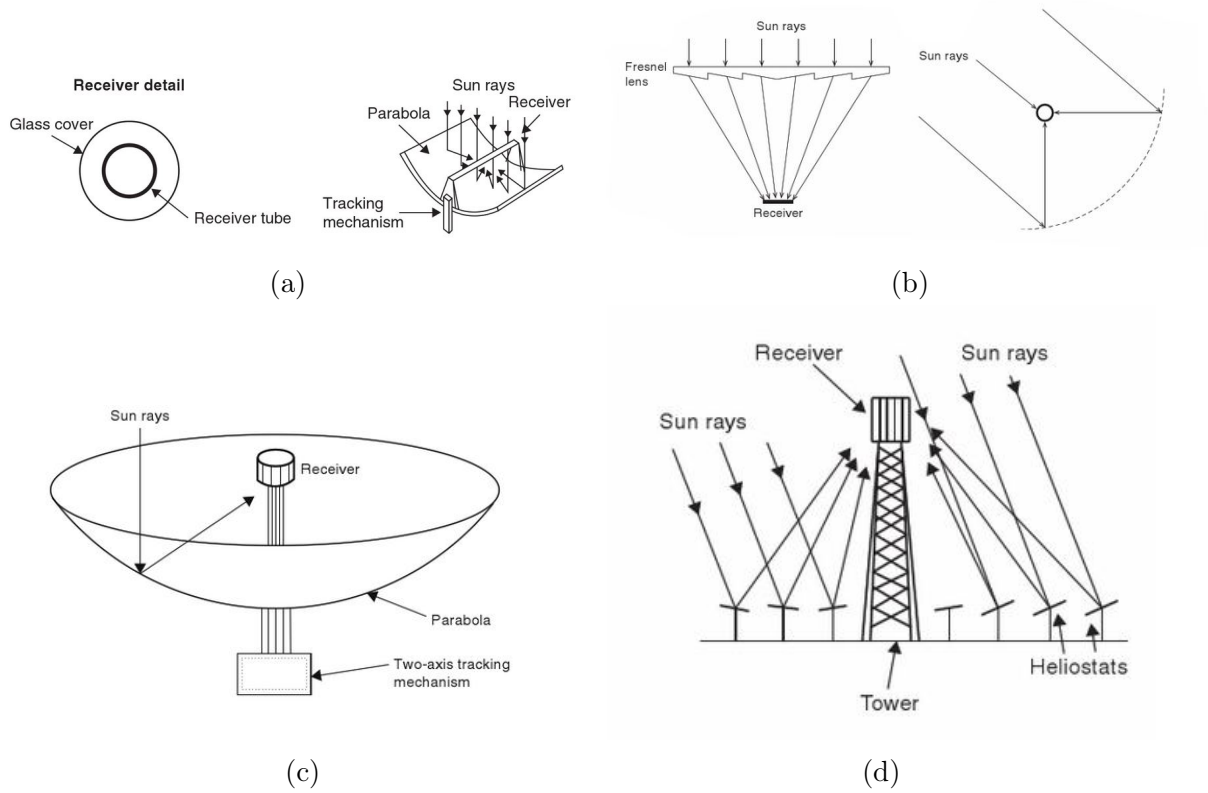

Figure B.2 Sun-tracking collector configurations: (a) parabolic trough collector, (b) Fresnel reflector, (c) Parabolic dish reflectors and (d) heliostat field collectors [117, 118].

a high-efficiency engine is used [86], as the case of the EuroDish-Stirling project where a Stirling engine is employed to generate electricity [22]. Finally, Heliostat Field collectors (Figure B.2d) are mirrors that reflect the incident solar radiation onto a common target. Because of the high energy concentration that can be reached, this target could be a steam generator [122].

Heat exchangers that use radiation are widely employed in space-power system applications [122, 125, 126]. An example of space power system is presented in Figure B.3; a working fluid following a Brayton cycle[1] is compressed, heated and then expanded into a turbine. In order to increase the efficiency of these engines, a regenerative heat exchanger, namely, a preheater, is introduced. The working fluid needs to be cooled before being sent back to the compressor. Therefore, the fluid passes though the finned tubes of a serpentine settled into a radiator; in this way, cooling takes place by means of radiation of excess heat to the free space (Figure B.3). Unlike solar collectors, which absorb the radiation as heat, a working fluid is cooled down.

The radiator is the most critical and complicated component to be designed in a space-power system and it is the largest and the heaviest of the equipments [126]. In order to evaluate its surface (A_{rad}) as a function of the thermal energy to be rejected, a heat transfer study must be implemented. Thus, the area of the radiator A_{rad} is given by:

$$A_{rad} = \frac{\dot{Q}_{cold}}{U \Delta T_{ml}} \tag{1}$$

where $\dot{Q}_{cold}$ is the heat to be rejected, U is the global heat exchange coefficient and ΔT_{ml} is the logarithmic mean temperature of the working fluid to be cooled. The global heat exchange coefficient can be calculated as:

$$U = \left(\frac{1}{h_c} + \frac{t}{k} + \frac{1}{h_r} \right)^{-1} \tag{2}$$

where h_c is the convective heat transfer coefficient, t is the tube thickness, k is the thermal conductivity of the finned tube and h_r is the radiative heat transfer coefficient. For internal

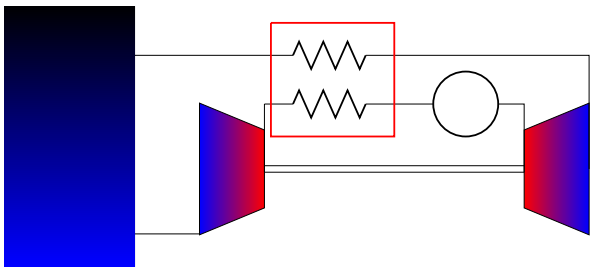

Figure B.3 Brayton power engine for space application.

[1] However, Rankine engines find application in space power system as well.

convection, h_c could be evaluated from the well known Dittus-Boelter equation [43]:

$$\mathrm{Nu} = \frac{h_c D}{k} = 0.023 \mathrm{Re}^{0.8} \mathrm{Pr}^{0.3} \tag{3}$$

with Nu the Nusselt number, D the diameter of the tube and Re and Pr are respectively the Reynolds and Prandtl dimensionless groups. The logarithmic mean temperature of the working fluid is given as:

$$\Delta T_{ml} = \frac{T_{in} - T_{out}}{\log \frac{T_{in} - T_s}{T_{out} - T_s}} \tag{4}$$

with T_{in}, T_{out} are the inlet and outlet working fluid temperatures, respectively, and T_s is the space temperature. Finally, h_r is calculated by [125]:

$$h_r = \epsilon_r \sigma \left(\Delta T_{ml} + T_s\right) \left(\Delta T_{ml}^2 + T_s^2\right) \tag{5}$$

where ϵ_r is the emissivity of the radiator, which is close to unity [43, 125].
The heat transfer analysis illustrated above highlights the parameters affecting the surface of the radiator (A_{rad}), that is, the rejected thermal power ($\dot{Q}_{cold}$), the thermodynamic properties of both the radiator material (t/k), and working fluid (Re, Pr), as well as the inlet and outlet temperatures (T_{in}, T_{out}). Other power plant variables deeply affect the radiator surface. For instance, according to Glassman [126], who analyzed a Brayton space engine, the A_{rad} can be minimized through the optimization of the turbine ratio temperature; still, turbomachinery efficiency and preheater effectiveness should be taken into account.
Finally, another coefficient analyzed by Toro and Lior [125] should be employed to understand the influence of the radiator on the whole power plant, namely, the ratio Ψ between the power output W, and the surface A_{rad}:

$$\Psi = \frac{W}{A_{rad}} \tag{6}$$

which varies between 0.78 to 0.87 kWm^2 for a regenerative Brayton engine and between 0.008 to 0.014 kWm^2 for a regenerative Rankine engine [125]. Assuming η to be the power-plant efficiency, Ψ can be expressed as a function of the heat transfer variables listed above, that is [125]:

$$\Psi = \frac{\eta}{1 - \eta} \frac{\Delta T_{ml}}{\frac{1}{h_c} + \frac{t}{k} + \frac{1}{h_r}} \tag{7}$$

APPENDIX C

THE $k\varepsilon$ AND THE $k\omega$ TURBULENCE MODELS

In this appendix, the turbulence models tested in this document are presented, that is, the $k\varepsilon$ turbulence model with buoyancy term [80] and the standard $k\omega$ model [18];

- In the $k\varepsilon$ turbulence model with buoyancy term, the turbulence kinetic energy k and the dissipation rate ε are estimated from the following equations:

$$\frac{\partial k}{\partial t} + U_j \frac{\partial k}{\partial x_j} = P_k - \varepsilon + \frac{\partial}{\partial x_j}\left[\left(\nu + \frac{\nu_t}{\sigma_k}\right)\frac{\partial k}{\partial x_j}\right] + G_k \tag{1}$$

$$\frac{\partial \varepsilon}{\partial t} + U_j \frac{\partial \varepsilon}{\partial x_j} = \frac{\partial}{\partial x_j}\left[\left(\nu + \frac{\nu_t}{\sigma_\varepsilon}\right)\frac{\partial \varepsilon}{\partial x_j}\right] + \left[c_{1\varepsilon}\left(P_k + G_k\right) - c_{2\varepsilon}\varepsilon\right]\frac{\varepsilon}{k} \tag{2}$$

where

$$P_k = -\overline{u_i' u_j'}\frac{\partial U_j}{\partial x_i}, \quad G_k = -\frac{\nu_t}{\sigma_T} g\beta \frac{\partial T}{\partial x_j}, \quad \nu_t = c_\mu \frac{k^2}{\varepsilon} \tag{3}$$

with $c_\mu = 0.09$, $c_{1\varepsilon} = 1.44$, $c_{2\varepsilon} = 1.92$, $\sigma_T = \sigma_k = 1$, $\sigma_\varepsilon = 1.3$.

- In the standard $k\omega$ turbulence model, the turbulence kinetic energy k and the frequency of turbulence dissipation ω are estimated from the following equations:

$$\frac{\partial k}{\partial t} + U_j \frac{\partial k}{\partial x_j} = \tau_{ij}\frac{\partial U_i}{\partial x_j} - \beta^* k\omega + \frac{\partial}{\partial x_j}\left[\left(\nu + \sigma^* \nu_t\right)\frac{\partial k}{\partial x_j}\right] \tag{4}$$

$$\frac{\partial \omega}{\partial t} + U_j \frac{\partial \omega}{\partial x_j} = \alpha \frac{\omega}{k}\tau_{ij}\frac{\partial U_i}{\partial x_j} - \beta\omega^2 + \frac{\partial}{\partial x_j}\left[\left(\nu + \sigma \nu_t\right)\frac{\partial \omega}{\partial x_j}\right] \tag{5}$$

where

$$\tau_{ij} = -\overline{u_i' u_j'}, \quad \nu_t = \frac{k}{\omega} \tag{6}$$

and $\alpha = \frac{5}{9}$, $\beta = \frac{3}{40}$, $\beta^* = \frac{9}{100}$, $\sigma^* = \sigma = \frac{1}{2}$.

APPENDIX D

GENERAL TRANSPORT EQUATION IN THE FINITE VOLUME METHOD

For a given control volume V_p (see Figure D.1), the conservation of the quantity ϕ can be written as [19]:

$$\int_{V_p} \underbrace{\frac{\partial \rho\phi}{\partial t}}_{\text{Rate of change}} \mathrm{d}V_p + \int_{V_p} \underbrace{\nabla \cdot (\rho \mathbf{u}\phi)}_{\text{Convection}} \mathrm{d}V_p = \int_{V_p} \underbrace{\nabla \cdot (\rho \Gamma_\phi \nabla \phi)}_{\text{Diffusion}} \mathrm{d}V_p + \int_{V_p} \underbrace{S_\phi(\phi)}_{\text{Source}} \mathrm{d}V_p \quad (1)$$

The FVM is based on the application of the Gauss theorem (also known as the divergence theorem or Ostrogradsky's theorem) to Equation 1. For a scalar field $\mathbf{F}$, the Gauss theorem states that:

$$\int_V (\nabla \cdot \mathbf{F}) \, \mathrm{d}V = \oint_S (\mathbf{F} \cdot \mathbf{n}) \, \mathrm{d}S, \quad S = \partial V \quad (2)$$

Thus:

$$\frac{\partial}{\partial t} \int_{V_p} (\rho\phi) \, \mathrm{d}V_p + \oint_{\partial V_p} \mathrm{d}\mathbf{S} \cdot (\rho \mathbf{u}\phi) = \oint_{\partial V_p} \mathrm{d}\mathbf{S} \cdot (\rho \Gamma_\phi \nabla \phi) + \int_{V_p} S_\phi(\phi) \, \mathrm{d}V_p \quad (3)$$

Each term of Equation 3 is then approximated according to the mean value theorems for definite integrals. Therefore:

$$\int_{V_p} \phi(\mathbf{x}) \, \mathrm{d}V = \phi_P V_p \quad (4)$$

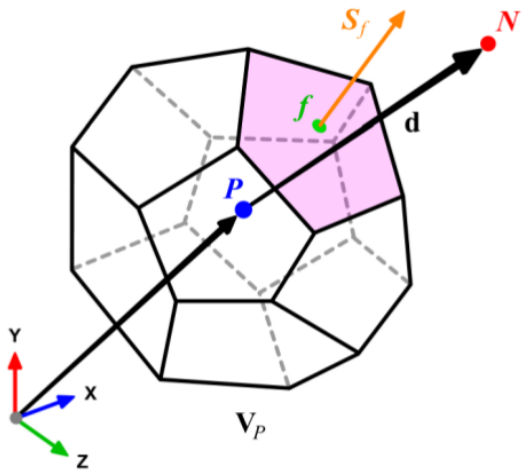

Figure D.1 Control volume V_p for the definition of the FVM.

$$\oint_{\partial V_p} \mathrm{d}\mathbf{S} \cdot (\rho \mathbf{u} \phi) \approx \sum_f \mathbf{S}_f \cdot (\rho \mathbf{u} \phi)_f \tag{5}$$

$$\oint_{\partial V_p} \mathrm{d}\mathbf{S} \cdot (\rho \Gamma_\phi \nabla \phi) \approx \sum_f \mathbf{S}_f \cdot (\rho \Gamma_\phi \nabla \phi)_f \tag{6}$$

Finally, we obtain the transport equation of the quantity ϕ according to the FVM:

$$\boxed{\frac{\partial}{\partial t} \rho \phi V_p + \sum_f \mathbf{S}_f \cdot (\rho \mathbf{u} \phi)_f = \sum_f \mathbf{S}_f \cdot (\rho \Gamma_\phi \nabla \phi)_f + S_\phi V_p} \tag{7}$$

Each term of this equation needs to be discretized according to the rules of the CFD.

APPENDIX E

THE SEMI IMPLICIT METHOD FOR PRESSURE LINKED EQUATIONS (SIMPLE) OF PATANKAR [19]

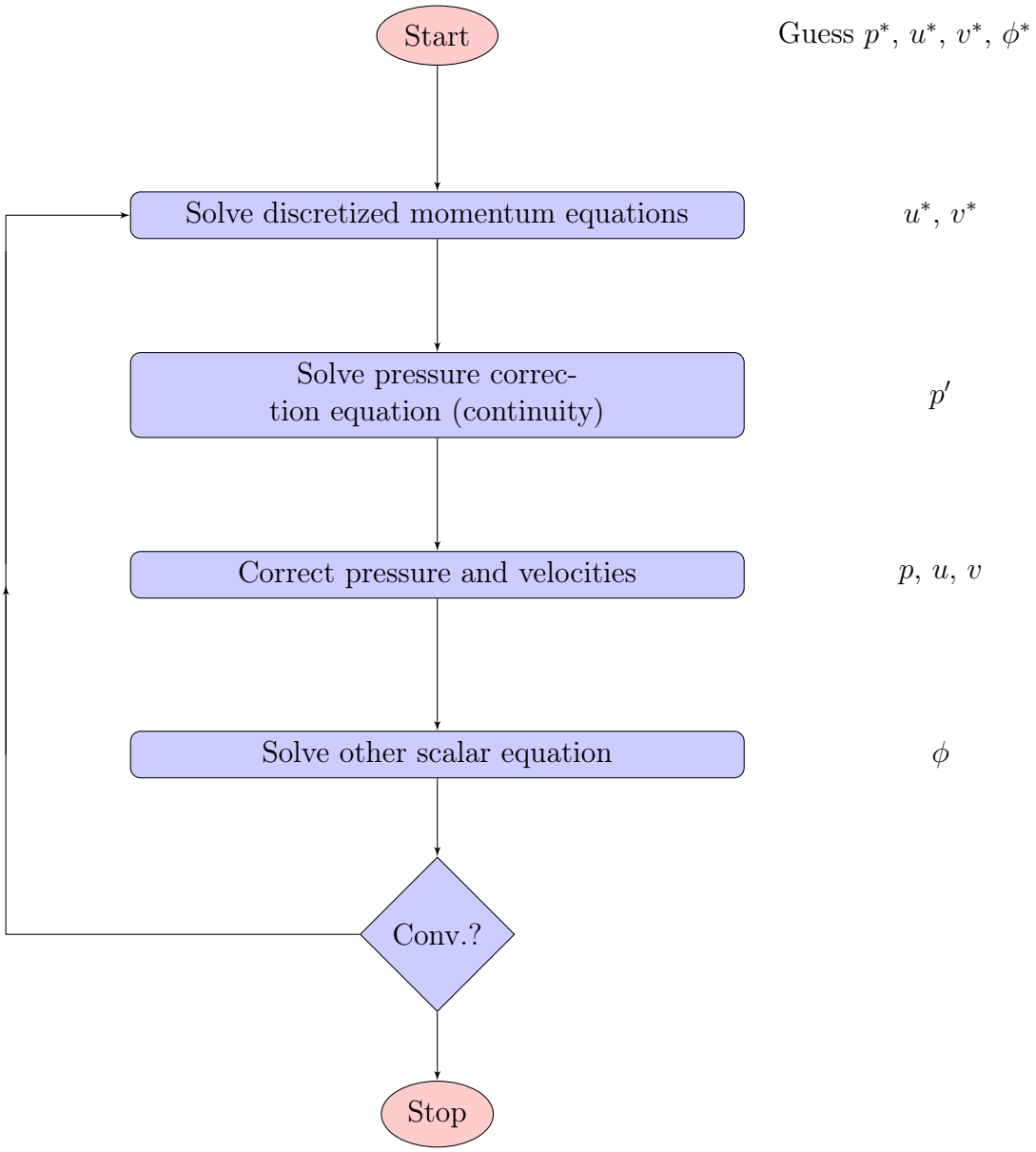

APPENDIX F
RE-1000 TECHNICAL DATA [49]

Working Fluid	He
Design frequency [Hz]	30
Design pressure [MPa]	7.0
Design power [W]	1000
Design phase angle [°]	45
Displace stroke (maximal) [cm]	4.01
Power piston stroke (maximal) [cm]	4.35
Compression space	
Mean volume [cm^3]	103.6
Cooler	
Number of rectangular passages	135
Passage width [cm]	0.0508
Passage depth [cm]	0.376
Length [cm]	7.92
Flow area [cm^2]	2.58
Wetted perimeter [cm]	115.2
Dead volume [cm^3]	28.5
Temperature [°C]	25
Heater	
Number of tubes	34
Tube length [cm]	18.34
Tube inside diameter [cm]	0.2362
Flow area [cm^2]	1.4898
Dead volume [cm^3]	39.6
Temperature [°C]	600
Regenerator	
Length [cm]	6.446
Outside diameter [cm]	7.18
Inside diameter [cm]	6.07
Wire diameter [µm]	88.9
Porosity [%]	75.9
Dead volume [cm^3]	59.41
Expansion space	
Mean volume [cm^3]	63.6

Power piston	
Mass [kg]	6.2
Diameter [cm]	5.718
Displacer	
Mass [kg]	0.426
Diameter [cm]	5.67
Rod diameter [cm]	1.663
Gas spring mean volume [cm^3]	31.8

LIST OF REFERENCES

[1] International Energy Agency, URL "https://www.iea.org/publications/freepublications/publication/KeyWorld2014.pdf", 2014.

[2] N. Oreskes, The scientific consensus on climate change: How do we know we're not wrong?, in: Climate Modelling, Springer, 31–64, 2018.

[3] A. Sandmo, Pigouvian taxes. The New Palgrave Dictionary of Economics, 2008.

[4] M. Fleer, O.-A. Lorentsen, W. Harvey, H. Palsson, G. Saevarsdottir, Heat recovery from the exhaust gas of aluminum reduction cells, 2010.

[5] B. L. Lostec, H. Nasreddine, Rapport Technique–Conversion of low grade waste heat to power in smelters, Tech. Rep., HydroQuebec LTE, 2011.

[6] C. Nowicki, L. Gosselin, An overview of opportunities for waste heat recovery and thermal integration in the primary aluminum industry, JOM 64 (8) (2012) 990–996.

[7] W. E. H. William B. Frank, Ullmann's Encyclopedia of Industrial Chemistry, Aluminium, Wiley-VCH, 2000.

[8] E. Saloux, M. Sorin, H. Nesreddine, A. Teyssedou, Reconstruction procedure of the thermodynamic cycle of organic Rankine cycles (ORC) and selection of the most appropriate working fluid, Applied Thermal Engineering 129 (2018) 628–635.

[9] K. H. Touchette, The Aluminum Industry In Canada, URL "http://www.jamec.ca/en/blog/aluminum-industry-canada/", 2017.

[10] Rio Tinto Alcan, URL "http://www.usinealmariotintoalcan.com/fr/page/usine-alma/", 2014.

[11] I. Johnson, W. T. Choate, A. Davidson, Waste heat recovery. Technology and opportunities in US industry, Tech. Rep., BCS, Inc., Laurel, MD (United States), 2008.

[12] RioTinto, Valorisation énrgie thermique dissipée par les cuves, Tech. Rep., Rio Tinto Alcan Métal primaire – Aluminium Pechiney SAS – 725, rue Aristide Bergès - 38340 Voreppe - France, 2014.

[13] F. Formosa, A. Badel, J. Lottin, Equivalent electrical network model approach applied to a double acting low temperature differential Stirling engine, Energy Conversion and Management 78 (2014) 753–764.

[14] W. R. Martini, Stirling engine design manual, US Department of Energy, Office of Conservation and Solar Applications, Division of Transportation Energy Conservation, 1978.

[15] G. T. Reader, et al., Stirling engines, E. and F. Spon, New York, NY, USA, 1983.

[16] I. Bayer, B. R. Olmstead, Combined Thermoelectric and Thermomagnetic Generator, uS Patent App. 13/120,962, 2011.

[17] M. A. Saad, M. A. Saad, Thermodynamics: principles and practice, Prentice Hall New Jersey, 1997.

[18] D. C. Wilcox, Turbulence modeling for CFD, DCW industries, La Canada, CA, 1998.

[19] H. K. Versteeg, W. Malalasekera, An Introduction to Computational Fluid Dynamics: The Finite Volume Method, Pearson Education, Pearson Education edn., 2011.

[20] D. Anderson, J. C. Tannehill, R. H. Pletcher, Computational Fluid Mechanics and Heat Transfer, CRC Press, ISBN 9781591690375, 2012.

[21] H. G. Weller, G. Tabor, H. Jasak, C. Fureby, A tensorial approach to computational continuum mechanics using object-oriented techniques, Computers in Physics 12 (6) (1998) 620–631, ISSN 0894-1866, URL http://aip.scitation.org/doi/abs/10.1063/1.168744.

[22] F. J. G. Granados, V. Ruiz-Hernández, M. A. Silva Pérez, Thermal Model of the EuroDish Solar Stirling Engin, J. Sol. Energy Eng URL http://solarenergyengineering.asmedigitalcollection.asme.org/article.aspx?articleid=1473951.

[23] F. Cascella, M. Sorin, F. Formosa, A. Teyssedou, Modeling the dynamic and thermodynamic operation of Stirling engines by means of an equivalent electrical circuit, Energy Conversion and Management 150 (2017) 295–303, ISSN 0196-8904, URL http://www.sciencedirect.com/science/article/pii/S0196890417307380.

[24] H. Kvande, P. A. Drabløs, The Aluminum Smelting Process and Innovative Alternative Technologies, Journal of Occupational and Environmental Medicine 56 (5 Suppl) (2014) S23.

[25] C. M. Hall, Process of reducing aluminium from its fluoride salts by electrolysis, US Patent App. 0/400,664, 1886.

[26] C. M. Hall, Manufacture of aluminium, US Patent 400,665, 1889.

[27] W. T. Choate, J. A. S. Green, US energy requirements for aluminum production, in: Energy efficient manufacturing processes symposium TMS, San Diego, CA, 99–113, 2003.

[28] V. Gusberti, D. S. Severo, B. J. Welch, M. Skyllas-Kazacos, Modeling the mass and energy balance of different aluminium smelting cell technologies, Light Metals 2012 (2012) 929–934.

[29] M. Taylor, W. Zhang, V. Wills, S. Schmid, A dynamic model for the energy balance of an electrolysis cell, Chemical Engineering Research and Design 74 (8) (1996) 913–933.

[30] R. G. Ehl, A. J. Ihde, Faraday's electrochemical laws and the determination of equivalent weights, Journal of Chemical Education 31 (5) (1954) 226.

[31] Y. A. Cengel, M. A. Boles, M. Kanoglu, Thermodynamics: an engineering approach, vol. 1056, McGraw-Hill New York, 1998.

[32] C. Nowicki, L. Gosselin, C. Duchesne, Waste heat integration potential assessment through exergy analysis in an aluminium production facility, TMS-Energy Technology 2012: Carbon Dioxide Management and Other Technologies (2012) 165–172.

[33] J. Bos, B. Feve, P. Homsi, Electrolytic pot for production of aluminum using the Hall-Héroult process comprising cooling means, US Patent 6,251,237, 2001.

[34] R. Zhao, Analysis, Simulation and Optimization of Ventilation of Aluminum Smelting Cells and Potrooms for Waste Heat Recovery, Ph.D. thesis, Université Laval, 2015.

[35] M. Dupuis, V. Bojarevics, J. Freibergs, Demonstration thermo-electric and MHD mathematical models of a 500 kA Al electrolysis cell, in: Proceedings of the 42nd Conference on Light Metals, CIM, Citeseer, 2003.

[36] I. Galasiu, R. Galasiu, C. Nicolescu, 9 Metallic Inert Anodes for Aluminium Electrolysis, Molten Salts and Ionic Liquids: Never the Twain? (2010) 123–131.

[37] S. Namboothiri, P. Lavoie, D. Cotton, M. P. Taylor, Controlled cooling of aluminium smelting cell sidewalls using heat exchangers supplied with air, TMS Light Metals (2009) 317–22.

[38] S. Dobric, Utilizing waste heat from metal industry for drying of organic waste, Master's thesis, Institutt for energi-og prosessteknikk, 2014.

[39] M. Planck, The theory of heat radiation, Courier Corporation, 1959.

[40] J. R. Howell, M. P. Menguc, R. Siegel, Thermal radiation heat transfer, CRC press, 2015.

[41] M. T. Johansson, M. Söderström, Options for the Swedish steel industry – Energy efficiency measures and fuel conversion, Energy 36 (1) (2011) 191–198.

[42] Hubblesite, URL "http://hubblesite.org/reference_desk/faq/answer.php.id=72&cat=light", 2018.

[43] F. P. Incropera, Introduction to heat transfer, John Wiley & Sons, 2011.

[44] Y. Rao, et al., Chemical engineering thermodynamics, Universities Press, 1997.

[45] A. Bejan, Entropy generation through heat and fluid flow, Wiley, 1982.

[46] T. J. Seebeck, Ueber die magnetische Polarisation der Metalle und Erze durch Temperaturdifferenz, (Magnetic polarization of metals and minerals by temperature differences), Annalen der Physik 82 (3) (1826) 253–286.

[47] I. Urieli, D. M. Berchowitz, Stirling cycle engine analysis, Taylor & Francis, 1984.

[48] G. Walker, Stirling engines, Oxford University Press, New York, NY, 1980.

[49] J. G. Schreiber, S. M. Geng, G. V. Lorenz, RE-1000 free-piston Stirling engine sensitivity test results, National Aeronautics and Space Administration Report .

[50] S. Abdullah, B. F. Yousif, K. Sopian, Design consideration of low temperature differential double-acting Stirling engine for solar application, Renewable Energy 30 (12) (2005) 1923–1941.

[51] A. Der Minassians, S. R. Sanders, Multiphase Free-Piston Stirling Engine for Solar-Thermal-Electric Power Generation Applications, in: 5th International Energy Conversion Engineering Conference, vol. 139, 2007.

[52] S. D. Wilson, W. A. Wong, NASA Glenn Research Center Support of the Advanced Stirling Radioisotope Generator Project .

[53] A. Romanelli, Alternative thermodynamic cycle for the Stirling machine, American Journal of Physics 85 (12) (2017) 926–931.

[54] M. W. Zemansky, Heat and thermodynamics: an intermediate textbook for students of physics, chemistry, and engineering .

[55] B. Kongtragool, S. Wongwises, A review of solar-powered Stirling engines and low temperature differential Stirling engines, Renewable and Sustainable energy reviews 7 (2) (2003) 131–154.

[56] K. Wang, S. R. Sanders, S. Dubey, F. H. Choo, F. Duan, Stirling cycle engines for recovering low and moderate temperature heat: A review, Renewable and Sustainable Energy Reviews 62 (2016) 89–108.

[57] B. Kongtragool, S. Wongwises, Testing of a low-temperature differential Stirling engine by using actual solar energy, International Journal of Green Energy 5 (6) (2008) 491–507.

[58] H. Karabulut, C. Çınar, E. Oztürk, H. Yücesu, Torque and power characteristics of a helium charged Stirling engine with a lever controlled displacer driving mechanism, Renewable Energy 35 (1) (2010) 138–143.

[59] A. R. Tavakolpour, A. Zomorodian, A. A. Golneshan, Simulation, construction and testing of a two-cylinder solar Stirling engine powered by a flat-plate solar collector without regenerator, Renewable Energy 33 (1) (2008) 77–87.

[60] Y. Kato, Indicated diagrams of a low temperature differential Stirling engine using flat plates as heat exchangers, Renewable Energy 85 (2016) 973–980.

[61] N. Tongdee, M. Jandakaew, T. Dolwichai, C. Thumthae, Thermodynamics Analysis for Optimal Geometrical Parameters and Influence of Heat Sink Temperature of Gamma-configuration Stirling Engine, Energy Procedia 105 (2017) 1782–1788.

[62] R. Redlich, D. Berchowitz, Linear dynamics of free-piston Stirling engines, Proceedings of the Institution of Mechanical Engineers, Part A: Power and process engineering 199 (3) (1985) 203–213.

[63] M. D. Kankam, J. S. Rauch, W. Santiago, Dynamic analysis of free-piston Stirling engine/linear alternator-load system-experimentally validated .

[64] N. Chen, F. Griffin, Linear harmonic analysis of free-piston Stirling engines, Tech. Rep., Oak Ridge National Lab., TN (USA), 1986.

[65] S. Bégot, G. Layes, F. Lanzetta, P. Nika, Stability analysis of free piston Stirling engines, The European Physical Journal-Applied Physics 61 (3).

[66] F. Formosa, Coupled thermodynamic–dynamic semi-analytical model of free piston Stirling engines, Energy Conversion and Management 52 (5) (2011) 2098–2109.

[67] N. Ulusoy, Dynamic analysis of free piston Stirling engines, Ph.D. thesis, Case western reserve university, 1994.

[68] G. W. Swift, Thermoacoustics, Acoustical Society of America, 2002.

[69] B. Kongtragool, S. Wongwises, Performance of a twin power piston low temperature differential Stirling engine powered by a solar simulator, Solar Energy 81 (7) (2007) 884–895.

[70] N. Nakajima, K. Ogawa, I. Fujimasa, Study on micro engines-miniaturizing Stirling engines for actuators and heatpumps, in: Micro Electro Mechanical Systems, 1989, Proceedings, An Investigation of Micro Structures, Sensors, Actuators, Machines and Robots., IEEE, 145–148, 1989.

[71] F. Formosa, L. G. Fréchette, Scaling laws for free piston Stirling engine design: Benefits and challenges of miniaturization, Energy 57 (2013) 796–808.

[72] S. Kwankaomeng, B. Silpsakoolsook, P. Savangvong, Investigation on stability and performance of a free-piston Stirling engine, Energy Procedia 52 (2014) 598–609.

[73] H. Karabulut, H. S. Yücesu, C. Çınar, F. Aksoy, An experimental study on the development of a β-type Stirling engine for low and moderate temperature heat sources, Applied Energy 86 (1) (2009) 68–73.

[74] G. R. Dochat, Stirling space power demonstrator engine test/analytical comparison, Acta Astronautica 15 (6-7) (1987) 341–346.

[75] M. Planck, Treatise on thermodynamics, Courier Corporation, 2013.

[76] J. Thonstad, P. Fellner, G. Haarberg, J. Híveš, H. Kvande, Å. Sterten, Aluminium electrolysis: fundamentals of the Hall-Héroult process. 3rd, 2001.

[77] A. Faux, A. de Gromard, A. Gonzalez, E. H. Bouhabila, M. Coulon, Waste heat recovery solutions, Aluminium International Today 28 (5) (2016) 45.

[78] E. Naess, T. Slungaard, B. Moxnes, O. K. Sonju, Experimental investigation of particulate fouling in waste heat recovery from the aluminum industry, in: International Heat Transfer Conference 13, Begel House Inc., 2006.

[79] L. E. Bell, Cooling, heating, generating power, and recovering waste heat with thermoelectric systems, Science 321 (5895) (2008) 1457–1461.

[80] R. Henkes, F. Van Der Vlugt, C. Hoogendoorn, Natural-convection flow in a square cavity calculated with low-Reynolds-number turbulence models, International Journal of Heat and Mass Transfer 34 (2) (1991) 377–388.

[81] B. Nebenführ, OpenFOAM: A tool for predicting automotive relevant flow fields .

[82] A. Shouman, An exact general solution for the temperature distribution and the composite radiation convection heat exchange along a constant cross-sectional area fin, Quarterly of Applied Mathematics 25 (4) (1968) 458–462.

[83] S. Churchill, M. Bernstein, A correlating equation for forced convection from gases and liquids to a circular cylinder in crossflow, Journal of Heat Transfer 99 (2) (1977) 300–306.

[84] G. Abramovich, The Theory of Turbulent Jets, 75, 1963.

[85] F. Lemoine, Y. Antoine, M. Wolff, M. Lebouche, Simultaneous temperature and 2D velocity measurements in a turbulent heated jet using combined laser-induced fluorescence and LDA, Experiments in fluids 26 (4) (1999) 315–323.

[86] V. Siva Reddy, S. Kaushik, S. Tyagi, Exergetic analysis and performance evaluation of parabolic dish Stirling engine solar power plant, International Journal of Energy Research 37 (11) (2013) 1287–1301.

[87] E. Fermi, Thermodynamics, Dover Publications, New York, (1956).

[88] N. Chen, F. Griffin, Review of Stirling-engine mathematical models, Tech. Rep., Oak Ridge National Lab., TN (USA), 1983.

[89] B. Huang, M. Chuang, System design of orifice pulse-tube refrigerator using linear flow network analysis, Cryogenics 36 (11) (1996) 889–902.

[90] P. Nika, Y. Bailly, Comparison of two models of a double inlet miniature pulse tube refrigerator: Part A thermodynamics, Cryogenics 42 (10) (2002) 593–603.

[91] Y. Bailly, P. Nika, Comparison of two models of a double inlet miniature pulse tube refrigerator: Part B electrical analogy, Cryogenics 42 (10) (2002) 605–615.

[92] T. Iwase, T. Biwa, T. Yazaki, Acoustic impedance measurements of pulse tube refrigerators, Journal of Applied Physics 107 (3) (2010) 034903.

[93] J. Tan, H. Dang, An electrical circuit analogy model for analyses and optimizations of the Stirling-type pulse tube cryocooler, Cryogenics 71 (2015) 18–29.

[94] G. Féniès, F. Formosa, J. Ramousse, A. Badel, Double acting Stirling engine: Modeling, experiments and optimization, Applied energy 159 (2015) 350–361.

[95] F. Cascella, M. Sorin, F. Formosa, A. Teyssedou, Modelling Stirling engines by means of an electrical analogy, Energy Production and Management in the 21st Century II: The Quest for Sustainable Energy 205 (2016) 59–72.

[96] R. B. Bird, Transport phenomena, vol. 55, American Society of Mechanical Engineers, (2002).

[97] N. Rott, Damped and thermally driven acoustic oscillations in wide and narrow tubes, Zeitschrift für angewandte Mathematik und Physik ZAMP 20 (2) (1969) 230–243.

[98] G. Benvenuto, F. De Monte, Analysis of free-piston Stirling engine/linear alternator systems. Part I-Theory., Journal of propulsion and power 11 (5) (1995) 1036–1046.

[99] I. H. Bell, J. Wronski, S. Quoilin, V. Lemort, Pure and Pseudo-pure Fluid Thermophysical Property Evaluation and the Open-Source Thermophysical Property Library CoolProp, Industrial & Engineering Chemistry Research 53 (6) (2014) 2498–2508, URL http://pubs.acs.org/doi/abs/10.1021/ie4033999.

[100] B. Huang, H. Chen, Modeling of integral-type Stirling refrigerator using system dynamics approach, International journal of refrigeration 23 (8) (2000) 632–641.

[101] P. Roach, K. Bell, Analysis of pressure drop and heat transfer data from the reversing flow test facility Report No, Tech. Rep., ANL/MCT-88-2, Argonne National Laboratory, Argonne, IL, 1989.

[102] M. Tanaka, I. Yamashita, F. Chisaka, Flow and heat transfer characteristics of the Stirling engine regenerator in an oscillating flow, JSME international journal. Ser. 2, Fluids engineering, heat transfer, power, combustion, thermophysical properties 33 (2) (1990) 283–289.

[103] B. Thomas, D. Pittman, Update on the evaluation of different correlations for the flow friction factor and heat transfer of Stirling engine regenerators, in: Energy Conversion Engineering Conference and Exhibit, 2000.(IECEC) 35th Intersociety, vol. 1, IEEE, 76–84, 2000.

[104] L.-S. Tong, A. London, Heat-transfer and flow-friction characteristics of woven-screen and crossed-rod matrices, Tech. Rep., Westinghouse Electric Corp. Pittsburgh, PA, 1956.

[105] W. T. Beale, Free piston Stirling engines-some model tests and simulations, Tech. Rep., SAE Technical Paper, 1969.

[106] K. Mahkamov, Design improvements to a biomass Stirling engine using mathematical analysis and 3D CFD modeling, Journal of Energy Resources Technology 128 (3) (2006) 203–215.

[107] J. J. Weygandt, P. D. Kimmel, D. E. Kieso, Financial & managerial accounting, John Wiley & Sons, 2015.

[108] P. Jain, Theory and problems in financial management, Tata McGraw-Hill Education, 1999.

[109] EPRI, Stirling Engine Assessment, Tech. Rep., Palo Alto, CA, 2002.

[110] HydroQuébec, Rate L - Industrial rate for large-power customers, URL "http://www.hydroquebec.com/business/customer-space/rates/rate-l-industrial-rate-large-power-customers.html", 2018.

[111] H. Analytics, Economic and Financial Indicators, The Economist (May, 2018) .

[112] CleanTech, "New Stirling Engine with Higher Temperature, Efficiency", URL "http://www.cleantech.org/2001/02/25/new-stirling-engine-with-higher-temperature-efficiency/", 2001.

[113] M. Kuosa, K. Saari, A. Kankkunen, T.-M. Tveit, Oscillating flow in a stirling engine heat exchanger, Applied Thermal Engineering 45 (2012) 15–23.

[114] T. Finkelstein, Thermodynamic analysis of Stirling engines., Journal of Spacecraft and Rockets 4 (9) (1967) 1184–1189.

[115] I. Boldea, S. A. Nasar, Linear electric actuators and generators, in: Electric Machines and Drives Conference Record, 1997. IEEE International, IEEE, MA1–1, 1997.

[116] E. Arroyo, A. Badel, F. Formosa, Y. Wu, J. Qiu, Comparison of electromagnetic and piezoelectric vibration energy harvesters: Model and experiments, Sensors and Actuators A: Physical 183 (2012) 148–156.

[117] F. Huet, F. Formosa, A. Badel, J.-F. Capsal, M. Lallart, Vibration energy harvesting device using P (VDF-TrFE) hybrid fluid diaphragm, Sensors and Actuators A: Physical 247 (2016) 12–23.

[118] L. L. Beranek, T. Mellow, Acoustics: sound fields and transducers, Academic Press, 2012.

[119] S. D. Senturia, Microsystem design, Springer Science & Business Media, 2007.

[120] F. Formosa, L. Fréchette, Multi-physics modelling approach for oscillatory micro-engines: application for a microStirling generator design, in: Journal of Physics: Conference Series, vol. 660, IOP Publishing, 012071, 2015.

[121] F. Cascella, M. Sorin, F. Formosa, A. Teyssedou, Analogie thermoacoustique appliquée à la modélisation d'un moteur Stirling, in: XIIème Colloque Interuniversitaire Franco-Québécois sur la Thermique des Systèmes, Université de Sherbrooke, 2015.

[122] A. P. Fraas, Heat exchanger design, John Wiley & Sons, 1989.

[123] R. K. McMordie, M. C. Brown, Solar Energy Fundamentals, Fairmont Press, 2012.

[124] S. A. Kalogirou, Solar energy engineering: processes and systems, Academic Press, 2013.

[125] C. Toro, N. Lior, Analysis and comparison of different thermal cycles for power generation in space, in: The 27th International Conference on Efficiency, Cost, Optimization, Simulation and Environmental Impact of Energy Systems, ECOS 2014, Proceedings of ECOS 2014, Turku, Finland, 2014.

[126] A. J. Glassman, Summary of Brayton cycle analytical studies for space-power system applications .